NTNU
Norwegian University of
Science and Technology

Andreev bound states in Josephson junctions: unconventional pairing symmetries in weak magnetic field and strong-field formalism

Anna Ursula Birkeland Brøyn

Master of Science in Physics and Mathematics
Submission date: June 2017
Supervisor: Jacob Rune Wüsthoff Linder, IFY
Co-supervisor: Jeroen Danon, IFY

Norwegian University of Science and Technology
Department of Physics

Abstract

The supercurrent in the normal region of a superconductor - normal metal - superconductor structure (SNS), when exposed to an external magnetic field, is studied. The current is found via the energy levels of the Andreev bound states of the system. For an ordinary low-T_c SNS-junction in a weak magnetic field it is found that a linear vortex pattern occurs in the current density. If the normal metal is substituted by a ferromagnet (SFS) it is found that the strength and direction of the current vortices can be controlled by the Zeeman field strength. The vortex pattern changes significantly if the low-T_c superconductors in the SNS-junction are substituted by high-T_c superconductors with d-wave pairing. Interestingly, it is found that in the presence of a subdominant s-wave gap in the high-T_c superconductors, the symmetry of the vortex pattern is lost. Analytical expressions for the precise gap orientation producing this phenomenon are derived. Numerical simulations of the system demonstrate that the supercurrent vortex pattern can be spatially controlled via the orientation of the d-wave gap and via the Zeeman field, and could open new perspectives with regard to tailored quantum current distributions. A conventional SNS-junction in a strong magnetic field is also studied in which semiclassical orbits could be classified from energy levels found quantum mechanically with use of numerical calculations. It is found that if the radius of the Lorentz cyclotron is small enough the energy levels will not contribute to the Josephson current.

Sammendrag

Superstrømmen i en superleder - normalmetall - superleder struktur (SNS), i et ytre magnetfelt, studeres. Strømmen blir funnet via Andreev bundende tilstander i systemet. For en normal SNS-overgang med lav kritisk temperatur i et svakt magnetisk felt finner vi et lineært mønster av virvler i strømtettheten. Hvis vi bytter ut det normale metallet med en ferromagnet (SFS) vil styrken og retningen til virvlene kunne bli styrt via Zeeman-feltstyrken. Virvelmønsteret endres betydelig hvis superlederne med lav kritisk temperatur og normal s-bølgegap byttes ut med superledere med høy kritisk temperatur og d-bølgegap. Dersom et mindre dominerende s-bølgegap er tilstede sammen med d-bølgegapet finner vi at symmetrien i virvelmønsteret forsvinner. Analytiske uttrykk for hvilke orienteringer av gapet som skaper dette fenomenet er utledet og numeriske simuleringer av strømtettheten i systemet viser at mønsteret kan kontrolleres via orienteringen til d-bølgegapet og av Zeeman-feltet. Vi har også studert en normal SNS-overgang i et sterkt magnetfelt der de semiklassiske banene blir klassifisert fra energinivåene funnet kvantemekanisk ved hjelp av numeriske beregninger.

Preface

This thesis on quantum condensed matter theory is submitted as the conclusion of a five year integrated master program in Applied Physics and Mathematics at the Norwegian University of Science and Technology. I would like to thank my supervisor Prof. Jacob Linder for introducing me to the fascinating topic of superconductivity in hybrid structures and for providing excellent help and guidance. I would also like to thank Assoc. Prof. Jeroen Danon for many insightful discussions on the topic and finally, I want to thank Jabir Ali Ouassou for helpful guidance concerning numerical simulations.

Anna Brøyn
Trondheim, Norway
June 2017

Contents

Chapter 1

Introduction

In 1911, H. K. Onnes discovered that the electrical resistance in mercury vanished when it was cooled down to a temperature of 4.2 K [1]. This was the first observation of superconductivity and it would go two more decades before W. Meissner and R. Ochsenfeld, in 1933, discovered a second fundamental property of superconductivity, namely the expulsion of magnetic fields below a certain threshold value, and that above this critical value the superconductivity breaks down [2, 3]. The absence of electrical resistance and the expulsion of the magnetic field are macroscopic quantum mechanical effects of which a microscopical description was missing for another two decades. This was finally presented by Bardeen, Cooper and Schieffer in 1957 and is now known as the BCS theory [4]. The theory propose that the supercurrent in a superconductor is transported via pairs of electrons, known as *Cooper pairs*, which condense into an electronic superfluid in which the Cooper pairs can travel without resistance.

More than 70 years after Onnes' discovery of low-T_c superconductivity with a critical temperature $T_c \approx 4\,\mathrm{K}$, Bednorz and Müller discovered high-T_c superconductivity at about 30 K in cuprates [5]. The high-T_c superconductors typically possess a d-wave pair symmetry which is different from the conventional s-wave pairing in the low-T_c superconductors in the way that it gives nodes in the excitation energy spectrum [6–9]. Experiments has shown that this gives far-reaching consequences for the properties of the superconducting state of the material [10, 11], and the origin of high-T_c superconductivity remains one of the most important unresolved problems in condensed matter physics.

When a superconductor (S) is placed in contact with a normal metal (N), Cooper pairs will leak from the superconductor and into the normal metal. This effect is known as the *proximity effect* [12], and allow for superconducting-like properties in materials which originally were non-superconducting. As the Meissner effect expels magnetic fields, superconductivity and magnetism rarely coexists in bulk materials. However, when hybrid structures are exposed to magnetic fields,

the proximity effect allows for interplay between superconductivity and magnetism, giving rise to a variety of interesting effects. In recent years new techniques have allowed resolving properties on smaller length scales and lower temperatures, and this has renewed the interest of the subject [13, 14]. There is now a good understanding of many electronic and transport properties of hybrid SN structures, but there are still many unexplored aspects of the dependency the magnetic field has on those properties. The interplay between superconductivity and magnetism is further manifested if the normal metal in the hybrid structures is substituded by magnetic materials, such as ferromagnets, in which the spin, in addition to the charge, of electrons is exploited [15, 16].

J. Rowell observed in 1963 that a superconductor-insulator-superconductor structure, exposed to a magnetic field, would have critical current that oscillates in a certain manner, known as Fraunhofer oscillations [17], see figure 1.1(b). It is understood that these oscillations are a consequence of circulating current vortices which appear in the insulator between the superconductors, due to quantum interference. The vortices are known as Josephson vortices and have later been observed in several SNS junctions [18, 19], as well as junctions with other materials such as graphene [20–23] and topological insulators [24–27]. In figure 1.1(a) supercurrent vortices in an SNS junction is illustrated. They are different from Abrikosov vortices [28], located in the superconductor, which have normal cores and a phase-winding of 2π of the superconducting order parameter.

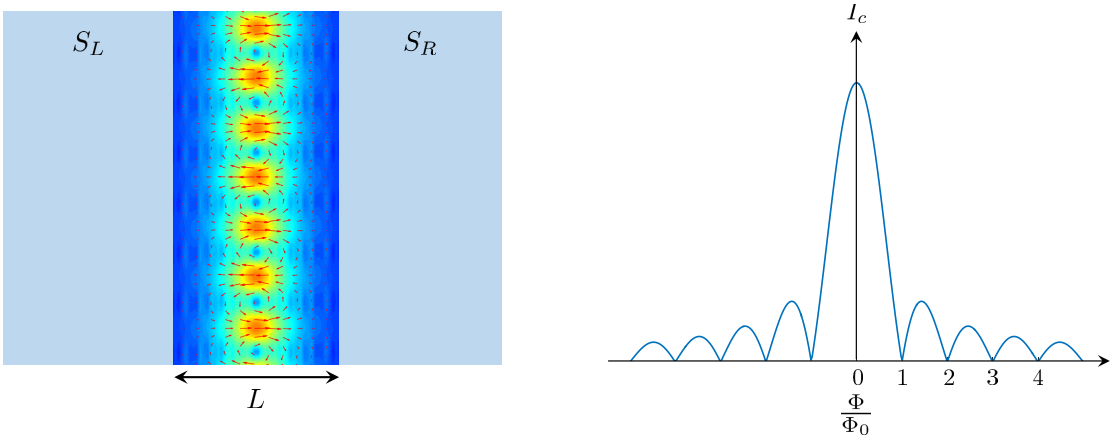

(a) (b)

Figure 1.1: Figure (a) illustrates the supercurrent vortices in the normal region of an SNS-junction when exposed to a uniform magnetic field. The length of the normal region is L while the width is $W \gg L$. Figure (b) shows the Fraunhofer oscillations, with period Φ_0, of the corresponding critical current versus the magnetic flux, Φ.

In wide SNS-junctions, $W \gg L$, of isotropic superconductors exposed to a spatially uniform mag-

netic field, research has shown that the vortices are arranged in a chain along the superconducting interface [29–33], like the pattern shown in figure 1.1(a). It is well-known that this pattern is modified by the insulating barriers if $W \simeq L$ [34–36], and in newer research it was found that if the Fermi surface is warped, the vortices are modified into a two-dimensional vortex lattice [37]. In any cases the critical current decays as Fraunhofer oscillations when the field strength is increased, although the decay rate under certain conditions has varied [37, 38]. In a modulated magnetic field the vortex pattern is somewhat modified and for certain modulations the current is left unaffected, even for arbitrary large field strengths. Thus the vortex pattern and the critical current can be controlled with modulated fields [39]. To our knowledge the research done on the supercurrent pattern in Josephson junctions has so far mainly been on SNS junctions with conventional s-wave superconductors. The d-wave symmetry of high-T_c superconductors will allow for different energy levels than the conventional s-wave superconductors and it is of interest to investigate how this in turn influence the supercurrent density. Moreover, if the normal metal in the junction is substituted by a ferromagnet (SFS), the external magnetic field will interact with the magnetic moments in the material and this may in turn influence the supercurrent density. One of the main objectives in this thesis is to understand how the supercurrent pattern in d-wave SNS-junctions and in s-wave SFS junctions responds to external magnetic fields on a microscopic level.

As already stated, the superconductivity breaks down if the magnetic field exceeds a critical value. Nevertheless, experiments have been done with strong magnetic fields large enough for the Landau-level quantization of the electronic motion to be of importance [40], but still without exceeding the critical value[41, 42]. At single NS interfaces with semi-infinite superconductors and normal regions exposed to such strong magnetic fields it is found that edge states consisting of coherent superposition of electron and hole excitations are formed and propagate along the interface [43]. Similar systems, but with finite width of the normal region has also been studied in both a quantum mechanical and semi-classical point of view [44]. There has, however, to the best of our knowledge not been any research on SNS junctions in strong magnetic fields and another main objective in this thesis is to understand how the energy levels and current in such junctions are affected by strong magnetic fields.

The outline of the thesis is as follows. In chapter 2 we will give the necessary background theory, explaining the Meissner effect, BCS theory and supercurrent transport theory in hybrid structures. We will also give a brief explanation of the d-wave pairing in high-T_c superconductors as well as some relevant properties of magnetic materials. The remaining chapters will consider a two-dimensional Josephson junction in an external magnetic field, but we will treat two somewhat different concepts. The first part (chapter 3 and 4) will focus on the current density pattern in weak magnetic fields, while the second part (chapter 5) will focus on the effect of a strong magnetic field on the energy levels in the junction. In chapter 3 we define the system and identify the energy lev-

els in the weak magnetic field. We will here consider three different situations: (1) an ordinary SNS junction of low-T_c superconductors with s-wave pairing, (2) an SNS junction of high-T_c superconductors with d-wave pairing and (3) an SFS junction with s-wave superconductors separated by a ferromagnet. In chapter 4 we use the energy levels found in chapter 3 to find the current density and the total current of the three situation. In chapter 5 we consider the second part of the thesis in which the external magnetic field is strong. Here we will use an analytical approach to set up the necessary equations for finding the energy levels and then use numerical calculations to identify the energy levels in the junction. We will use different methods to find the energy levels in the first and second part, the first being based on the Bohr-Sommerfeld quantization condition [45], while the second being based on matching of the wave functions at the interfaces. In chapter 6 we summarize the results in a conclusion followed by an outlook for future work.

Chapter 2

Fundamental theory

2.1 The Meissner effect

Meissner and Ochsenfeld discovered in 1933 [2] that applied magnetic field, H, below some critical limit H_c, would be expelled in the superconductor for temperatures below T_c, resulting in zero field inside the superconductor. This is called the Meissner effect and is a consequence of induced screening supercurrents at the surface of the superconductor. No current can exist only on the surface of a material as this would imply a finite current in a layer of zero thickness requiring infinite density of free charge. Consequently, the screening current must exist at some finite distance, λ_L, into the superconductor and thus letting the external magnetic field penetrate to a depth λ_L. On a deeper level, the Meissner effect represents that the photon has become massive inside a superconductor as a result of the spontaneous local U(1) symmetry breaking. The Meissner effect breaks down as the external field is increased to above the critical limit H_c. Depending on the material we will then get full (in type I superconductors) or partial (in type II superconductors) penetration of magnetic flux and the superconductor will go from the superconducting state into the normal or mixed state, respectively.

2.2 BCS theory

The discovery of the Cooper pairs, which can loosely be thought of as bosonic, was truly remarkable, as it is the key origin of superconductivity. In low-T_c superconductors the conventional mechanism behind the formation of Cooper pairs is phonon-mediated attractive interaction which is overwinning the Coulomb repulsion. In high-T_c superconductors the mechanism is still not clear, but the exact mechanism of the pairing is not of importance in this thesis, and the following derivation applies for any attractive interaction [1].

[1] The derivation in this section is inspired by Fossheim and Sudbø 2004, pp. 57-83 [46].

The Hamiltonian of the system will consist of two parts, describing the non-interacting and interacting electrons, respectively. A given state is defined by the momentum $\boldsymbol{k}$ and spin σ. In the second quantization formalism the annihilation- and creation operators, $c_{\boldsymbol{k},\sigma}$ and $c^\dagger_{\boldsymbol{k},\sigma}$, will destroy and create an electron in the corresponding state, respectively. The number operator $n_{\boldsymbol{k},\sigma} = c^\dagger_{\boldsymbol{k},\sigma} c_{\boldsymbol{k},\sigma}$ counts the number of electrons in the state. The non-interacting part of the Hamiltonian will simply be the energy of each state, $\epsilon_{\boldsymbol{k}} = \hbar^2 k^2/2m$, times the number operator and summed over all states. This will thus be the first term in the Hamiltonian (2.1). The interacting part of the Hamiltonian will describe a scattering process where two electrons in the states $(\boldsymbol{k}, \sigma)$ and $(\boldsymbol{k}', \sigma')$ are scattered into the states $(\boldsymbol{k}+\boldsymbol{q}, \sigma)$ and $(\boldsymbol{k}'-\boldsymbol{q}, \sigma')$, i.e. $(\boldsymbol{k}, \sigma)$ and $(\boldsymbol{k}', \sigma')$ are destroyed by the annihilation operators while $(\boldsymbol{k}+\boldsymbol{q}, \sigma)$ and $(\boldsymbol{k}'-\boldsymbol{q}, \sigma')$ are created by the creation operators. We must also include a matrix element $V_{\boldsymbol{k},\boldsymbol{k}'}$ including both the attractive phonon-mediated interaction and the repulsive Coulomb interaction, between the electrons. The total Hamiltonian including both the non-interacting and the interacting term is thus given as

$$H = \sum_{\boldsymbol{k},\sigma} \epsilon_{\boldsymbol{k}} c^\dagger_{\boldsymbol{k},\sigma} c_{\boldsymbol{k},\sigma} + \sum_{\mathbf{k},\mathbf{k}',\mathbf{q},\sigma,\sigma'} V_{\mathbf{k},\mathbf{k}'}(\mathbf{q},\omega) \mathbf{c}^\dagger_{\mathbf{k}+\mathbf{q},\sigma} \mathbf{c}^\dagger_{\mathbf{k}'-\mathbf{q},\sigma'} \mathbf{c}_{\mathbf{k},\sigma} \mathbf{c}_{\mathbf{k}',\sigma'}. \tag{2.1}$$

We define $\varepsilon_{\boldsymbol{k}} \equiv \epsilon_{\boldsymbol{k}} - \mu$ as the energy above the Fermi surface. The chemical potential, μ, is used in place of the Fermi energy, ϵ_F, as these two quantities are essentially the same in all relevant cases. The attractive interaction will only be valid in a small energy range, ω, above the Fermi-surface, and for electrons on opposite sides of the Fermi-surface. We may therefore let $\boldsymbol{k}' = -\boldsymbol{k}$. Due to the Pauli principle the electrons in the Cooper pairs will in most cases be found in opposite spin states, so we will also let $\sigma' = -\sigma$. By now changing the dummy indices, the Hamiltonian takes the form

$$H - \mu N = \sum_{\boldsymbol{k},\sigma} \varepsilon_{\boldsymbol{k}} c^\dagger_{\boldsymbol{k},\sigma} c_{\boldsymbol{k},\sigma} + \sum_{\boldsymbol{k},\boldsymbol{k}'} V_{\boldsymbol{k},\boldsymbol{k}'} c^\dagger_{\boldsymbol{k},\uparrow} c^\dagger_{-\boldsymbol{k},\downarrow} c_{\boldsymbol{k}',\uparrow} c_{-\boldsymbol{k}',\downarrow}, \tag{2.2}$$

where N is the number of electrons. Henceforth we will write H in place of $H - \mu N$.

We will use mean field approximation to simplify the Hamiltonian and assume the fluctuations around the expectation values to be small such that we can write

$$c_{-\boldsymbol{k},\downarrow} c_{\boldsymbol{k},\uparrow} = \langle c_{-\boldsymbol{k},\downarrow} c_{\boldsymbol{k},\uparrow} \rangle + c_{-\boldsymbol{k},\downarrow} c_{\boldsymbol{k},\uparrow} - \langle c_{-\boldsymbol{k},\downarrow} c_{\boldsymbol{k},\uparrow} \rangle \equiv \langle c_{-\boldsymbol{k},\downarrow} c_{\boldsymbol{k},\uparrow} \rangle + \delta_{\boldsymbol{k}}, \tag{2.3}$$

and only keep $\delta_{\boldsymbol{k}}$ to the first order. By also defining the *gap parameter* as follows

$$\Delta_{\boldsymbol{k}'} = \sum_{\boldsymbol{k}} V_{\boldsymbol{k},\boldsymbol{k}'} \langle c_{-\boldsymbol{k},\downarrow} c_{\boldsymbol{k},\uparrow} \rangle, \tag{2.4}$$

the Hamiltonian will simplify to

$$H = = E_0 + \sum_{\boldsymbol{k}} \varphi'^\dagger_{\boldsymbol{k}} H'_{\boldsymbol{k}} \varphi'_{\boldsymbol{k}}. \tag{2.5}$$

where we have used the standard commutation relations for fermions

$$\left[c^\dagger_{\boldsymbol{k},\sigma}, c_{\boldsymbol{k}',\sigma'}\right]_+ = \delta_{\boldsymbol{k},\boldsymbol{k}'}\delta_{\sigma,\sigma'}, \qquad \left[c^\dagger_{\boldsymbol{k},\sigma}, c^\dagger_{\boldsymbol{k}',\sigma'}\right]_+ = 0, \qquad \left[c_{\boldsymbol{k},\sigma}, c_{\boldsymbol{k}',\sigma'}\right]_+ = 0 \tag{2.6}$$

and defined

$$E_0 \equiv \sum_{\boldsymbol{k}} \left[\varepsilon_{\boldsymbol{k}} - \Delta_{\boldsymbol{k}} \langle c^\dagger_{\boldsymbol{k},\uparrow} c^\dagger_{-\boldsymbol{k},\downarrow}\rangle\right], \quad H'_{\boldsymbol{k}} = \begin{pmatrix} \varepsilon_{\boldsymbol{k}} & \Delta_{\boldsymbol{k}} \\ \Delta^*_{\boldsymbol{k}} & -\varepsilon_{\boldsymbol{k}} \end{pmatrix} \quad \text{and} \quad \varphi'_{\boldsymbol{k}} \equiv \begin{pmatrix} c_{\boldsymbol{k},\uparrow} \\ c^\dagger_{-\boldsymbol{k},\downarrow} \end{pmatrix}.$$

The Hamiltonian (2.5) can be diagonalized by inserting $U_{\boldsymbol{k}} U^\dagger_{\boldsymbol{k}} = I$, where I is the identity matrix and U is a unitary matrix:

$$U_{\boldsymbol{k}} = \begin{pmatrix} u_{\boldsymbol{k}} & -v^*_{\boldsymbol{k}} \\ v_{\boldsymbol{k}} & u^*_{\boldsymbol{k}} \end{pmatrix}, \qquad U^\dagger_{\boldsymbol{k}} = \begin{pmatrix} u^*_{\boldsymbol{k}} & v^*_{\boldsymbol{k}} \\ -v_{\boldsymbol{k}} & u_{\boldsymbol{k}} \end{pmatrix}. \tag{2.7}$$

The coherence factors

$$u_{\boldsymbol{k}} = e^{i\varphi/2}\cos\theta_{\boldsymbol{k}}, \qquad v_{\boldsymbol{k}} = e^{-i\varphi/2}\sin\theta_{\boldsymbol{k}}, \tag{2.8}$$

defined by the new variables, φ and $\theta_{\boldsymbol{k}}$, satisfy the relation $|u_{\boldsymbol{k}}|^2 + |v_{\boldsymbol{k}}|^2 = 1$ and will therefore leave the matrix U unitary. If we now let φ and $\theta_{\boldsymbol{k}}$ be such that $H_{\boldsymbol{k}} = U^\dagger_{\boldsymbol{k}} H'_{\boldsymbol{k}} U_{\boldsymbol{k}}$ is diagonal, our Hamiltonian will be on the diagonal form

$$H = E_0 + \sum_{\boldsymbol{k}} \varphi^\dagger_{\boldsymbol{k}} H_{\boldsymbol{k}} \varphi_{\boldsymbol{k}} \tag{2.9}$$

with $\varphi_{\boldsymbol{k}} \equiv U^\dagger_{\boldsymbol{k}} \varphi'_{\boldsymbol{k}}$:

$$\varphi_{\boldsymbol{k}} \equiv \begin{pmatrix} \gamma_{\boldsymbol{k},\uparrow} \\ \gamma^\dagger_{-\boldsymbol{k},\downarrow} \end{pmatrix} = \begin{pmatrix} u^*_{\boldsymbol{k}} & v^*_{\boldsymbol{k}} \\ -v_{\boldsymbol{k}} & u_{\boldsymbol{k}} \end{pmatrix} \begin{pmatrix} c_{\boldsymbol{k},\uparrow} \\ c^\dagger_{-\boldsymbol{k},\downarrow} \end{pmatrix}. \tag{2.10}$$

The new fermionic operators $\gamma_{\boldsymbol{k},\uparrow}$ and $\gamma^\dagger_{-\boldsymbol{k},\downarrow}$ are describing excitation of single quasi-particles. We find that $H_{\boldsymbol{k}}$ is diagonal if $\theta_{\boldsymbol{k}}$ satisfy

$$\begin{aligned} u^2_{\boldsymbol{k}} &= \cos^2\theta = \frac{1}{2}\left(1 \pm \frac{\varepsilon^\pm_{\boldsymbol{k}}}{\sqrt{\varepsilon^{\pm 2}_{\boldsymbol{k}} + |\Delta_{\boldsymbol{k}}|^2}}\right) \\ v^2_{\boldsymbol{k}} &= \sin^2\theta = \frac{1}{2}\left(1 \mp \frac{\varepsilon^\pm_{\boldsymbol{k}}}{\sqrt{\varepsilon^{\pm 2}_{\boldsymbol{k}} + |\Delta_{\boldsymbol{k}}|^2}}\right) \end{aligned} \tag{2.11}$$

and φ is the phase of the gap parameter, $\Delta_{\boldsymbol{k}} = |\Delta_{\boldsymbol{k}}|\, e^{i\varphi}$. We will see in the following chapters that the superconducting phase, φ, plays an extremely important role in hybrid structures such as Josephson junctions. We let $\varepsilon^+_{\boldsymbol{k}} > 0$ and $\varepsilon^-_{\boldsymbol{k}} < 0$ and notice that we get $u^2_{\boldsymbol{k}} = 1$ and $v^2_{\boldsymbol{k}} = 0$ when $\Delta_{\boldsymbol{k}} = 0$, that is in the limit of the normal state when there is no attraction between the electrons, according to

equation (2.4). The resulting diagonal Hamiltonian is now on the form

$$H_{\boldsymbol{k}} = \begin{pmatrix} E_{\boldsymbol{k}} & 0 \\ 0 & -E_{\boldsymbol{k}} \end{pmatrix} \tag{2.12}$$

where we have defined

$$E_{\boldsymbol{k}} = \sqrt{\varepsilon_{\boldsymbol{k}}^2 + |\Delta_{\boldsymbol{k}}|^2} \tag{2.13}$$

as the quasiparticle excitation energy. It is now clear why $\Delta_{\boldsymbol{k}}$ is refered to as the *gap-parameter* as it gives a gap in the excitation spectrum of the quasiparticles $\varphi_{\boldsymbol{k}}$. Below the gap there are no allowed single particle states and we understand that the presence of the Cooper pairs has crucial consequences for the single particle density of states. Moreover, we have

$$k^{\pm} = k_F \sqrt{1 + \frac{\varepsilon_{\boldsymbol{k}}^{\pm}}{\mu}} = k_F \sqrt{1 \pm \frac{\sqrt{E_{\boldsymbol{k}}^2 - |\Delta_{\boldsymbol{k}}|^2}}{\mu}} \tag{2.14}$$

where $\mu = \hbar^2 k_F^2/2m$ and $\varepsilon_{\boldsymbol{k}}^{\pm} = \pm\sqrt{E_{\boldsymbol{k}} - |\Delta_{\boldsymbol{k}}|^2}$ is obtained from equation (2.13). We notice how we get a fourfold degeneracy of relevant states, $(k^+, k^-, -k^+, -k^-)$, for each $E_{\boldsymbol{k}}$. The quasiparticle excitation $\gamma_{\boldsymbol{k},\uparrow}^{\dagger}$ in equation (2.10) will be electronlike since we, according to equation (2.11), have $u_{\boldsymbol{k}}^2 \to 1$ and $v_{\boldsymbol{k}}^2 \to 0$ as $\Delta \to 0$ and $c_{\boldsymbol{k},\uparrow}^{\dagger}$ creates an electron while $c_{-\boldsymbol{k},\downarrow}$ destroys an electron, leaving a hole. Similarly, $\gamma_{\boldsymbol{k},\uparrow}$ will be holelike. Moreover, from equation (2.14) we see that $\pm k^+$ ($\pm k^-$) correspond to energy above (below) the Fermi surface and thus $\pm k^+$ ($\pm k^-$) are electron (hole)-like excitations. The direction of the waves is determined from the group velocity,

$$\boldsymbol{v}_g = \frac{1}{\hbar}\frac{\partial E_{\boldsymbol{k}}}{\partial \boldsymbol{k}} = \frac{\varepsilon_{\boldsymbol{k}}^{\pm}}{E_{\boldsymbol{k}}}\frac{\hbar \boldsymbol{k}^{\pm}}{m}, \tag{2.15}$$

and as $\varepsilon_{\boldsymbol{k}}^{-} < 0$ we realize that the holes travel in opposite direction of their wave vector, $\boldsymbol{k}^{-}$.

For convenience we introduce a new variable, η, defined as

$$\eta \equiv \begin{cases} \arccos\left(\frac{E_{\boldsymbol{k}}}{|\Delta_{\boldsymbol{k}}|}\right), & \text{if } E_{\boldsymbol{k}} < |\Delta_{\boldsymbol{k}}| \\ i\,\text{arccosh}\left(\frac{E_{\boldsymbol{k}}}{|\Delta_{\boldsymbol{k}}|}\right), & \text{if } E_{\boldsymbol{k}} > |\Delta_{\boldsymbol{k}}|\,. \end{cases} \tag{2.16}$$

By using this new variable in the expressions for $u_{\boldsymbol{k}}$ and $v_{\boldsymbol{k}}$ in equation (2.11) we find the quantity,

$$\frac{u_{\boldsymbol{k}}}{v_{\boldsymbol{k}}} = e^{i(\eta+\varphi)}, \tag{2.17}$$

which we will find useful in the following chapters.

2.3 Bogoliubov-de Gennes equations

In the description above we assumed the Hamiltonian to be position-invariant so that the wave functions could be considered as simple plane waves, $\sim \exp(i\boldsymbol{k}\cdot\boldsymbol{r})$. We took the potential $V(\boldsymbol{r})$ and the vector potential, $\boldsymbol{A}(\boldsymbol{r})$, to be zero and simply replaced the Hamiltonian for a single particle system,

$$h(\boldsymbol{r}) = \frac{1}{2m}\left(\frac{\hbar}{i}\nabla - q\boldsymbol{A}(\boldsymbol{r})\right)^2 - \mu(\boldsymbol{r}) + V(\boldsymbol{r}), \tag{2.18}$$

with $\varepsilon_{\boldsymbol{k}} = \hbar^2 k^2/2m - \mu$. For systems where the momentum is position-dependent we can not do this simplification and introduce instead field operators:

$$\psi(\boldsymbol{r},t) \equiv \sum_{\boldsymbol{k}} U(\boldsymbol{r},t)\varphi_{\boldsymbol{k}}, \qquad \psi^\dagger(\boldsymbol{r},t) \equiv \sum_{\boldsymbol{k}} \varphi^\dagger_{\boldsymbol{k}} U^\dagger(\boldsymbol{r},t). \tag{2.19}$$

The Hamiltonian in equation (2.5) will now be given as

$$H = E_0 + \int d^3r\, \psi^\dagger(\boldsymbol{r},t)\begin{pmatrix} h(\boldsymbol{r}) & \Delta(\boldsymbol{r}) \\ \Delta^*(\boldsymbol{r}) & -h(\boldsymbol{r}) \end{pmatrix}\psi(\boldsymbol{r},t) \equiv E_0 + \int d^3r\, \psi^\dagger(\boldsymbol{r},t) H'(\boldsymbol{r})\psi(\boldsymbol{r},t). \tag{2.20}$$

Again the Hamiltonian may be diagonalized by setting $U^\dagger(\boldsymbol{r},t)H'(\boldsymbol{r})U(\boldsymbol{r},t) = H_{\boldsymbol{k}}$, or equally $H'(\boldsymbol{r})U(\boldsymbol{r},t) = U(\boldsymbol{r},t)H_{\boldsymbol{k}}$, where $H_{\boldsymbol{k}}$ is on the diagonal form in equation (2.12). By separating these equations for each eigenvalue in $H_{\boldsymbol{k}}$ we get the *Bogoliubov de Gennes equations* (BdG equations) [47]:

$$\begin{pmatrix} h(\boldsymbol{r}) & \Delta(\boldsymbol{r}) \\ \Delta^*(\boldsymbol{r}) & -h(\boldsymbol{r}) \end{pmatrix}\begin{pmatrix} u(\boldsymbol{r},t) \\ v(\boldsymbol{r},t) \end{pmatrix} = E_{\boldsymbol{k}}\begin{pmatrix} u(\boldsymbol{r},t) \\ v(\boldsymbol{r},t) \end{pmatrix}, \tag{2.21a}$$

$$\begin{pmatrix} -h(\boldsymbol{r}) & -\Delta^*(\boldsymbol{r}) \\ -\Delta(\boldsymbol{r}) & h(\boldsymbol{r}) \end{pmatrix}\begin{pmatrix} -v(\boldsymbol{r},t) \\ u(\boldsymbol{r},t) \end{pmatrix} = E_{\boldsymbol{k}}\begin{pmatrix} -v(\boldsymbol{r},t) \\ u(\boldsymbol{r},t) \end{pmatrix}. \tag{2.21b}$$

which is equivalent to writing

$$\begin{pmatrix} h(\boldsymbol{r}) & 0 & 0 & \Delta(\boldsymbol{r}) \\ 0 & h(\boldsymbol{r}) & -\Delta(\boldsymbol{r}) & 0 \\ 0 & -\Delta^*(\boldsymbol{r}) & -h(\boldsymbol{r}) & 0 \\ \Delta^*(\boldsymbol{r}) & 0 & 0 & -h(\boldsymbol{r}) \end{pmatrix}\begin{pmatrix} u(\boldsymbol{r},t) \\ u(\boldsymbol{r},t) \\ -v(\boldsymbol{r},t) \\ v(\boldsymbol{r},t) \end{pmatrix} = E_{\boldsymbol{k}}\begin{pmatrix} u(\boldsymbol{r},t) \\ u(\boldsymbol{r},t) \\ -v(\boldsymbol{r},t) \\ v(\boldsymbol{r},t) \end{pmatrix}. \tag{2.22}$$

2.4 Superconducting wave functions

From equation (2.10) we have $\gamma^\dagger_{\boldsymbol{k},\uparrow} = u_{\boldsymbol{k}} c^\dagger_{\boldsymbol{k},\uparrow} + v_{\boldsymbol{k}} c_{-\boldsymbol{k},\downarrow}$. By letting $u_\sigma(\boldsymbol{r},t)$ and $v_{-\sigma}(\boldsymbol{r},t)$ be the position space representation of $u_{\boldsymbol{k}}$ and $v_{\boldsymbol{k}}$ we can represent $\gamma^\dagger_{\boldsymbol{k},\sigma}$ and $\gamma_{\boldsymbol{k},\sigma}$ by the vectors $\Psi_{e,\sigma}$ and $\Psi_{h,\sigma}$,

respectively, where Ψ is a vector of the form $\left(u_\uparrow, u_\downarrow, v_\uparrow, v_\downarrow\right)^T$. This gives:

$$\begin{aligned}
\gamma^\dagger_{\boldsymbol{k},\uparrow} \to \Psi_{e,\uparrow} &= \begin{pmatrix} u(\boldsymbol{r},t) \\ 0 \\ 0 \\ v(\boldsymbol{r},t) \end{pmatrix}, & \gamma^\dagger_{-\boldsymbol{k},\downarrow} \to \Psi_{e,\downarrow} &= \begin{pmatrix} 0 \\ u(\boldsymbol{r},t) \\ -v(\boldsymbol{r},t) \\ 0 \end{pmatrix}, \\
\gamma_{\boldsymbol{k},\uparrow} \to \Psi_{h,\uparrow} &= \begin{pmatrix} 0 \\ -v^*(\boldsymbol{r},t) \\ u^*(\boldsymbol{r},t) \\ 0 \end{pmatrix}, & \gamma_{-\boldsymbol{k},\downarrow} \to \Psi_{h,\downarrow} &= \begin{pmatrix} v^*(\boldsymbol{r},t) \\ 0 \\ 0 \\ u^*(\boldsymbol{r},t) \end{pmatrix}.
\end{aligned} \tag{2.23}$$

We can often ignore the spin degeneracy and only consider the 2×2 matrix in (2.21a) as the BdG-equations. In that case the wave functions reduces to 2-vectors:

$$\Psi_e = \begin{pmatrix} u(\boldsymbol{r},t) \\ v(\boldsymbol{r},t) \end{pmatrix}, \qquad \Psi_h = \begin{pmatrix} v^*(\boldsymbol{r},t) \\ u^*(\boldsymbol{r},t) \end{pmatrix}. \tag{2.24}$$

We will in this thesis assume the magnetic field to be completely expelled by the superconductors and let the vector potential be zero in this region. The Hamiltonian from equation (2.18) will simplify to

$$h_S(\boldsymbol{r}) = -\frac{\hbar^2\nabla^2}{2m} - \mu_S. \tag{2.25}$$

Ignoring the spin-degeneracy and using the above Hamiltonian (2.25) in the BdG-equations (2.21a), the wave functions satisfying the equations will be plane waves on the form

$$\Psi_e(\boldsymbol{r}) = \begin{pmatrix} u_{\boldsymbol{k}} \\ v_{\boldsymbol{k}} \end{pmatrix} e^{i\boldsymbol{k}^+\cdot\boldsymbol{r}}, \qquad \Psi_h(\boldsymbol{r}) = \begin{pmatrix} v^*_{\boldsymbol{k}} \\ u^*_{\boldsymbol{k}} \end{pmatrix} e^{i\boldsymbol{k}^-\cdot\boldsymbol{r}}, \tag{2.26}$$

and we find

$$h_S(\boldsymbol{r})\Psi_{e/h}(\boldsymbol{r}) = \left(\frac{\hbar^2 k^{\pm 2}}{2m} - \mu\right)\Psi_{e/h}(\boldsymbol{r}) \equiv \varepsilon^\pm_k \Psi_{e/h}(\boldsymbol{r}). \tag{2.27}$$

The eigenvalue problem in the BdG-equations (2.21a) has non-trivial solutions if the energies, $E_{\boldsymbol{k}}$ satisfy

$$\begin{aligned}
0 &= \det\begin{pmatrix} \varepsilon^\pm_{\boldsymbol{k}} - E_{\boldsymbol{k}} & \Delta \\ \Delta^* & -\varepsilon^\pm_{\boldsymbol{k}} - E_{\boldsymbol{k}} \end{pmatrix} \\
&= -\varepsilon^{\pm 2} + E^2_{\boldsymbol{k}} - |\Delta|^2
\end{aligned} \tag{2.28}$$

which gives the energies $E^2_{\boldsymbol{k}} = \varepsilon^{\pm 2}_{\boldsymbol{k}} + |\Delta|^2$ in correspondence with the energies obtained in equation (2.13), and $k^\pm$ and $\varepsilon^\pm_{\boldsymbol{k}}$ will be as in equation (2.14). Electronlike quasiparticles will have excitation

energy above the fermi surface, $\varepsilon_{\boldsymbol{k}}^{+} = +\sqrt{E_{\boldsymbol{k}}^2 - \Delta^2} = i\Delta\sin\eta$, for which we find the wave-functions

$$\Psi_e(\boldsymbol{r}) = \begin{pmatrix} u_0 e^{i\varphi/2} \\ v_0 e^{-i\varphi/2} \end{pmatrix} e^{i\boldsymbol{k}_e\boldsymbol{r}} \propto \begin{pmatrix} e^{i\eta}e^{i\varphi} \\ 1 \end{pmatrix} e^{i\boldsymbol{k}_e\boldsymbol{r}}, \tag{2.29}$$

where Ψ_e^{+} are right-going waves, while Ψ_e^{-} are left-going waves. Similarly, for $\varepsilon_k^{-} = -\sqrt{E_k^2 - \Delta^2} = -i\Delta\sin\eta$, we get the wave-functions describing holelike quasiparticles:

$$\Psi_h(\boldsymbol{r}) = \begin{pmatrix} v_0 e^{i\varphi/2} \\ u_0 e^{-i\varphi/2} \end{pmatrix} e^{i\boldsymbol{k}_h\boldsymbol{r}} \propto \begin{pmatrix} e^{-i\eta}e^{i\varphi} \\ 1 \end{pmatrix} e^{i\boldsymbol{k}_h\boldsymbol{r}}, \tag{2.30}$$

where Ψ_h^{+} are left-going waves, while Ψ_h^{-} are right-going waves. When spin is taken into account the wave functions are modified to

$$\Psi_{e,\uparrow} \propto \begin{pmatrix} e^{i\eta}e^{i\varphi} \\ 0 \\ 0 \\ 1 \end{pmatrix} e^{i\boldsymbol{k}_{e,\uparrow}\boldsymbol{r}}, \quad \Psi_{e,\downarrow} \propto \begin{pmatrix} 0 \\ e^{i\eta}e^{i\varphi} \\ -1 \\ 0 \end{pmatrix} e^{i\boldsymbol{k}_{e,\downarrow}\boldsymbol{r}}, \quad \Psi_{h,\uparrow} \propto \begin{pmatrix} e^{-i\eta}e^{i\varphi} \\ 0 \\ 0 \\ 1 \end{pmatrix} e^{i\boldsymbol{k}_{h,\uparrow}\boldsymbol{r}}, \quad \Psi_{h,\downarrow} \propto \begin{pmatrix} 0 \\ e^{-i\eta}e^{i\varphi} \\ -1 \\ 0 \end{pmatrix} e^{i\boldsymbol{k}_{e,\downarrow}\boldsymbol{r}}. \tag{2.31}$$

2.5 Andreev reflection

Andreev reflection is the underlying mechanism in the superconducting proximity effect which was mentioned in the introduction 1. It describes supercurrent transport in hybrid structures consisting of a normal metal and a superconductor [2]. The complete model was described by Blonder, Tinkham and Klapwijk in 1982 and is now known as the BTK-theory [48].

When an electron with momentum, $\boldsymbol{k}^{+} = k_x^{+}\hat{x} + k_y^{+}\hat{y} + k_z^{+}\hat{z}$, and spin, σ, in the normal metal is propagating towards the superconducting interface, it will be scattered with certain probabilities of transmission and reflection. We choose the coordinate system such that the intersection is placed in the yz-plane, see figure 2.1. There are two possible ways the electron could be transmitted and reflected. The electron may be transmitted into the superconductor as an electron-like quasiparticle, with momentum $\boldsymbol{q}^{+} = q_x^{+}\hat{x} + q_y^{+}\hat{y} + q_z^{+}\hat{z}$ and spin σ, or as a hole-like quasiparticle, with momentum $\boldsymbol{q}^{-} = -q_x^{-}\hat{x} + q_y^{-}\hat{y} + q_z^{-}\hat{z}$ and spin σ. The x-component has negative sign since the wave direction of a hole is opposite of the direction of its wave vector, as explained in section 2.2. The electron may be reflected, either in the normal way, i.e. as an electron with momentum $\boldsymbol{k}_r^{+} = -k_x^{+}\hat{x} + k_y^{+}\hat{y} + k_z^{+}\hat{z}$, and the same spin σ or by Andreev reflection [49]. In Andreev reflection

[2] The non-superconducting material can be replaced by other materials, such as ferromagnets which will be considered in this thesis

the incoming electron goes into the superconductor and form a Cooper pair with an electron of opposite spin, leaving a reflected hole with momentum $\boldsymbol{k}^- = k_x^-\hat{x} + k_y^-\hat{y} + k_z^-\hat{z}$ and spin $-\sigma$.

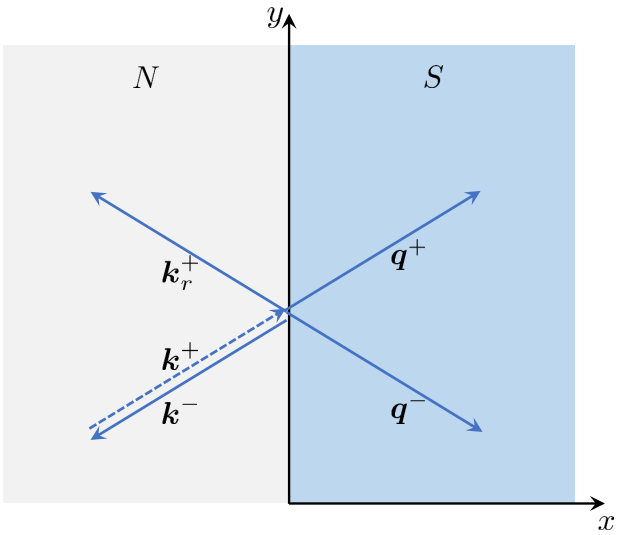

Figure 2.1: A normal metal is in contact with a superconductor. An electron of momentum $\boldsymbol{k}^+$ (dashed line) is either transmitted into the superconductor with momentum $\boldsymbol{q}^+$ (electron-like) or $\boldsymbol{q}^-$ (hole-like), or it is reflected back into the normal metal with momentum $\boldsymbol{k}_r^+$ (electron) or $\boldsymbol{k}^-$ (hole). The arrows indicate the direction of the group velocities (not necessarily the direction of the momentum vectors).

We will in this section ignore the spin degeneracy and use the wave functions from equation (2.29) and (2.30) with energies $E_{\boldsymbol{k}}$ (2.13) and corresponding wave numbers, $\boldsymbol{k}^\pm$ (2.14). The incoming, reflected and transmitted wave vectors will in this notation take the form

$$\begin{aligned}
\psi_i(\boldsymbol{r}) &= \begin{pmatrix} 1 \\ 0 \end{pmatrix} e^{i\boldsymbol{k}^+\boldsymbol{r}} \\
\psi_r(\boldsymbol{r}) &= r_{ee}\begin{pmatrix} 1 \\ 0 \end{pmatrix} e^{i\boldsymbol{k}_r^+\boldsymbol{r}} + r_{eh}\begin{pmatrix} 0 \\ 1 \end{pmatrix} e^{i\boldsymbol{k}^-\boldsymbol{r}} \\
\psi_t(\boldsymbol{r}) &= t_{ee}\begin{pmatrix} u_0 e^{i\varphi/2} \\ v_0 e^{-i\varphi/2} \end{pmatrix} e^{i\boldsymbol{q}^+\boldsymbol{r}} + t_{eh}\begin{pmatrix} v_0 e^{i\varphi/2} \\ u_0 e^{-i\varphi/2} \end{pmatrix} e^{i\boldsymbol{q}^-\boldsymbol{r}},
\end{aligned} \tag{2.32}$$

where r_{ee}, r_{eh}, t_{ee}, and t_{eh} represent the probabilities of normal reflection, Andreev reflection, electron-like transmission and hole-like transmission, respectively. The Andreev reflection is retro reflective [50, 51] and the hole will move along the same path as the incoming electron as illustrated in figure 2.1. In the opposite situation in which an incoming hole is Andreev reflected into an electron, a Cooper pair is "dragged" from the superconductor and into the normal metal. This illustrates how the Andreev reflection is the mechanism behind the proximity effect.

In equation (2.13) we found that only energies above the energy gap, Δ, are allowed for the quasiparticles. Consequently, when $E_{\boldsymbol{k}} < \Delta$, the amplitudes t_{ee} and t_{eh} will be zero and only reflection (either normal or Andreev reflection) is allowed. If there is no barrier at the interface, there will be no normal reflection, r_{ee}, and only Andreev reflection, r_{eh}, will be allowed. States with such energies in SNS junctions would thus be trapped in the normal metal by the Andreev reflections and are referred to as Andreev bound states (ABS).

2.6 Josephson current

A Josephson junction is a device consisting of two superconductors that is brought into contact via a *weak link*, in which the *critical current* is much lower than in the bulk superconductor. In the SNS junction the normal metal plays the role as the weak link. The critical current is the maximum supercurrent that can exist in the structure and is related to the density of Cooper pairs. The proximity effect allows for leakage of Cooper pairs into the normal metal, but the density of Cooper pairs will be much lower than in the bulk superconductor, and consequently so will the critical current. Brian D. Josephson predicted in 1962 that supercurrents would flow through the junction even without any applied voltage [52]. Instead, the current was driven by a difference in the superconducting phase, φ, between the two superconductors. We will in this section derive the Josephson current and how it is related to the free energy of the system.

The number operator, N, of the Cooper pairs in the superconductor, and the superconducting phase φ are canonical conjugate variables [53]:

$$\hbar\dot{N} = -\frac{\partial H}{\partial \varphi} \qquad \hbar\dot{\varphi} = \frac{\partial H}{\partial N}. \tag{2.33}$$

The tunneling current through a weak link from a superconductor, S_L, with number of Cooper pairs, N_L, to a superconductor, S_R, of N_R Cooper pairs will be given as

$$I = q\dot{N}_L = -q\dot{N}_R, \tag{2.34}$$

where $q = -2e$ is the charge of a Cooper pair. Combining equation (2.33) and (2.34) yields

$$I = \frac{2e}{\hbar}\frac{\partial H}{\partial \varphi_L} = -\frac{2e}{\hbar}\frac{\partial H}{\partial \varphi_R}. \tag{2.35}$$

We define the phase difference $\Delta\varphi = \varphi_L - \varphi_R$, and as only this quantity, not the individual phases, has physical meaning, we let $\partial\varphi_L \to \partial\Delta\varphi$ and $\partial\varphi_R \to -\partial\Delta\varphi$. Hence

$$I = \frac{2e}{\hbar}\frac{\partial H}{\partial(\Delta\varphi)}. \tag{2.36}$$

Taking the expectation value of this gives the Josephson current in terms of the free energy, F:

$$\langle I\rangle = \frac{2e}{\hbar}\frac{\partial F}{\partial(\Delta\varphi)}, \tag{2.37}$$

since we have

$$\frac{\partial F}{\partial(\Delta\varphi)} = -\frac{1}{\beta}\frac{1}{Z}\frac{\partial Z}{\partial(\Delta\varphi)} = -\frac{1}{\beta Z}\mathrm{Tr}\left[-\beta\frac{\partial H}{\partial(\Delta\varphi)}e^{-\beta H}\right] = \frac{1}{Z}\mathrm{Tr}\left[\frac{\partial H}{\partial(\Delta\varphi)}e^{-\beta H}\right] = \left\langle\frac{\partial H}{\partial(\Delta\varphi)}\right\rangle \tag{2.38}$$

with Z as the partition function:

$$Z = e^{-\beta F} = \mathrm{Tr}\left[e^{-\beta H}\right] \tag{2.39}$$

and $\beta = 1/k_B T$. As we find the derivative of the phase difference, $\Delta\varphi$, in the expression for the Josephson current, we realize that the current is *phase*-driven. These predictions have been confirmed experimentally for a large number of systems [54–56].

2.7 Free energy

In order to relate the Josephson current to the energy levels, $E_{\boldsymbol{k}}$, we will here derive the free energy, F, in terms of the energy levels of the superconducting system. The diagonal Hamiltonian in equation (2.9) is on the form of a free fermion gas:

$$\begin{aligned} H &= E_0 + \sum_{\boldsymbol{k}}\begin{pmatrix}\gamma^\dagger_{\boldsymbol{k},\uparrow} & \gamma_{-\boldsymbol{k},\downarrow}\end{pmatrix}\begin{pmatrix}E_{\boldsymbol{k}} & 0\\ 0 & -E_{\boldsymbol{k}}\end{pmatrix}\begin{pmatrix}\gamma_{\boldsymbol{k},\uparrow}\\ \gamma^\dagger_{-\boldsymbol{k},\downarrow}\end{pmatrix} \\ &= E_0 + \sum_{\boldsymbol{k}}\left[E_{\boldsymbol{k}}\gamma^\dagger_{\boldsymbol{k},\uparrow}\gamma_{\boldsymbol{k},\uparrow} - E_{\boldsymbol{k}}\left(1-\gamma^\dagger_{-\boldsymbol{k},\downarrow}\gamma_{-\boldsymbol{k},\downarrow}\right)\right] \\ &= E_0 + \sum_{\boldsymbol{k}} E_{\boldsymbol{k}}\left(N_\uparrow + N_\downarrow - 1\right) \end{aligned} \tag{2.40}$$

where $N_\uparrow$ and $N_\downarrow$ denotes the number of single particles of respective spin up and down in each state $\boldsymbol{k}$. We find the partition function of the system using the Pauli exclusion principle of fermions such that $N_\uparrow$ and $N_\downarrow$ can take the values 0 or 1. Hence, the partition function is

$$\begin{aligned} Z &= \sum e^{-\beta H} = e^{-\beta E_0}\sum_{N_\uparrow,N_\downarrow} e^{-\beta\sum_k E_{\boldsymbol{k}}(N_\uparrow+N_\downarrow-1)} = e^{-\beta E_0}\prod_{\boldsymbol{k}} e^{\beta E_{\boldsymbol{k}}}\sum_{N_\uparrow} e^{-\beta E_{\boldsymbol{k}}N_\uparrow}\sum_{N_\downarrow} e^{-\beta E_{\boldsymbol{k}}N_\downarrow} \\ &= e^{-\beta E_0}\prod_{\boldsymbol{k}} e^{\beta E_{\boldsymbol{k}}}\left(1+e^{-\beta E_{\boldsymbol{k}}}\right)^2 = e^{-\beta E_0}\prod_{\boldsymbol{k}}\left(2\cosh\left(\frac{\beta E_{\boldsymbol{k}}}{2}\right)\right)^2. \end{aligned} \tag{2.41}$$

We can now easily use the relation between the partition function and the free energy to obtain the free energy in terms of the energy levels, $E_{\boldsymbol{k}}$:

$$F = -\frac{1}{\beta}\ln(Z) = E_0 - 2k_B T \sum_{\boldsymbol{k}} \ln\left[2\cosh\left(\frac{E_{\boldsymbol{k}}}{2k_B T}\right)\right]. \tag{2.42}$$

In chapter 3 and 5 we will find the energy levels of selected systems and by using this expression for the free energy along with the Josephson current (2.37), we are able to find the supercurrent in the systems.

2.8 High-T_c superconductors

As stated in the introduction, 1, the high-T_c superconductors have typically d-wave pair symmetry [57, 58], with a gap parameter, Δ, which is dependent on the momentum, $\boldsymbol{k}$, of the quasi-particles. This is different from the isotropic s-wave pairing in low-T_c superconductors. The gap-parameter in d-wave superconductors is given as

$$\Delta(\theta_{\boldsymbol{k}}) = \Delta_0 \cos\left[2(\theta_{\boldsymbol{k}} - \alpha)\right], \tag{2.43}$$

with the direction of the momentum given by $\theta_{\boldsymbol{k}}$ and α being the orientation of the d-wave superconductor. An important property with such gap parameter is that it will change sign when the momentum is rotated by 90 degrees. This has been confirmed experimentally by the observation of a phase shift π in the superconducting phase, which is equivalent to the sign change of the gap parameter [59]. A tunneling theory for the d-wave pairing, similar to the BTK theory [48], was presented by Tanaka and Kashiwaya [60] and allows us to find the reflection amplitudes in a similar fashion as in section 2.5 where s-wave pairing was assumed.

2.9 Zeeman energy

In magnetic materials, such as ferromagnets, the energy band is spin split when exposed to an external magnetic field and electrons with up and down spin will experience different potential. This is due to the interaction between the magnetic moments in the material and the external magnetic field, known as the Zeeman interaction. The Zeeman effect results in the microscopic energy, $-\sigma h = -\sigma\mu B$, with $\sigma = \pm 1$ and μ being the spin and the magnetic moment of the electron or hole and B being the external magnetic field strength.

2.10 Rashba effect

In two-dimensional condensed matter physics asymmetry of the potential perpendicular to the plane of motion and spin-orbit coupling may cause a momentum-dependent splitting of the spin bands. This is known as the Rashba effect and is modeled by the Bychkov-Rashba term [61]

$$H_R = \alpha(\boldsymbol{\sigma} \times \boldsymbol{k}) \cdot \hat{z} \tag{2.44}$$

where $\alpha_{e/h}$ depend on the material and may be different for electrons and holes. $\boldsymbol{\sigma} = \sigma_x \hat{x} + \sigma_y \hat{y} + \sigma_z \hat{z}$ is a vector of the Pauli matrices, $\boldsymbol{k}$ is the momentum of the electrons or holes and $\hat{z}$ is the unit vector perpendicular to the plane of motion.

Chapter 3

Andreev bound state energies in a weak magnetic field

The current through a Jospehson junction will mainly be carried by Andreev bound states [62], which are described in section 2.5. We will in this chapter find the Andreev bound state energies of a Josephson junction exposed to a weak external magnetic field, $\boldsymbol{B}$, and the energy levels will in the following chapter be used to find the current through the junction. We start by defining the system in section 3.1 and will then consider three different situations; (1) an ordinary SNS-junction of low-T_c superconductors with s-wave pairing, (2) an SNS-junction of high-T_c superconductors with d-wave pairing and (3) an SFS-junction with s-wave superconductors separated by a ferromagnet. We will in all three situations identify the Andreev reflection amplitudes which was introduced in section 2.5. The phase accumulated by the Andreev bound state when traveling across the junction and when being Andreev reflected at the superconducting interfaces will next be used in Bohr-Sommerfeld quantization condition [45] and from this condition the energy levels are easily found.

3.1 Physical system

The two-dimensional SNS junction of consideration is of length L and width W and is placed in the xy-plane, with the interfaces parallel to the y-axis at $x = -L/2$ and $x = L/2$, see figure 3.1. We allow the gap parameter to have different phases, φ_L and φ_R, in the left and right superconductor, respectively, such that the superconducting phase difference between the two superconductors is $\Delta\varphi = \varphi_L - \varphi_R$. Necessarily, the gap parameter is zero in the normal metal and the overall gap parameter is

$$\Delta(x) = \Delta\left(e^{i\phi_L}\Theta(-x - L/2) + e^{i\phi_R}\Theta(x - L/2)\right), \tag{3.1}$$

where $\Theta(x)$ is the Heaviside step function.

We allow for different chemical potential, μ_N and μ_S, and effective mass, m_N and m_S, in the normal and superconducting region and we let the superconducting interfaces be completely transparent. The Hamiltonian of a normal electron excitation is given as

$$h_N(x,y) = \frac{1}{2m}\left(-i\hbar\nabla - q\boldsymbol{A}(x,y)\right)^2 - \mu_N \tag{3.2}$$

in the normal metal (N) where $\boldsymbol{A}$ is the vector potential allowing for an external magnetic field $\boldsymbol{B} = \nabla \times \boldsymbol{A}$. We will assume the magnetic field to be completely screened from the superconductors and will in these regions let the vector potential be zero. The Hamiltonian in the superconducting region is thus given as

$$h_S(x,y) = -\frac{\hbar^2}{2m}\nabla^2 - \mu_S. \tag{3.3}$$

In section 3.4 the normal metal in the SNS junction will be substituted by a ferromagnet and we will get an extra contribution from the Zeeman energy, h, as discussed in section 2.9. The single particle Hamiltonian will thus be given as

$$h_F(x,y) = \frac{1}{2m}\left(-i\hbar\nabla - q\boldsymbol{A}(x,y)\right)^2 - \sigma h - \mu_F. \tag{3.4}$$

The spin-orbit Rashba splitting discussed in section 2.10 will also give a contribution to the Hamiltonian, as given in equation (2.44).

For the analytical calculations we will consider the semiclassical limit $k_F L \gg 1$, in which the Andreev bound states can be associated with classical trajectories. Due to the Lorentz force the trajectories will be arcs of cyclotron radius $l_{\text{cycl}} = \hbar k_F / eB$. We will start by considering a weak magnetic field strength, B, so that $l_{\text{cycl}}/L \gg 1$ and we can neglect the curvature of the trajectories, as illustrated in figure 3.1. These trajectories can be thought of as single-mode waveguides connecting the two superconductors. The Fermi surface is assumed to be circular with isotropic dependency on the wave vector $\boldsymbol{k} = (k_x, k_y) = (k_F\cos\theta, k_F\sin\theta)$ and we work in the short-junction regime $L \ll \xi$, with $\xi = \hbar v_f/\Delta$ being the superconducting coherence length induced by the proximity effect [37].

We will in this and in the following chapter look at three different situations. First, in section 3.2, we consider an SNS-junction with s-wave superconductors in which the gap parameter, Δ, is position- and angle independent. Next, in section 3.3, the gap parameter is angle-dependent as we let the superconductors be high-temperature superconductors with d-wave pairing, as described in section 2.8. We will then go back to the s-wave pairing, but substitute the normal metal in the junction with a ferromagnet (SFS) and allow for Zeeman splitting and spin-orbit coupling. In all cases the ABS energies will be identified and then, in chapter 4, be used to find the Josephson current density and total current in the junction. There has been research on junctions exposed to a uniform external magnetic field, both for one-dimensional and two-dimensional systems [29–37, 39]. High

temperature junctions exposed to magnetic field has also been investigated [63], but to the extend of our knowledge there has been far less theoretical research on how the current density pattern is affected by the d-wave pairing when exposed to an external magnetic field. Zeeman splitting and spin orbit coupling has shown to give an anisotropic dependence of the total current on the direction of the magnetic field [64], but the effect from these spin sensitive properties on the current density pattern has been unexplored, as far as we know.

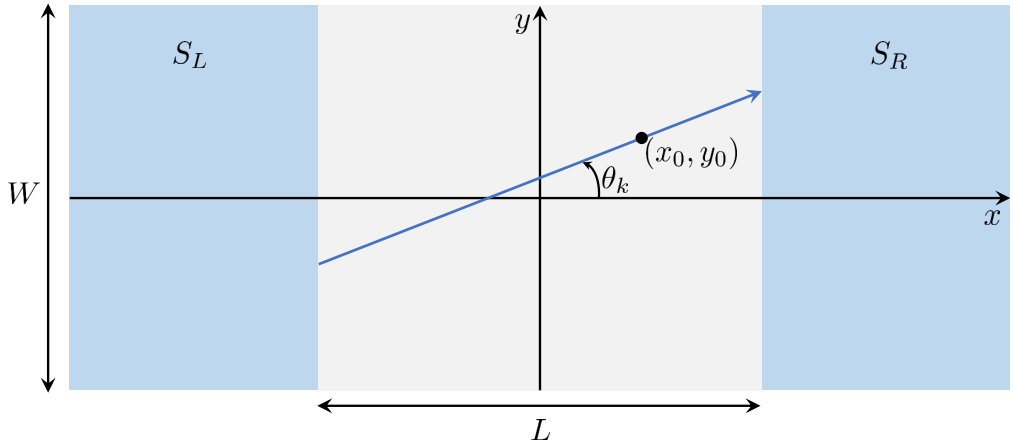

Figure 3.1: A Josephson junction formed by two superconductors of phase difference $\Delta\varphi$ connected by a normal metal (or ferromagnet) of length L and width W. An electron trajectory used for semi-classical calculations of the supercurrent density at (x_0, y_0) in the weak field is indicated.

3.2 Low-T_c SNS junction in weak magnetic field

We will first consider an SNS junction with s-wave pairing in the superconductors [1]. These are typically low-T_c superconductors with isotropic gap parameter, Δ. We use the same material in both superconductors so that the magnitude of Δ is equal in left and right superconductor, but we allow for different phases. In section 3.2.1 the theory from section 2.5 will be used to find the phase shift accumulated over a penetration depth in the superconductor when an electron or a hole is Andreev reflected at the superconducting interface. This will next be added to the phase accumulated when the electron or hole is traveling along the trajectory from figure 3.1. The total phase shift of the Andreev bound state is used in the Bohr-Sommerfeld quantization condition from which the energy levels are found.

[1] The derivation of this section has already been considered by A. Brøyn in a specialization project [39] and is meant to introduce the reader to the relevant approach and for comparison with later derivations and results.

3.2.1 Andreev reflection amplitude

The probability amplitudes from section 2.5 may be determined by using the boundary conditions at an interface between the normal metal and the superconductor, placed at $x = 0$. With transparent interfaces, the boundary conditions yield

$$\begin{aligned} \psi_i(0,y) + \psi_r(0,y) &= \psi_t(0,y) \\ \frac{\partial}{\partial x}\psi_i(0,y) + \frac{\partial}{\partial x}\psi_r(0,y) &= \frac{\partial}{\partial x}\psi_t(0,y), \end{aligned} \tag{3.5}$$

in which the wave functions, given in equation (2.32), will be inserted. In the Andreev approximation [49] we let $k_x^{\pm} \approx q_x^{\pm}$ and find the Andreev reflection amplitudes

$$r_{eh} = e^{-i\eta}e^{-i\varphi}, \qquad r_{ee} = 0 \tag{3.6}$$

where η is as defined in equation (2.16). Similarly, the amplitudes for an incoming hole which is Andreev reflected to an electron will be

$$r_{he} = \frac{v_0}{u_0}e^{i\varphi} = e^{-i\eta}e^{i\varphi}, \qquad r_{hh} = 0. \tag{3.7}$$

Hence, the Andreev reflection gives a phase shift of $-\eta \mp \varphi$, where we use the upper (lower) sign if the incoming particle is an electron (hole).

3.2.2 Bohr-Sommerfeld quantization

In the short junction regime, the continuous quasiparticle excitation spectrum ($E_{\boldsymbol{k}} > \Delta$) will not contribute to the Josephson current [62] and it is sufficient to restrict our selves to energies below the gap $E_{\boldsymbol{k}} < \Delta$. For such energies we have $\eta = \arccos(E_{\boldsymbol{k}}/\Delta)$, according to equation (2.16). The Bohr-Sommerfeld quantization condition require the total phase obtained by the state in a whole cycle to be a multiple of 2π [45]. An electron starting at the left interface traveling in the xy-plane towards the right interface along a trajectory at an angle θ (see figure 3.1) would gain a phase of $L(k_x^+ + k_y^+ \tan\theta)$, before it is Andreev reflected at the right interface with the amplitude r_{eh} and thus gaining a phase of $-\eta - \varphi_R$. The state would then continue as a hole traveling back along the same trajectory, accumulating a phase of $-L(k_x^- + k_y^- \tan\theta)$, and finally be Andreev reflected back to its original state. In appendix A it is shown that if a vector potential, $\boldsymbol{A}$, is present the gauge invariant phase gives rise to an extra phase shift, $-\frac{q}{\hbar}\int \boldsymbol{A}\cdot d\boldsymbol{r}$, as given in equation (A.6). In a magnetic field,

the total phase in the quantization condition is thus

$$\begin{aligned} 2\pi n = \oint d\phi &= \int_L^R \pm\boldsymbol{k}^{\pm}\cdot d\boldsymbol{l} \pm \frac{e}{\hbar}\int_L^R \boldsymbol{A}\cdot d\boldsymbol{l} + \phi^R_{(eh)(he)} + \int_R^L \pm\boldsymbol{k}^{\mp}\cdot d\boldsymbol{l} \mp \frac{e}{\hbar}\int_R^L \boldsymbol{A}\cdot d\boldsymbol{l} + \phi^L_{(he)(eh)} \\ &= L(k_x^+ - k_x^-) + L\tan\theta(k_y^+ - k_y^-) - 2\eta \pm \left(\Delta\varphi + \frac{2e}{\hbar}\int_L^R \boldsymbol{A}\cdot d\boldsymbol{l}\right), \end{aligned} \tag{3.8}$$

where $\phi^{R/L}_{(eh)(he)} = -\eta \mp \varphi_{R/L}$ is the phase from Andreev reflection of an electron (hole) of charge $\mp e$. The upper sign indicate that the state starts out as a right-going electron, while the lower sign indicate that it starts as a right-going hole. Again we use the Andreev approximation and let $k_x^+ \approx k_x^-$ and $k_y^+ \approx k_y^-$, such that the two first terms vanish and the quantization condition is simply

$$2\pi n = -2\eta \pm \left(\Delta\varphi - \gamma\right), \tag{3.9}$$

where

$$\gamma = -\frac{2e}{\hbar}\int_L^R \boldsymbol{A}\cdot d\boldsymbol{l} \tag{3.10}$$

is the Aharonov-Bohm phase shift [65].

3.2.3 ABS energy

The energy levels are found by inserting for η (2.16) in equation (3.9) and solving for $E_{\boldsymbol{k}}$:

$$E_{\boldsymbol{k}} = \Delta\cos\eta = \pm\Delta\cos\left(\frac{\Delta\varphi}{2} - \frac{\gamma}{2}\right). \tag{3.11}$$

This is the well known Andreev levels in an SNS Josephson junction [66] with an extra phase shift, γ, in the superconducting phase, resulting from the external magnetic field. As the Aharonov-Bohm phase shift appear in the energies in the same manner as the superconducting phase, it is expected to have the same driving force of the Josephson current as the superconducting phase. In the absense of magnetic field, the minimum energies are found at $\Delta\varphi = 0$ and the junction is an ordinary 0-junction.

3.3 High-T_c SNS junction in weak magnetic field

We now replace the low-T_c superconductors in the junction by high-T_c superconductors with d-wave pairing as described in section 2.8. The superconducting gap will in this case be angle dependent,

$$\Delta(\theta) = \Delta_0\cos\left[2(\theta_\pm - \alpha)\right], \tag{3.12}$$

where $\theta_\pm$ is the angle between the momentum of the incoming electron (hole) and the surface normal. α is the orientation of the gap parameter and we allow for different orientations in the left

(α_L) and right (α_R) superconductor. The situation is illustrated in figure 3.2. We introduce the new variable $\beta(\theta)$ which can take the values 0 or π depending on the sign of $\Delta(\theta)$:

$$e^{i\beta} = \frac{\Delta(\theta)}{|\Delta(\theta)|}. \tag{3.13}$$

In figure 3.2 the sign of the gap parameter is indicated for the orientations α_L and α_R. With η defined in a similar manner as for the s-wave pairing,

$$\eta = \arccos \frac{E_{\boldsymbol{k}}}{|\Delta(\theta)|}, \tag{3.14}$$

the new variable, β, takes care of the sign of Δ and will appear along with the superconducting phase, φ.

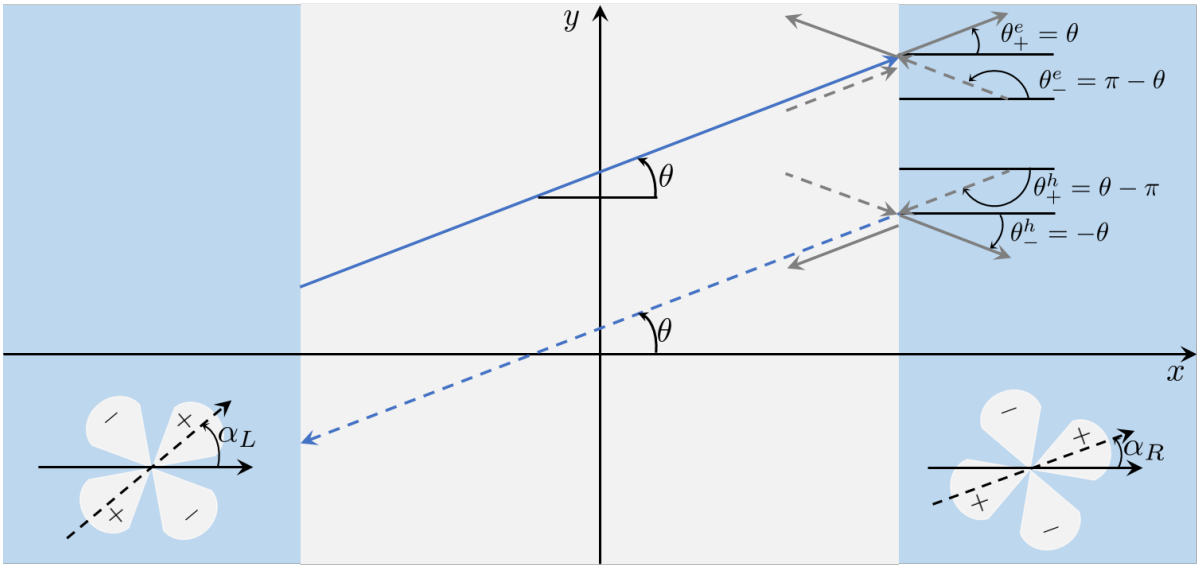

Figure 3.2: A d-wave superconductor junction with orientation α_L and α_R in left and right superconductor. An electron (hole) traveling to the right along a semiclassical trajectory at an angle θ above the surface normal has momentum illustrated by a blue, solid (dashed) line. The transmitted quasi-electron (quasi-hole) has momentum with an angle $\theta^{e/h}_+$ above the surface normal, while the transmitted quasi-hole (quasi-electron) has momentum with an angle $\theta^{e/h}_-$.

3.3.1 Andreev reflection amplitude

The Andreev reflection amplitude is found in the same manner as in section 3.2.1. However, we must be careful in the calculations as the momentum of an incoming hole is opposite of the group velocity. When an incoming electron traveling along the trajectory with angle θ is transmitted into

the superconductor, the electronlike quasiparticle will experience a gap parameter $\Delta(\theta_+^e) = \Delta(\theta)$ where $\Delta(\theta)$ is given in equation (3.12). The holelike quasiparticle, however, will experience a gap parameter $\Delta(\theta_-^e) = \Delta(\pi-\theta)$. If the incoming particle is a hole, the transmitted electronlike quasiparticle will experience a gap parameter $\Delta(\theta_-^h) = \Delta(-\theta)$, while the transmitted holelike quasiparticle will experience the gap parameter $\Delta(\theta_+^h) = \Delta(\theta-\pi)$. Both cases are illustrated in figure 3.2. The expression of the d-wave superconducting gap, (3.12), makes it is clear that

$$\begin{aligned}\Delta(\theta_+^e) &= \Delta(\theta_+^h) = \Delta(\theta),\\ \Delta(\theta_-^e) &= \Delta(\theta_-^h) = \Delta(-\theta),\end{aligned} \tag{3.15}$$

and we define

$$\eta_\pm \equiv \arccos\left(\frac{E}{|\Delta(\pm\theta)|}\right), \qquad e^{i\beta_\pm} \equiv \frac{\Delta(\pm\theta)}{|\Delta(\pm\theta)|}, \tag{3.16}$$

which is valid for both holes and electrons. We consider an NS interface placed at $x = 0$ like we did in section 2.5 with incoming, reflected and transmitted wave functions given as

$$\begin{aligned}\psi_{i,e} &= \begin{pmatrix}1\\0\end{pmatrix} e^{ik_x x}, \qquad \psi_{i,h} = \begin{pmatrix}0\\1\end{pmatrix} e^{-ik_x x}\\ \psi_r &= r_e \begin{pmatrix}1\\0\end{pmatrix} e^{-ik_x x} + r_h \begin{pmatrix}0\\1\end{pmatrix} e^{ik_x x}\\ \psi_t &= \tilde{t}_e \begin{pmatrix}e^{i\beta_\pm} e^{i\varphi} e^{\eta_\pm}\\ 1\end{pmatrix} e^{ik_x x} + \tilde{t}_h \begin{pmatrix}e^{i\beta_\mp} e^{i\varphi} e^{\eta_\mp}\\ 1\end{pmatrix} e^{-ik_x x}.\end{aligned} \tag{3.17}$$

We choose the upper (lower) sign of the index in β and η if the incoming particle is $\psi_{i,e}$ ($\psi_{i,h}$). We have taken $k_x = \sqrt{k_F^2 - k_y^2}$ in the Andreev approximation and absorbed some factors in the transmission amplitudes $\tilde{t}_e$ and $\tilde{t}_h$. The wave functions and their derivatives must be continuous at the interface which we assume to be transparent and we find the Andreev amplitudes:

$$\begin{aligned}r_{eh} &= e^{-i\varphi} e^{-i\eta_+} e^{-i\beta_+} \equiv e^{-i\varphi} e^{-i\eta} e^{-i\beta}\\ r_{he} &= e^{i\varphi} e^{-i\eta_+} e^{i\beta_+} \equiv e^{i\varphi} e^{-i\eta} e^{i\beta}\end{aligned} \tag{3.18}$$

where $r_{eh} = r_h$ when we let the incoming particle be the electron, $\psi_{i,e}$, and $r_{he} = r_e$ when we let the incoming particle be the hole, $\psi_{i,h}$.

3.3.2 Bohr-Sommerfeld quantization

The quantization condition is found in the same manner as in section 3.2.2. An electron (hole) traveling towards the right superconductor along a trajectory of an angle θ will be Andreev reflected into a hole (electron) and gain a phase shift $-\eta_R(\theta) \mp \beta_R(\theta) \mp \varphi_R$. The hole (electron) would then travel towards the left superconductor with a group velocity of an angle $\theta + \pi$ and be Andreev

reflected back to its original state, gaining a phase $-\eta_L(\theta+\pi)\pm\beta_L(\theta+\pi)\pm\varphi_L$. In the Andreev approximation the phase accumulated in the normal metal will be canceled, just like in the s-wave case, but a magnetic field will result in an extra phase shift, γ. This results in the quantization condition

$$2\pi n = -\left(\eta_R+\eta_L\right)\pm\left(\Delta\varphi+\Delta\beta-\gamma\right). \tag{3.19}$$

We have allowed for different orientations in left (L) and right (R) superconductor with

$$\eta_{L/R} = \arccos\left(\frac{E_{\boldsymbol{k}}}{|\Delta_0\cos(2(\theta-\alpha_{L/R}))|}\right) \tag{3.20}$$

and

$$\Delta\beta = \beta_L-\beta_R, \qquad e^{i\beta_{L/R}} = \frac{\Delta_0\cos(2(\theta-\alpha_{L/R}))}{|\Delta_0\cos(2(\theta-\alpha_{L/R}))|}. \tag{3.21}$$

3.3.3 ABS energy

Since, in general, $\eta_R\neq\eta_L$, the dispersion relation (3.19) gives a rather complicated expression for the ABS energies,

$$E_{\boldsymbol{k}} = \pm\frac{\Delta_0\left|\cos(2(\theta-\alpha_L))\cos(2(\theta-\alpha_R))\sin\left(\Delta\beta+\Delta\varphi-\gamma\right)\right|}{\sqrt{\cos(2(\theta-\alpha_L))^2+\cos(2(\theta-\alpha_R))^2-2|\cos(2(\theta-\alpha_L))\cos(2(\theta-\alpha_R))|\cos\left(\Delta\beta+\Delta\varphi-\gamma\right)}}, \tag{3.22}$$

and in order to get more insight we will in the following consider some special orientations, α_L and α_R.

$\underline{\alpha_L=\alpha_R=\alpha}$

When the left and right superconductor is oriented equally with $\alpha_L=\alpha_R\equiv\alpha$, equation (3.21) yields $\Delta\beta=0$ and we have $\eta_R=\eta_L$. Thus the ABS energies (3.22) simplify to

$$E_{\boldsymbol{k}} = \pm|\Delta_0\cos(2(\theta-\alpha))|\cos\left(\frac{\Delta\varphi}{2}-\frac{\gamma}{2}\right). \tag{3.23}$$

Comparing this to the s-wave energies (3.11) we notice that they have the same dependency of the superconducting phase difference, $\Delta\varphi$, and of the magnetic field, γ. In the absence of magnetic field the minimum energies are found when $\Delta\varphi=0$ and we have an ordinary 0-junction, like in the s-wave case. The d-wave energy levels are, however, different from the s-wave energies in the way that they are suppressed by the gap parameter at certain angles, θ, of the momentum. With $\theta=\alpha+n\pi/2$ and $n=0,\pm1$ we find the absolute values of the energies to be maximized and we expect states of such angles to give a large contribution to the current. The gap parameter will have nodes at $\theta=\alpha+(n/2+1/4)\pi$ and thus no ABS states of finite energies will have momentum of such

directions and contribute to the current.

$\underline{\alpha_L = \alpha,\ \alpha_R = \alpha - \pi/2}$

We will now rotate one of the superconductors by 90 degrees such that the orientation in left and right superconductor is given by $\alpha_L = \alpha$ and $\alpha_R = \alpha - \pi/2$. This will change the sign of the gap parameter in the right superconductor and from equation (3.21) we get the phase change $\Delta\beta = \pi$. On the other hand, the magnitude of the gap parameters will not change so we will still have the relation $\eta_L = \eta_R$. The Andreev levels will in this case be simplified to

$$E_{\boldsymbol{k}} = \pm|\Delta_0 \cos(2(\theta - \alpha))| \sin\left(\frac{\Delta\varphi}{2} - \frac{\gamma}{2}\right). \tag{3.24}$$

As the gap parameters will have the same magnitude as in the $\alpha_L = \alpha_R$ case we expect the same ABS state, to contribute to the current. The only difference now is that the π-shift will minimize the energy at $\Delta\varphi = \pi$ in the absence of magnetic field. The junction is thus a π-junction. This is an important property of d-wave junctions and has been used to prove the existence of d-wave pairing [59].

In the general case with arbitrary orientations α_L and α_R the value of $\Delta\varphi$ that minimizes the energies will depend on the angle θ of the respective state. And the junction will not be a pure 0-junction or π-junction.

$\underline{\Delta = \Delta_d + i\Delta_s}$

We have so far considered pure d-wave superconductors or pure s-wave superconductors. However, at low temperatures and where the d-wave gap is suppressed, a subdominant gap of s-wave pairing may appear near the surface if a weak secondary interaction is present [67–73]. The gap parameter is now given as the complex combination

$$\Delta = \Delta_0 \cos(2(\theta - \alpha)) + i\Delta_s = \sqrt{\Delta_0^2 \cos^2(2(\theta - \alpha)) + \Delta_s^2}\, e^{\pm i\beta} \tag{3.25}$$

where β is modified to

$$\beta = \arctan \frac{\Delta_s/\Delta_0}{\cos(2(\theta - \alpha))} + n\pi \tag{3.26}$$

and we choose n such that β is in the first or second quadrant for positive values of Δ_s. The energies will for arbitrary orientations, α_L and α_R, in left and right superconductor be

$$E_{\boldsymbol{k}} = \pm \frac{\Delta_0 \sqrt{c_L^2 + \frac{\Delta_s^2}{\Delta_0^2}} \sqrt{c_R^2 + \frac{\Delta_s^2}{\Delta_0^2}} \sin\left(\Delta\varphi + \Delta\beta - \gamma\right)}{\sqrt{c_L^2 + c_R^2 + 2\frac{\Delta_s^2}{\Delta_0^2} - 2\sqrt{c_L^2 + \frac{\Delta_s^2}{\Delta_0^2}} \sqrt{c_R^2 + \frac{\Delta_s^2}{\Delta_0^2}} \cos\left(\Delta\varphi + \Delta\beta - \gamma\right)}}. \tag{3.27}$$

where $c_{L/R}$ are defined as

$$c_{L/R} \equiv \cos\left(2(\theta - \alpha_{L/R})\right). \tag{3.28}$$

We will especially consider the cases with $\alpha_R = \alpha_L$ and $\alpha_R = \alpha_L \pm \pi/2$ in which the above expression can be simplified to

$$E_{\boldsymbol{k}} = \pm \sqrt{\Delta_0^2 \cos^2\left(2(\theta - \alpha)\right) + \Delta_s^2} \cos\left(\frac{\Delta\varphi}{2} - \frac{\gamma}{2} + \frac{\Delta\beta_n}{2}\right), \tag{3.29}$$

where

$$\Delta\beta_n = \begin{cases} 0 & \text{for } n \ \alpha_R = \alpha_L \\ 2\arctan\frac{\Delta_s/\Delta_0}{\cos(2(\theta-\alpha))} - \pi \mathrm{sgn}\left[\cos\left(2(\theta-\alpha)\right)\right] & \text{for } n \ \alpha_R = \alpha_L \pm \pi/2. \end{cases} \tag{3.30}$$

An important feature of these energies compared to the pure d-wave energies is that we now have a phase shift $\Delta\beta$ which is θ-dependent. We will in the next chapter see that this angle-dependency has an important effect on the current pattern in the junction when exposed to a magnetic field.

In section 3.2.2 we claimed that the continuum quasi-particle excitation spectrum would not contribute to the Josephson junction in a conventional s-wave junction in the short junction regime. In the d-wave junction the continuum states will contribute to a greater degree as the subgap states are suppressed. However, in this thesis we focus on the current carried by the ABS states ad will not consider the continuum state contribution.

3.4 Low-T_c SFS junction in weak magnetic field

We will now again consider s-wave superconductors in the junction. However, the normal metal is replaced with a ferromagnet. It is reasonable to neglect the Zeeman-effect for the SNS junction considered here as the effect from the vector potential will be much more dominant. However, if one replace the normal metal in the SNS junction with a ferromagnet (SFS), the Zeeman-effect will be much more prominent, and we will study how this, as well as the spin-orbit coupling, affects the current in the junction. We will first consider each effect individually, starting with the Zeeman effect. The magnetic field will, like for the situations already considered, be weak such that the electrons and holes are following the semi-classical path from section 3.1. The strategy here is

similar to the one used in the SNS case. The Bohr-Sommerfeld quantization condition is used to find the energy levels. We do this by first identifying the Hamiltonian in the ferromagnet and from this we find the wave vectors and wave functions. The ferromagnetic wave functions can then be used in the matching conditions together with the superconducting wavefunctions (2.31) to find the Andreev reflection amplitudes. The phase of these amplitudes, and from the propagation in the ferromagnet, will finally be used in the Bohr-Sommerfeld quantization condition in a similar manner as for the SNS junction.

3.4.1 Zeeman splitting

Hamiltonian

The effective Zeeman energy for a state $\boldsymbol{k}$ will be $-\sigma h$ where $\sigma = \pm 1$ indicates the spin of the particle and h is a measure of the exchange interaction. In second quantization the Hamiltonian is

$$H - \mu N = \sum_{\sigma \boldsymbol{k}} (\varepsilon_{\boldsymbol{k}} - \sigma h) c^{\dagger}_{\boldsymbol{k},\sigma} c_{\boldsymbol{k},\sigma} \tag{3.31}$$

where $\varepsilon_{\boldsymbol{k}} = \hbar^2 k^2 / 2m - \mu$. Using the commutation relations for the creation and annihiliation operators this can be rewritten to

$$H - \mu N = E_0 + \frac{1}{2} \sum_{\boldsymbol{k}} \psi^{\dagger}_{\boldsymbol{k}} H_{\boldsymbol{k}} \psi_{\boldsymbol{k}} \tag{3.32}$$

where

$$H_{\boldsymbol{k}} = \begin{pmatrix} \varepsilon_{\boldsymbol{k}} - h & 0 & 0 & 0 \\ 0 & \varepsilon_{\boldsymbol{k}} + h & 0 & 0 \\ 0 & 0 & -\varepsilon_{\boldsymbol{k}} + h & 0 \\ 0 & 0 & 0 & -\varepsilon_{\boldsymbol{k}} - h \end{pmatrix}, \qquad \psi_{\boldsymbol{k}} = \begin{pmatrix} c_{\boldsymbol{k},\uparrow} \\ c_{\boldsymbol{k},\downarrow} \\ c^{\dagger}_{-\boldsymbol{k},\uparrow} \\ c^{\dagger}_{-\boldsymbol{k},\downarrow} \end{pmatrix} \tag{3.33}$$

and $E_0 = \sum_{\boldsymbol{k}} \varepsilon_{\boldsymbol{k}}$ is the ground energy. The elements of $\psi^{\dagger}_{\boldsymbol{k}}$ represent creation of electrons and holes with spin up and down, respectively.

Wave functions

$H_{\boldsymbol{k}}$ is already on a diagonal form and we see immediately that the excitation energies of the single-particles are

$$E^{e/h}_{\boldsymbol{k}\sigma} = \pm(\varepsilon_{\boldsymbol{k}} - \sigma h) \tag{3.34}$$

where the upper (lower) sign indicate that the particle is an electron (hole) and $\sigma = \pm 1$ is the spin of the particle. The corresponding wave functions are

$$\psi^e_{\boldsymbol{k},\uparrow} = \begin{pmatrix}1\\0\\0\\0\end{pmatrix} e^{i\boldsymbol{k}_{e,\uparrow}}, \qquad \psi^e_{\boldsymbol{k},\downarrow} = \begin{pmatrix}0\\1\\0\\0\end{pmatrix} e^{i\boldsymbol{k}_{e,\downarrow}}, \qquad \psi^h_{\boldsymbol{k},\uparrow} = \begin{pmatrix}0\\0\\1\\0\end{pmatrix} e^{i\boldsymbol{k}_{h,\uparrow}}, \qquad \psi^h_{\boldsymbol{k},\downarrow} = \begin{pmatrix}0\\0\\0\\1\end{pmatrix} e^{i\boldsymbol{k}_{h,\downarrow}}. \tag{3.35}$$

The wave vectors $\boldsymbol{k}_{e/h,\sigma}$ are found from the excitation energy (3.34):

$$\begin{aligned} k_{e/h,\sigma} &= k_F \sqrt{1 + \sigma\frac{h}{\mu} \pm \frac{E^{e/h}_{\boldsymbol{k}\sigma}}{\mu}} \\ &\approx k_F\left(1 + \sigma\frac{1}{2}\frac{h}{\mu}\right), \end{aligned} \tag{3.36}$$

where we in the last equality have taken $E^{e/h}_{\boldsymbol{k}\sigma}/\mu$ to zero in the Andreev approximation [49] and assumed $h/\mu \ll 1$ and expanded the square root.

An electron with spin up and wave vector $k_{e\uparrow}$, travelling along a trajectory with an angle $\theta_\uparrow$ above the surface normal will, with a probability amplitude $r^{\uparrow\downarrow}_{eh}$, be Andreev reflected into a hole with spin down and wave vector $k_{h\downarrow}$ once it reaches the superconducting interface. Next, the hole will travel back along a trajectory at $\theta_\downarrow$ above the surface normal. The incoming electron will, with a probability amplitude $t_{ee/eh}$, be transmitted as a quasiparticle into the superconductor with wave vector $q_{e\uparrow/h\downarrow}$. The y-component of the wave vector must be conserved as our system is invariant in the y-direction. The y-components of wave vectors of the incoming electron, the outgoing hole and the transmitted quasiparticle are

$$\begin{aligned} k_{e\uparrow,y} &= k_F\left(1 + \frac{1}{2}\frac{h}{\mu}\right)\sin\theta_\uparrow \\ k_{h\downarrow,y} &= k_F\left(1 - \frac{1}{2}\frac{h}{\mu}\right)\sin\theta_\downarrow \\ q_{e,y} &= q_{h,y} = k_F \sin\theta_S. \end{aligned} \tag{3.37}$$

Letting these expressions be equal to each other we find

$$\begin{aligned} \sin\theta_\downarrow &= \frac{1+\frac{1}{2}\frac{h}{\mu}}{1-\frac{1}{2}\frac{h}{\mu}}\sin\theta_\uparrow \approx \left(1+\frac{1}{2}\frac{h}{\mu}\right)^2\sin\theta_\uparrow \approx \left(1+\frac{h}{\mu}\right)\sin\theta_\uparrow \\ \sin\theta_S &= \left(1+\frac{1}{2}\frac{h}{\mu}\right)\sin\theta_\uparrow \end{aligned} \tag{3.38}$$

where we have kept h/μ to first order. We will in the following use the same approach as in the previous section, that is letting a bound state travel along a semiclassical trajectory through the point (x_0, y_0). This approach makes us able to find the current density, not just the total current. However, from the above equation it is clear that the incoming electron and reflected hole are not traveling along the same trajectory as $\theta_\uparrow \neq \theta_\downarrow$, and in general the desired approach is not applicable. However, we may restrict the angle θ to be small and keep h/μ and θ to first order, but take the product $\theta h/\mu$ to zero. Hence, from the above expressions we get $\theta_\uparrow = \theta_\downarrow = \theta_S \equiv \theta$ and one bound state can be associated to one trajectory.

Andreev reflection amplitude

The Andreev reflection amplitude may be found in the same manner as in section 3.2, but with modified wave vectors:

$$\begin{aligned} k_{\uparrow,x} &= k_F\left(1+\frac{1}{2}\frac{h}{\mu}\right)\cos\theta \\ k_{\downarrow,x} &= k_F\left(1-\frac{1}{2}\frac{h}{\mu}\right)\cos\theta \\ q_x &= k_F\cos\theta. \end{aligned} \tag{3.39}$$

We use these wave vectors in the ferromagnetic and superconducting wave functions (3.35), (2.31), and insert the wave functions in the matching condition with both continuous wave functions and derivatives. By solving the system and only keeping h/μ to first order one finds the amplitudes to be

$$\begin{aligned} r_{eh}^{\uparrow\downarrow} = r_{eh}^{\downarrow\uparrow} = e^{-i\varphi}e^{-i\eta} \\ r_{he}^{\uparrow\downarrow} = r_{he}^{\downarrow\uparrow} = e^{-i\varphi}e^{i\eta}. \end{aligned} \tag{3.40}$$

These are identical with the amplitudes found in the SNS junction from section 3.2. Thus the Andreev reflection amplitudes are unaffected by a weak Zeeman effect.

Bohr-Sommerfeld quantiztion

We are now ready to use the quantization condition to find the Andreev bound states. Since the probability amplitudes remain the same after adding the Zeeman term we only need to modify the terms involving the wave vectors:

$$\begin{aligned} 2\pi n &= L\left(k_{\sigma,x}-k_{-\sigma,x}\right)+L\tan\theta\left(k_{\sigma,y}-k_{-\sigma,y}\right)-2\eta\pm(\Delta\varphi-\gamma) \\ &= \sigma k_F L\frac{h}{\mu}\cos\theta-2\eta\pm(\Delta\varphi-\gamma). \end{aligned} \tag{3.41}$$

We have in this kept terms of $\frac{h}{\mu}\cos\theta$ and let terms of $\frac{h}{\mu}\tan\theta$ go to zero as h/μ and θ are small.

ABS energies

The Andreev bound state energies can now be found from the quantization condition:

$$E_{\boldsymbol{k}} = \pm\Delta\cos\left(\frac{\Delta\varphi}{2} - \frac{\gamma}{2} + \sigma\frac{k_F L h}{2\mu}\cos\theta\right). \tag{3.42}$$

With $h = 0$ the two spin-degenerate energy levels (3.11) in the SNS-junction are re-obtained. However, with $h > 0$ each energy level is split into two spin-dependent levels and we will in this have four energy bands transferring the Josephson current. We notice that the new phase shift is θ-dependent and expect the spin effect to influence the current pattern in a fashion different from a phase shift in $\Delta\varphi$.

3.4.2 Spin orbit coupling

In this section we will include the energy contribution from the spin-orbit coupling as explained in section 2.10.

Hamiltonian

The spin-orbit coupling is modeled by the Bychkov-Rashba term (2.44) and in the second quantization formalism the Hamiltonian takes the form

$$H - \mu N = \sum_{\sigma\boldsymbol{k}}(\varepsilon_{\boldsymbol{k}} - \sigma h)c^\dagger_{\boldsymbol{k},\sigma}c_{\boldsymbol{k},\sigma} + \alpha\sum_{\boldsymbol{k}\alpha\beta} c^\dagger_{\mathbf{k},\alpha}\left[(\boldsymbol{\sigma}\times\boldsymbol{k})\cdot\hat{z}\right]_{\alpha\beta}c_{\mathbf{k},\beta}, \tag{3.43}$$

where α depend on the material. $\boldsymbol{\sigma} = \sigma_x\hat{x} + \sigma_y\hat{y} + \sigma_z\hat{z}$ is a vector of the Pauli matrices and the indices α and β represent the spin and are summed over up- and down-spins. We have kept the Zeeman field h finite, but will in later steps take this to zero in order to only consider the spin-orbit effect. By using the commutation relations for fermionic operators and rewriting the sums in equation (3.43) the Hamiltonian can be rewritten to

$$H - \mu N = E_0 + \frac{1}{2}\sum_{\boldsymbol{k}}\psi^\dagger_{\boldsymbol{k}}H_{\boldsymbol{k}}\psi_{\boldsymbol{k}} \tag{3.44}$$

where we have defined

$$E_0 = \sum_{\boldsymbol{k}}\varepsilon_{\boldsymbol{k}}, \qquad H_{\boldsymbol{k}} = \begin{pmatrix} \varepsilon_{\boldsymbol{k}} - h & is\alpha k e^{-is\theta} & 0 & 0 \\ -is\alpha k e^{is\theta} & \varepsilon_{\boldsymbol{k}} + h & 0 & 0 \\ 0 & 0 & -\varepsilon_{\boldsymbol{k}} + h & -is\alpha k e^{is\theta} \\ 0 & 0 & is\alpha k e^{-is\theta} & -\varepsilon_{\boldsymbol{k}} - h \end{pmatrix}, \qquad \psi_{\boldsymbol{k}} = \begin{pmatrix} c_{\boldsymbol{k},\uparrow} \\ c_{\boldsymbol{k},\downarrow} \\ c^\dagger_{-\boldsymbol{k},\uparrow} \\ c^\dagger_{-\boldsymbol{k},\downarrow} \end{pmatrix}. \tag{3.45}$$

θ is here the angle of the trajectory as indicated in figure 3.1 and $s = \pm 1$ indicate the direction of the x-component of the wave vector.

Wave functions

The problem can be expressed in the single-particle spectrum by diagonalizing $H_{\boldsymbol{k}}$ and introducing quasi-particle wave functions, $\psi^{e/h}_{\boldsymbol{k},\tilde{\sigma}}$, of pseudo-spin $\tilde{\sigma}$. The diagonalization is equivalent to the eigenvalue problem

$$H_{\boldsymbol{k}}\psi^{e/h}_{\boldsymbol{k},\tilde{\sigma}}(\boldsymbol{r}) = E^{e/h}_{\boldsymbol{k},\tilde{\sigma}}\psi^{e/h}_{\boldsymbol{k},\tilde{\sigma}}(\boldsymbol{r}). \tag{3.46}$$

from which one finds the quasiparticle excitation energies

$$E^{e/h}_{\boldsymbol{k},\tilde{\sigma}} = \pm\left(\varepsilon_{\boldsymbol{k}} - \tilde{\sigma}\sqrt{h^2 + \alpha^2 k^2}\right) \tag{3.47}$$

where the upper (lower) sign indicate that the particle is an electron (hole). The corresponding non-normalized wave functions are found to be

$$\begin{aligned}
\Psi^{e}_{\boldsymbol{k},\tilde{\uparrow}} &= \begin{pmatrix} 1 \\ isp_{e,\tilde{\uparrow}}e^{is\theta_{e,\tilde{\uparrow}}} \\ 0 \\ 0 \end{pmatrix} e^{i\boldsymbol{k}_{e,\tilde{\uparrow}}\boldsymbol{r}}, \qquad \Psi^{e}_{\boldsymbol{k},\tilde{\downarrow}} = \begin{pmatrix} isp_{e,\tilde{\downarrow}}e^{-is\theta_{e,\tilde{\downarrow}}} \\ 1 \\ 0 \\ 0 \end{pmatrix} e^{i\boldsymbol{k}_{e,\tilde{\downarrow}}\boldsymbol{r}}, \\
\Psi^{h}_{\boldsymbol{k},\tilde{\uparrow}} &= \begin{pmatrix} 0 \\ 0 \\ 1 \\ isp_{h,\tilde{\uparrow}}e^{-is\theta_{h,\tilde{\uparrow}}} \end{pmatrix} e^{i\boldsymbol{k}_{h,\tilde{\uparrow}}\boldsymbol{r}}, \qquad \Psi^{h}_{\boldsymbol{k},\tilde{\downarrow}} = \begin{pmatrix} 0 \\ 0 \\ isp_{h,\tilde{\downarrow}}e^{is\theta_{h,\tilde{\downarrow}}} \\ 1 \end{pmatrix} e^{i\boldsymbol{k}_{h,\tilde{\downarrow}}\boldsymbol{r}},
\end{aligned} \tag{3.48}$$

where we have defined

$$p_{e/h,\tilde{\sigma}}(\alpha, h) = \frac{\alpha k_{e/h,\tilde{\sigma}}}{h + \sqrt{h^2 + \alpha^2 k^2_{e/h,\tilde{\sigma}}}}. \tag{3.49}$$

In the limit $\alpha = 0$, that is without the spin-orbit effect, but with the Zeeman effect, we notice how $p = 0$ and we re-obtain the wave functions from equation (3.35). Moreover, we find $p = 1$ for any state in the limit $h = 0$, without the Zeeman effect, but with the spin-orbit effect. The wave vectors are given as

$$\boldsymbol{k}_{e/h,\tilde{\sigma}} = k_{e/h,\tilde{\sigma}}(s\cos\theta_{e/h,\tilde{\sigma}}\hat{x} + \sin\theta_{e/h,\tilde{\sigma}}\hat{y}) \tag{3.50}$$

where we find $k_{e/h,\tilde{\sigma}}$ from the excitation energy (3.47):

$$\begin{aligned} k_{e/h,\tilde{\sigma}} &= sk_F\sqrt{1+\frac{1}{2}\frac{k_F^2\alpha^2}{\mu^2}\pm\frac{E_k}{\mu}+\tilde{\sigma}\sqrt{\left(\frac{k_F^2\alpha^2}{2\mu^2}\right)^2+\frac{h^2}{\mu^2}+\frac{k_F^2\alpha^2}{\mu^2}\pm\frac{k_F^2\alpha^2}{\mu^2}\frac{E_k}{\mu}}} \\ &\approx sk_F\left(1+\tilde{\sigma}\frac{1}{2}\sqrt{\frac{h^2}{\mu^2}+\frac{k_F^2\alpha^2}{\mu^2}}\right) \end{aligned} \tag{3.51}$$

and we have taken $E^{e/h}_{\boldsymbol{k},\tilde{\sigma}}/\mu$ to zero in the Andreev approximation and let the Zeeman field strength and the spin orbit coupling be weak, $h/\mu \ll 1$, $\alpha k_F/\mu \ll 1$. At $\alpha = 0$ this corresponds to the wave vectors found in the pure Zeeman case, (3.36).

Like we argued in the previous section where Zeeman splitting was considered, we must have the particles of a bounded state to travel along the same trajectory, i.e. we must have $\theta_{e/h,\tilde{\sigma}} = \theta$ for all e, h, $\tilde{\uparrow}$, $\tilde{\downarrow}$. The angle $\theta_{e/h,\tilde{\sigma}}$ is determined by conservation of $k_y = k_{e/h,\tilde{\sigma}}\sin\theta_{e/h,\tilde{\sigma}}$ which yields

$$\sin\theta_{e/h,-\tilde{\sigma}} \approx \left(1+\sqrt{\frac{h^2}{\mu^2}+\frac{k_F^2\alpha^2}{\mu^2}}\right)\sin\theta_{e/h,\tilde{\sigma}}. \tag{3.52}$$

Even with $k_F\alpha/\mu$ and h/μ small and kept to first order the angle θ is not conserved in an Andreev reflection. However, we may assume θ small like we did for the Zeeman effect. We keep θ and $\alpha k_F/\mu$ to first order, but take the product $\theta\alpha k_F/2\mu$ to zero. In this approximation the above equality yields a conserved angle $\theta_{e/h,\tilde{\sigma}} = \theta_{e/h,-\tilde{\sigma}} \equiv \theta$, as required.

Andreev reflection amplitude

The Andreev reflection amplitude is found in a similar fashon as in the previous sections. However, the matching conditions will be modified due to the momentum operator $\hat{\boldsymbol{k}}$ entering at the off-diagonal of $H_{\boldsymbol{k}}$. When determining the reflection amplitudes we will consider an FS-interface placed at $x = 0$. The Hamiltonian considered above is only valid in the ferromagnet, but when considering the matching conditions we must consider the overall Hamiltonian which we may write as

$$\hat{H}(x,y) = \begin{pmatrix} \hat{h}(x,y) & \hat{w}(x,y) & 0 & \Delta(x,y) \\ \hat{w}^*(x,y) & \hat{h}(x,y) & -\Delta(x,y) & 0 \\ 0 & -\Delta^*(x,y) & -\hat{h}(x,y) & \hat{w}^*(x,y) \\ \Delta^*(x,y) & 0 & \hat{w}(x,y) & -\hat{h}(x,y) \end{pmatrix}, \tag{3.53}$$

where

$$\begin{aligned}\hat{h}(x,y) &= -\frac{\hbar^2\nabla^2}{2m} - (\mu_F + \bar{\sigma}h)\Theta(-x) - \mu_S\Theta(x),\\ \hat{w}(x,y) &= \alpha\left(\hat{k}_y(x,y) + i\hat{k}_x(x,y)\right),\\ \Delta(x,y) &= \Delta\Theta(x),\end{aligned} \tag{3.54}$$

with $\Theta(x)$ being the step function and $\hat{k}_x$ and $\hat{k}_y$ defined as

$$\begin{aligned}\hat{k}_x(x,y) &= -\frac{i}{2}\left(\frac{\partial}{\partial x}\Theta(-x) + \Theta(-x)\frac{\partial}{\partial x}\right),\\ \hat{k}_y(x,y) &= -i\frac{\partial}{\partial y}\Theta(-x).\end{aligned} \tag{3.55}$$

The symmetrical structure of $\hat{k}_x$ is important in order to keep the Hamiltonian hermitian, i.e. it must satisfy

$$\int_{-\infty}^{\infty}\Psi_1^*\hat{k}_x\Psi_2\,dx = \int_{-\infty}^{\infty}\Psi_2\left[\hat{k}_x\Psi_1\right]^*dx. \tag{3.56}$$

With the chosen structure of $\hat{k}_x$ one can show that this relation is satisfied, whereas an unsymmetrical choice such as $-i\Theta(-x)\partial/\partial x$ would leave the Hamiltonian non-hermitian.

Now that the overall Hamiltonian is determined, we can find the matching conditions at the interface. Charge conservation yields continuous wave functions at the interfaces:

$$\Psi_F(0,y) = \Psi_S(0,y). \tag{3.57}$$

The derivatives of the wave functions will not be continuous due to the momentum operators on the off-diagonal parts of the Hamiltonian. We find the matching conditions for the derivatives by integrating the BdG-equations (3.46) over a small distance ϵ around $x = 0$ and then let $\epsilon \to 0$:

$$\begin{aligned}0 &= \lim_{\epsilon\to0}\int_{-\epsilon}^{+\epsilon}E_{\boldsymbol{k}}\Psi(x,y)\,dx = \lim_{\epsilon\to0}\int_{-\epsilon}^{+\epsilon}\hat{H}(x,y)\Psi(x,y)\,dx\\ &= \lim_{\epsilon\to0}\sigma_h\int_{-\epsilon}^{+\epsilon}-\frac{\hbar^2}{2m}\frac{\partial^2}{\partial x^2}\Psi(x,y) + \lim_{\epsilon\to0}\sigma_w\int_{-\epsilon}^{+\epsilon}\frac{1}{2}\left(\frac{\partial}{\partial x}\Theta(-x) + \Theta(-x)\frac{\partial}{\partial x}\right)\Psi(x,y)\,dx\\ &= -\sigma_h\frac{\hbar^2}{2m}\left(\left.\frac{\partial\Psi_F}{\partial x}\right|_{x=0} - \left.\frac{\partial\Psi_S}{\partial x}\right|_{x=0}\right) - \frac{1}{2}\sigma_w\Psi\Big|_{x=0}.\end{aligned}$$

We have here defined the matrices

$$\sigma_h = \begin{pmatrix} 1 & 0 & 0 & 0 \\ 0 & 1 & 0 & 0 \\ 0 & 0 & -1 & 0 \\ 0 & 0 & 0 & -1 \end{pmatrix}, \qquad \sigma_w = \begin{pmatrix} 0 & -\alpha & 0 & 0 \\ \alpha & 0 & 0 & 0 \\ 0 & 0 & 0 & \alpha \\ 0 & 0 & -\alpha & 0 \end{pmatrix}, \tag{3.58}$$

and the resulting matching condition for the derivatives of the wave functions is

$$\left.\frac{\partial \Psi_F}{\partial x}\right|_{x=0} - \left.\frac{\partial \Psi_S}{\partial x}\right|_{x=0} = \alpha \frac{m}{\hbar^2} \begin{pmatrix} 0 & 1 & 0 & 0 \\ -1 & 0 & 0 & 0 \\ 0 & 0 & 0 & 1 \\ 0 & 0 & -1 & 0 \end{pmatrix} \Psi\Big|_{x=0}. \tag{3.59}$$

We will consider an incoming electron of pseudo spin $\tilde{\sigma}$ which will be reflected into an electron or hole of pseudo spin $\pm\tilde{\sigma}$ with probability amplitudes $r_{e\tilde{\sigma}e,\pm\tilde{\sigma}}$ and $r_{e\tilde{\sigma}h\pm\tilde{\sigma}}$, respectively, and it will be transmitted into quasi-electrons or quasi-holes in the superconductor of spin $\pm\sigma$ with probability amplitudes $t_{e\tilde{\sigma}\tilde{e}\pm\sigma}$ and $t_{e\tilde{\sigma}\tilde{h}\pm\sigma}$, respectively. We let $h = 0$ and consider only the effect from the spin-orbit coupling. The incoming, reflected and transmitted wave functions are constructed from the single particle wave functions from equation (3.48) and (2.31):

$$\begin{aligned}
\Psi_i(x) &= \begin{pmatrix} 1 \\ ie^{i\theta} \\ 0 \\ 0 \end{pmatrix} e^{ik_{x\uparrow}x}, \\
\Psi_r(x) &= a_1 \begin{pmatrix} 1 \\ ie^{-i\theta} \\ 0 \\ 0 \end{pmatrix} e^{-ik_{x\uparrow}x} + a_2 \begin{pmatrix} -ie^{i\theta} \\ 1 \\ 0 \\ 0 \end{pmatrix} e^{-ik_{x\downarrow}x} + a_3 \begin{pmatrix} 0 \\ 0 \\ 1 \\ ie^{-i\theta} \end{pmatrix} e^{ik_{x\uparrow}x} + a_4 \begin{pmatrix} 0 \\ 0 \\ ie^{i\theta} \\ 1 \end{pmatrix} e^{ik_{x\downarrow}x} \\
\Psi_t(x) &= b_1 \begin{pmatrix} e^{i\eta}e^{i\varphi} \\ 0 \\ 0 \\ 1 \end{pmatrix} e^{ik_{x\tilde{e}}x} + b_2 \begin{pmatrix} 0 \\ e^{i\eta}e^{i\varphi} \\ -1 \\ 0 \end{pmatrix} e^{ik_{x\tilde{e}}x} + b_3 \begin{pmatrix} e^{-i\eta}e^{i\varphi} \\ 0 \\ 0 \\ 1 \end{pmatrix} e^{-ik_{x\tilde{h}}x} + b_4 \begin{pmatrix} 0 \\ e^{-i\eta}e^{i\varphi} \\ -1 \\ 0 \end{pmatrix} e^{-ik_{x\tilde{h}}x}.
\end{aligned} \tag{3.60}$$

The wave functions found here are only valid for $\alpha \neq 0$ as one would have $p = 0$ in equation (3.49) if $\alpha = 0$ and the wave functions would be pure up- and down electrons and holes. Moreover, the wave functions considered above are not normalized. In fact, for them to represent single quasi-particles they must be columns of a unitary matrix as the diagonalization from equation (3.46) must leave the Hamiltonian (3.44) unchanged. This yields a modification in the reflection and transmission

amplitudes and we find the reflection amplitudes to be related to the coefficients a_i in the following way

$$r_{e\tilde{\uparrow}e\tilde{\uparrow}} = ie^{-i\theta}a_1, \qquad r_{e\tilde{\uparrow}e\tilde{\downarrow}} = -a_2, \qquad r_{e\tilde{\uparrow}h\tilde{\uparrow}} = ie^{-i\theta}a_3, \qquad r_{e\tilde{\uparrow}h\tilde{\downarrow}} = a_4. \tag{3.61}$$

In the Andreev approximation and with $\alpha k_F/\mu \ll 1$ the wave vectors are given as

$$k_{x\tilde{\uparrow}} = k_F\left(1-\frac{\alpha k_F}{2\mu}\right)\cos\theta, \qquad k_{x\tilde{\downarrow}} = k_F\left(1+\frac{\alpha k_F}{2\mu}\right)\cos\theta, \qquad k_{x\tilde{e}} = k_{x\tilde{h}} = k_F\cos\theta. \tag{3.62}$$

We let $\Psi_F = \Psi_i + \Psi_r$ and $\Psi_S = \Psi_t$ and insert the wave functions into the matching conditions (3.57) and (3.59). An algebraic tool can be used to solve the system and find the amplitudes. The resulting expressions are complicated, but when only keeping $\alpha k_F/\mu \ll 1$ to first order the amplitudes are found to be

$$\begin{aligned}
r_{e\tilde{\uparrow}e\tilde{\uparrow}} &= i\frac{\alpha k_F}{2\mu}e^{-i\eta}\sin\theta\sin\eta \\
r_{e\tilde{\uparrow}e\tilde{\downarrow}} &= \frac{\alpha k_F}{2\mu}e^{-i\eta}\sin\eta\left[\frac{1}{\cos\theta}+\cos\theta\right] \\
r_{e\tilde{\uparrow}h\tilde{\uparrow}} &= e^{-i\eta}e^{-i\varphi} \\
r_{e\tilde{\uparrow}h\tilde{\downarrow}} &= 0.
\end{aligned} \tag{3.63}$$

The corresponding probabilities are thus

$$\begin{aligned}
\left|r_{e\tilde{\uparrow}e\tilde{\uparrow}}\right|^2 &= \left(\frac{\alpha k_F}{2\mu}\right)^2\frac{v_0^2}{u_0^2}\sin^2\theta\sin^2\eta \approx 0, \\
\left|r_{e\tilde{\uparrow}e\tilde{\downarrow}}\right|^2 &= \left(\frac{\alpha k_F}{2\mu}\right)^2\frac{v_0^2}{u_0^2}\sin^2\eta\left[\frac{1}{\cos\theta}+\cos\theta\right]^2 \approx 0, \\
\left|r_{e\tilde{\uparrow}h\tilde{\uparrow}}\right|^2 &= \frac{v_0^2}{u_0^2}, \\
\left|r_{e\tilde{\uparrow}h\tilde{\downarrow}}\right|^2 &= 0,
\end{aligned} \tag{3.64}$$

where we again keep $\alpha k_F/\mu$ to first order. Thus the only non-zero probability, in the weak spin orbit coupling, is the probability for Andreev reflection from an electron of pseudo spin up to a hole of the same pseudo spin. This allows us to treat the incoming electron, which is reflected into a hole, as an Andreev bound state.

We do similar calculations for incoming electrons of pseudo spin down, and for incoming holes of pseudo spin up and down. In all cases there is only one non-zero probability for reflection. The corresponding amplitudes are found to be

$$r_{e\tilde{\uparrow}h\tilde{\uparrow}} = e^{-i\eta}e^{-i\varphi}, \qquad r_{e\tilde{\downarrow}h\tilde{\downarrow}} = e^{-i\eta}e^{-i\varphi}, \qquad r_{h\tilde{\uparrow}e\tilde{\uparrow}} = e^{-i\eta}e^{i\varphi}, \qquad r_{h\tilde{\downarrow}e\tilde{\downarrow}} = e^{-i\eta}e^{i\varphi}. \tag{3.65}$$

We have found that electrons (holes) in the ferromagnet of pseudo spin $\tilde{\alpha}$ are Andreev reflected to holes (electrons) with the same pseudo spin. This is different from what we found for the Zeeman effect where the reflected hole (electron) had opposite spin of the incomming electron (hole) and we will see that this is an essential difference when we in the following consider the quantization condition.

Bohr-Sommerfeld quantization

An incoming electron (hole) of pseudo spin $\tilde{\sigma}$ traveling along a trajectory with an angle θ, from the left superconductor towards the right superconductor, will accumulate a phase of

$$\begin{aligned}\pm\left(Lk_{x,\tilde{\sigma}}+L\tan\theta k_{y,\tilde{\sigma}}\right) &= \pm k_F L\left(1+\tilde{\sigma}\frac{\alpha k_F}{2\mu}\right)\cos\theta + k_F L\left(1+\tilde{\sigma}\frac{\alpha k_F}{2\mu}\right)\sin\theta\tan\theta \\ &\approx \pm k_F L\left[\left(1+\tilde{\sigma}\frac{\alpha k_F}{2\mu}\right)\cos\theta+\sin\theta\tan\theta\right].\end{aligned} \tag{3.66}$$

The electron (hole) will then be Andreev reflected into a hole (electron) of the same pseudo spin $\tilde{\sigma}$ and according to the amplitudes in equation (3.65) gain a phase $-\eta\mp\varphi_R$. Next, the reflected hole (electron) will travel back along the same trajectory and accumulate the phase

$$\mp\left(Lk_{x,\tilde{\sigma}}+L\tan\theta k_{y,\tilde{\sigma}}\right)\approx\mp k_F L\left[\left(1+\tilde{\sigma}\frac{\alpha k_F}{2\mu}\right)\cos\theta+\sin\theta\tan\theta\right]. \tag{3.67}$$

When arriving at the left superconductor the hole (electron) will be Andreev reflected back to it's original state and get an additional phase $-\eta\pm\varphi_L$.

Since the reflected hole (electron) has the same pseudo spin and thus the same momentum according to equation (3.62) the phase shift accumulated by the electron (hole) traveling from the left to the right superconductor will cancel the phase shift accumulated by the hole (electron) traveling from the right to the left superconductor. The total phase must be a multiple of 2π and the quantization condition yields

$$2n\pi = -2\eta\pm(\Delta\varphi-\gamma), \tag{3.68}$$

where we have allowed for a magnetic field and thus a phase shift γ like we did in the preveous sections. This quantization condition is identical to the quantization condition found for the ordinary SNS junction (3.9), and we find that the spin-orbit coupling alone has in fact no effect on the energy levels. This is in correspondence with what other research has shown, namely that the spin-orbit coupling has only an effect in the presence of a Zeeman field [64]. So far we have only considered the Zeeman effect and the spin-orbit coupling effect separately and it could be relevant to consider a combination of the two effects. However, one would then find that an incoming state will be reflected into multiple states with finite probabilities even when we let $h/\mu \ll 1$ and

$\alpha k_F/\mu \ll 1$. In that case the approach for finding the current density used in this thesis will not be applicable as we require the trajectories of section 3.1 to be traversed by single states.

Chapter 4

Andreev bound state current in a weak magnetic field

We will in this chapter find the current of the systems described in chapter 3. In section 2.6 and equation (2.37) we saw how the Josephson current can be expressed in terms of the free energy and the superconducting phase difference. In section 2.7 and equation (2.42) the free energy was expressed in terms of the energy levels, $E_{\boldsymbol{k}}$, and by combining equation (2.37) and (2.42) we can thus express the Josephson current along the junction in terms of the ABS energies and the phase difference:

$$I_x(\Delta\varphi) = \sum_{k_y} \delta I(\boldsymbol{r}, \boldsymbol{k}) \to \int dy \int \frac{dk_y}{2\pi} \delta I(\boldsymbol{r}, \boldsymbol{k}), \tag{4.1}$$

with

$$\delta I(\boldsymbol{r}, \boldsymbol{k}) \equiv -\frac{2e}{\hbar} \sum_i \tanh\left(\frac{E_{\boldsymbol{k},i}}{2k_B T}\right) \frac{\partial E_{\boldsymbol{k},i}}{\partial(\Delta\varphi)} \tag{4.2}$$

where the sum over i is the sum over all states for each wave vector $\boldsymbol{k}$. The current density will be given as

$$\begin{aligned} j_x(x_0, y_0) &= \int \frac{dk_y}{2\pi} \delta I(\boldsymbol{r}, \boldsymbol{k}) = \frac{k_F}{2\pi} \int_{-\pi/2}^{\pi/2} d\theta_k \cos\theta_k \delta I(\boldsymbol{r}, \boldsymbol{k}), \\ j_y(x_0, y_0) &= \int \frac{dk_x}{2\pi} \delta I(\boldsymbol{r}, \boldsymbol{k}) = \frac{k_F}{2\pi} \int_{-\pi/2}^{\pi/2} d\theta_k \sin\theta_k \delta I(\boldsymbol{r}, \boldsymbol{k}), \end{aligned} \tag{4.3}$$

in the x- and y-direction, respectively, where we have let

$$\begin{pmatrix} dk_x \\ dk_y \end{pmatrix} \to k_F \begin{pmatrix} \sin\theta_k \\ \cos\theta_k \end{pmatrix} d\theta_k \tag{4.4}$$

as we consider the circular Fermi surface, as stated in section 3.1.

In chapter 3 the ABS energy levels were found for the systems of interest and we will use these energies in equation (4.3) to find the current density and in equation (4.1) to find the total and critical current. For the analytical progress we will consider the high temperature regime, ($k_B T \gtrsim \Delta$), in which the calculations are simpler.

4.1 Low-T_c SNS junction in weak magnetic field

In equation (3.11) we found the ABS energies in a normal SNS junction with s-wave pairing. These energies may be inserted into equation (4.2) to obtain [1]

$$\delta I_k(\Delta\varphi) = 4\frac{e\Delta}{\hbar}\sin\left(\frac{\Delta\varphi}{2}-\frac{\gamma_k}{2}\right)\tanh\left(\frac{\Delta\cos\left(\frac{\Delta\varphi}{2}-\frac{\gamma_k}{2}\right)}{2k_BT}\right), \tag{4.5}$$

which in the high temperature regime ($k_B T \gtrsim \Delta$), can be approximated to

$$\delta I_k(\Delta\varphi) \approx \frac{e\Delta^2}{\hbar k_B T}\sin\left(\Delta\varphi-\gamma_k\right). \tag{4.6}$$

The Aharonov-Bohm phase shift, γ_k, will depend on the modulation and strength of the magnetic field, as well as the trajectory of the particle. In the uniform field the Aharonov-Bohm phase shift is

$$\gamma_k = \frac{2L}{l_m^2}(y_0 - x_0\tan\theta), \tag{4.7}$$

see appendix B for details. The total current is

$$I_x = I_{c,0}\frac{\sin\left(\frac{e}{\hbar}\Phi\right)}{\frac{e}{\hbar}\Phi}\sin\Delta\varphi \tag{4.8}$$

where

$$I_{c,0} = \frac{k_F W e\Delta^2}{2\pi\hbar k_B T} \tag{4.9}$$

is the critical current in the absence of magnetic field. The critical current in a magnetic field is found from (4.8) and plotted in figure 4.1(a). This is the well known Fraunhofer oscillations with decreasing critical current as the magnetic field strength is increased.

The current density is found numerically from equation (4.6) and (4.3) and shown in figure 4.1(b). The chain of current vortex-antivortex pairs appearing along the superconducting interfaces in the figure, is already a known result [37]. We emphasize here that we are discussing supercurrent vortices which are distinct from Abrikosov vortices, the latter having normal cores and a phase-

[1] The derivation of this section has already been considered by A. Brøyn in a specialization project [39] and will be used for comparison.

winding of 2π in the superconducting order parameter. The vortex distance is found to be

$$d_{\text{vortex}} = \pi \frac{l_m^2}{L}, \tag{4.10}$$

and it is clear that the distance between the vortices increases with the magnetic length. The vortex distance (4.10) is related to the period, $\Phi_0 = \pi\hbar/e$, of the Fraunhofer oscillations (4.8) by

$$d_{\text{vortex}} = W \frac{\Phi_0}{\Phi}, \tag{4.11}$$

and we realize that the oscillations are a direct consequence of the vortex pattern.

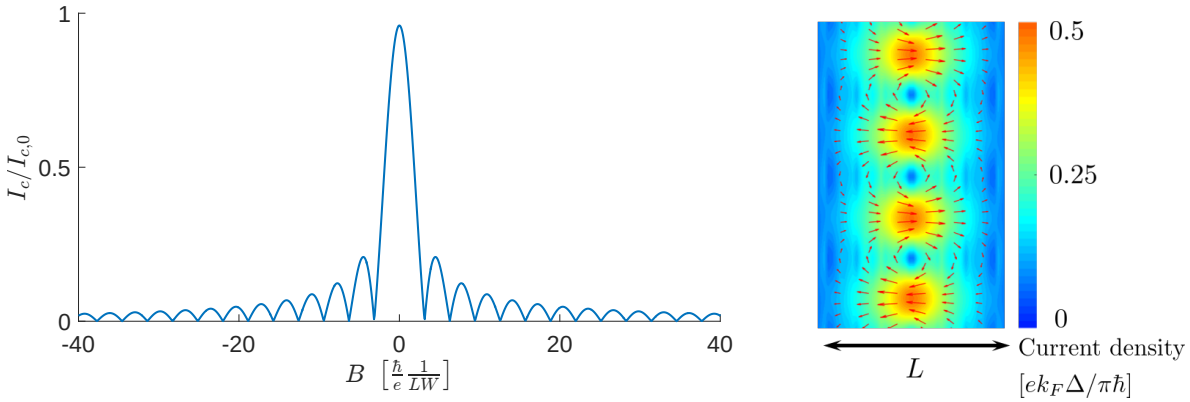

(a) (b)

Figure 4.1: The critical current $I_c(B)$ (a) and a scale plot of the current density (b) through the normal region of a Josephson junction exposed to a uniform field. The current is calculated numerically from equation (4.1), (4.3), (4.5) and (4.7) at $\Delta\varphi = \pi/2$ and $kBT = \Delta$. The magnetic length in the scale plot is $l_m/L = 0.6$.

4.2 High-T_c SNS junction in weak magnetic field

In section 3.3 we considered high-T_c superconductors in which the d-wave pairing gave rise to energy levels different from the low-T_c case considered above. We will here use the energy levels to find the supercurrent in the SNS junction and focus on some specific orientations of α in order to get a better physical understanding. We consider a uniform magnetic field with Aharanov-Bohm phase shift given in equation (4.7), but the approach is applicable with any modulation of the magnetic field and would only require to change γ.

4.2.1 Equal orientation in left and right superconductor: $\alpha_L = \alpha_R = \alpha$

With the order parameter oriented equally in the left and right superconductor the Andreev levels (3.23) were found to have the same dependency on the magnetic field and the superconducting phase difference, $\Delta\varphi$, as in the s-wave junction. But unlike the s-wave case, the energies were suppressed by the gap parameter at certain angles, θ, of the momentum. We will here use these Andreev levels to find the current density and the total current in the junction. We consider two special orientations of the gap parameter, $\alpha = 0$ and $\alpha = \pi/4$, before we consider the more general case with arbitrary α.

$\underline{\alpha = 0}$

With the order parameter oriented along the surface normal in both superconductors the Andreev levels in (3.23) are given as

$$E_{\boldsymbol{k}} = \pm|\Delta_0 \cos(2\theta))| \cos\left(\frac{\Delta\varphi}{2} - \frac{\gamma}{2}\right), \tag{4.12}$$

and in the high temperature regime we find from (4.2)

$$\begin{aligned} \delta I_k(\Delta\varphi) &= 4\frac{e\Delta_0}{\hbar}|\cos(2\theta)| \sin\left(\frac{\Delta\varphi}{2} - \frac{\gamma_k}{2}\right) \tanh\left(\Delta_0|\cos(2\theta)| \frac{\cos\left(\frac{\Delta\varphi}{2} - \frac{\gamma_k}{2}\right)}{2k_BT}\right) \\ &\approx \frac{e\Delta_0^2}{\hbar k_B T}\cos^2(2\theta)\sin\left(\Delta\varphi - \gamma_k\right). \end{aligned} \tag{4.13}$$

Using the same approach as in section 4.1 and appendix B the total current in the uniform low field, $l_m \gg L$, is found to be

$$\begin{aligned} I_x &= I_{c,0}\frac{\sin\left(\frac{e}{\hbar}\Phi\right)}{\frac{e}{\hbar}\Phi}\sin\Delta\varphi \int_0^{\pi/2} d\theta \cos\theta\cos^2(2\theta) \\ &= \frac{7}{15} I_{c,0}\frac{\sin\left(\frac{e}{\hbar}\Phi\right)}{\frac{e}{\hbar}\Phi}\sin\Delta\varphi. \end{aligned} \tag{4.14}$$

From this we see that the total current in the high-T_c junction has the same dependency on the superconducting phase difference, $\Delta\varphi$, and the magnetic flux Φ, as the low-T_c junction, but is suppressed by a factor 7/15. The suppression is expected as the gap is smaller for $|\theta| > 0$ and thus the number of subgap states has decreased.

The current density is found numerically by insertion of equation (4.14) into equation (4.3). The result is shown to the left in figure 4.2. Comparing this result to the s-wave junction we notice how the current vortices are modified to current channels between the superconductors. The current along the junction was already weighted by the factor $\cos\theta$ in (4.3), so that the main contribution

to the current comes from states of small angles, $\theta \approx 0$. In the d-wave case we have an additional factor $\cos^2(2\theta)$ which amplifies this effect, resulting in channels with current along the trajectories of $\theta = 0$.

From the Aharanov-Bohm shift it is clear that the x_0-dependence is weak for small angles θ. Since the main contribution to the current is from states of small angles we observe less variation of the current along the junction, compared to the s-wave case. Moreover, a change in y_0 corresponds to a phase shift of $\Delta\varphi$. To be exact a change δy_0 in y_0 corresponds to a change $2\delta y_0 L/l_m^2$ in the phase $\Delta\varphi$. A shift δy_0 along the interfaces corresponding to $2\delta y_0 L/l_m^2 = \pi$, would change the direction of the current and we observe that the current channels in figure 4.2 have alternating directions and are separated by a distance $\pi l_m^2/2L$.

$\underline{\alpha = \pi/4}$

With the gap orientation in both superconductors rotated by 45 degrees, we find the energy levels from (3.23) to be given as

$$E_{\boldsymbol{k}} = \pm|\Delta_0 \sin(2\theta))| \cos\left(\frac{\Delta\varphi}{2} - \frac{\gamma}{2}\right). \tag{4.15}$$

We do the same calculations as above and find the current density,

$$\begin{aligned} \delta I_k(\Delta\varphi) &= 4\frac{e\Delta_0}{\hbar}|\sin(2\theta)| \sin\left(\frac{\Delta\varphi}{2} - \frac{\gamma_k}{2}\right) \tanh\left(\Delta_0 |\sin(2\theta)| \frac{\cos\left(\frac{\Delta\varphi}{2} - \frac{\gamma_k}{2}\right)}{2k_B T}\right) \\ &\approx \frac{e\Delta_0^2}{\hbar k_B T} \sin^2(2\theta) \sin\left(\Delta\varphi - \gamma_k\right), \end{aligned} \tag{4.16}$$

and total current in the low field regime:

$$\begin{aligned} I_x &= I_{c,0} \frac{\sin\left(\frac{e}{\hbar}\Phi\right)}{\frac{e}{\hbar}\Phi} \sin\Delta\varphi \int_0^{\pi/2} d\theta \cos\theta \sin^2(2\theta) \\ &= \frac{8}{15} I_{c,0} \frac{\sin\left(\frac{e}{\hbar}\Phi\right)}{\frac{e}{\hbar}\Phi} \sin\Delta\varphi. \end{aligned} \tag{4.17}$$

Thus the total current is almost identical, but a factor 8/7 larger, than the total current when the orientation of the gap parameter is along the surface normal in the junction. With the orientation $\alpha = 0$ the current is maximized at $\theta = 0$ and we would think that this would give a large current as the small angle states are weighted by the factor $\cos\theta$ in the current along the junction, (4.3). However, at $\alpha = \pi/4$, there are two angles in which the current peaks, namely $\pm\pi/4$. Constructive interference between these states would thus give a large current, despite the node at $\theta = 0$.

In the right figure in 4.2 the current density is shown when $\alpha = \pi/4$ in both superconductors. Due

to the factor $\sin^2(2\theta)$ in the current density, which will be maximized at $\theta = \pm\pi/4$, we would expect channels in the $\theta = \pm\pi/4$ direction instead of the $\theta = 0$ direction. However, the channels of $\pm\theta$ will overlap and instead of pure channels we observe a diamond pattern. In contrast to the case with $\alpha = 0$ we will now have significant variation of the current density along the junction, since the dominant states at $\theta = \pm\pi/4$ yield an x_0-dependence in the Aharonov-Bohm phase shift, (4.7).

Arbitrary α

For the more general case with equal, but arbitrary, orientation, α, in both superconductors, the current density is given as

$$\begin{aligned}\delta I_k(\Delta\varphi) &= 4\frac{e\Delta_0}{\hbar}\left|\cos(2(\theta-\alpha))\right|\sin\left(\frac{\Delta\varphi}{2}-\frac{\gamma_k}{2}\right)\tanh\left(\Delta_0\left|\cos((2(\theta-\alpha))\right|\frac{\cos\left(\frac{\Delta\varphi}{2}-\frac{\gamma_k}{2}\right)}{2k_BT}\right)\\ &\approx \frac{e\Delta_0^2}{\hbar k_BT}\cos^2(2(\theta-\alpha))\sin\left(\Delta\varphi-\gamma_k\right).\end{aligned} \tag{4.18}$$

Again, we use the method in appendix B to find the total current. In the two special cases considered above, $|\Delta(\theta)|$ was an even function of θ. In the general situation with α arbitrary this is no longer the case and it is slightly more complicated to find the total current. The difficulty is solved by splitting the integrand into two parts, $\delta I_k = \delta I_{k,1} + \delta I_{k,2}$, with

$$\delta I_{k,i}(\Delta\varphi) = \frac{e\Delta_0^2}{\hbar k_BT} f_i(\theta)\sin\left(\Delta\varphi-\gamma_k\right) \tag{4.19}$$

where $i = 1,2$ and $f_1(\theta) + f_2(\theta) = \cos^2(2(\theta-\alpha))$ with

$$\begin{aligned}f_1(\theta) &= \cos^2(2\theta)\cos^2(2\alpha) + \sin^2(2\theta)\sin^2(2\theta)\\ f_2(\theta) &= \frac{1}{2}\sin(4\theta)\sin(4\alpha),\end{aligned} \tag{4.20}$$

so that $f_1(\theta) = f_1(-\theta)$ is an even function of θ while $f_2(\theta) = -f_2(-\theta)$ is an odd function of θ. We can then use the approach from appendix B on each integrand separately:

$$I_i = \frac{k_F}{2\pi}\frac{e\Delta_0^2}{2\hbar k_BT}\int_{-W/2}^{W/2} dy_0 \int_{-\pi/2}^{\pi/2} d\theta\cos\theta\delta I_{k,i}(\theta) \tag{4.21}$$

and let the total current be the sum of the two integrals: $I_x = I_1 + I_2$. We find

$$\begin{aligned} I_1 &= I_{c,0}\frac{\sin\left(\frac{LW}{l_m^2}\right)}{\frac{LW}{l_m^2}}\sin(\Delta\varphi)\cos\left(\frac{2L}{l_m^2}x_0\tan\theta\right)\int_0^{\pi/2}d\theta\cos\theta f_1(\theta) \approx \frac{7+\sin^2(2\alpha)}{15}I_{c,0}\frac{\sin\left(\frac{LW}{l_m^2}\right)}{\frac{LW}{l_m^2}} \\ I_2 &= I_{c,0}\frac{\sin\left(\frac{LW}{l_m^2}\right)}{\frac{LW}{l_m^2}}\cos(\Delta\varphi)\sin\left(\frac{2L}{l_m^2}x_0\tan\theta\right)\int_0^{\pi/2}d\theta\cos\theta f_2(\theta) \approx 0, \end{aligned} \tag{4.22}$$

where we have let $\cos\left(\frac{2L}{l_m^2}x_0\tan\theta\right) \approx 1$ and $\sin\left(\frac{2L}{l_m^2}x_0\tan\theta\right) \approx 0$ in the low field regime, $l_m \gg L$. Hence, the total current for a junction with the gap parameter equally, but arbitrary, oriented in left and right superconductor is

$$I_x = \frac{7+\sin^2(2\alpha)}{15}I_{c,0}\frac{\sin\left(\frac{e}{\hbar}\Phi\right)}{\frac{e}{\hbar}\Phi}\sin\Delta\varphi. \tag{4.23}$$

The critical current reveals the Fraunhofer pattern for any orientation α. Compared to s-wave pairing the total current is suppressed with a factor varying between 7/15 and 8/15, with smallest current at $\alpha = 0, \pm\pi/2$ and largest current at $\alpha = \pm\pi/4$.

The current density is found numerically by inserting the expression (4.18) into equation (4.3). In the middle figure 4.2 we show the result for $\alpha = \pi/8$. From equation (4.18) we realize that the states with the greatest contribution to the current are those of angles $\theta = \alpha + n\pi/2$, with n as an integer. Since θ can take values between $-\pi/2$ and $\pi/2$ there will be two angles (for α non-zero) that maximize the expression in equation (4.18), that is α and $\alpha \pm \pi/2$ where we choose the upper (lower) sign if α is negative (positive). When finding the current density along the junction the factor $\cos\theta$ will weight the angle with the smallest absolute value, so that these states give the greatest current contribution. In the special case with $\alpha = \pi/8$, shown in figure 4.2, equation (4.18) is maximized at $\alpha = \pi/8$ and $\alpha = -3\pi/8$. Since $|\pi/8| < |-3\pi/8|$, the greatest current contribution comes from states of angle $\theta = \pi/8$. Consequently, we observe current channels which are tilted with $\pi/8$ radians compared to the case with $\alpha = 0$. We have found that the largest contribution comes from the states of the direction with the largest gap, but with a weight at the directions of the smallest angles.

4.2.2 Orientation in right superconductor rotated 90 degrees: $\alpha_L = \alpha$, $\alpha_R = \alpha - \pi/2$

We will now consider the case in which the left and right superconductors have orientations which differ by $\pi/2$. In (3.24) we found that the Andreev levels are very similar to the situation with $\alpha_L = \alpha_R$. The difference is that we now have a π-junction which in the absence of magnetic field has minimum energy at $\Delta\varphi = \pi$. In the presence of a magnetic field the situation corresponds to a

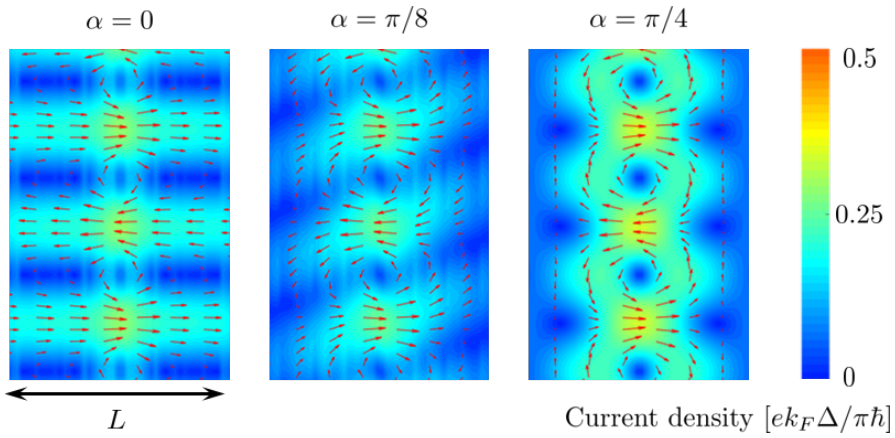

Figure 4.2: Scale plots of the current density through the normal region of a d-wave junction exposed to a uniform field when left and right superconductor have equal orientation, $\alpha = 0$, $\alpha = \pi/8$, $\alpha = \pi/4$ with $\Delta\varphi = \pi/2$, $k_B T = \Delta$, $l_m/L = 0.6$.

phase shift of π radians in $\Delta\varphi$, or as briefly discussed above, a shift $\delta y_0 = \pi l_m^2/2L$ along the interfaces. Thus, we expect the exact same patterns now as for the $\alpha_L = \alpha_R$ case, only shifted $\pi l_m^2/2L$ along the superconducting interface. As we are considering an infinitely wide junction we expect the total current to remain, and this can also be confirmed analytically using the same method as above.

4.2.3 Subdominant s-wave gap: $\Delta = \Delta_d + i\Delta_s$

Lastly, in section 3.3 we found the Andreev levels when the superconductors have sub-dominant s-wave gap. Using the Andreev levels from equation (3.29), with $\alpha_R = \alpha_L$ or $\alpha_R = \alpha_L \pm n\pi/2$, in (4.2), we find

$$\begin{aligned}\delta I_k(\Delta\varphi) &= \frac{4e}{\hbar}\sqrt{\Delta_0^2 c^2(\theta) + \Delta_s^2}\sin\left(\frac{\Delta\varphi}{2} - \frac{\gamma_k}{2} + \frac{\Delta\beta}{2}\right)\tanh\left(\sqrt{\Delta_0^2 c^2(\theta) + \Delta_s^2}\frac{\cos\left(\frac{\Delta\varphi}{2} - \frac{\gamma_k}{2} + \frac{\Delta\beta}{2}\right)}{2k_B T}\right) \\ &\approx \frac{e(\Delta_0^2 + \Delta_s^2)}{\hbar k_B T}\frac{\cos^2(2(\theta-\alpha)) + \Delta_s^2/\Delta_0^2}{1 + \Delta_s^2/\Delta_0^2}\sin\left(\Delta\varphi - \gamma_k + \Delta\beta\right)\end{aligned} \tag{4.24}$$

where $c(\theta) \equiv \cos(2(\theta - \alpha))$.

$\underline{\alpha_L = \alpha_R = \alpha}$

When the orientation of the d-wave gap is equal in the two superconductors and $\Delta\beta = 0$, this case is very similar to the pure d-wave pairing. However, we get an extra contribution from the term proportional to Δ_s^2/Δ_0^2. This term is of the same form as the s-wave pairing and when increasing Δ_s/Δ_0 we expect the current pattern to go from the pure d-wave pattern to an s-wave pattern. That is the current channels in the d-wave current are expected to shrink and the circular vortices along

the middle of the junction to re-appear. The current density is found numerically and shown in figure 4.2.3 for two different values of Δ_s/Δ_0.

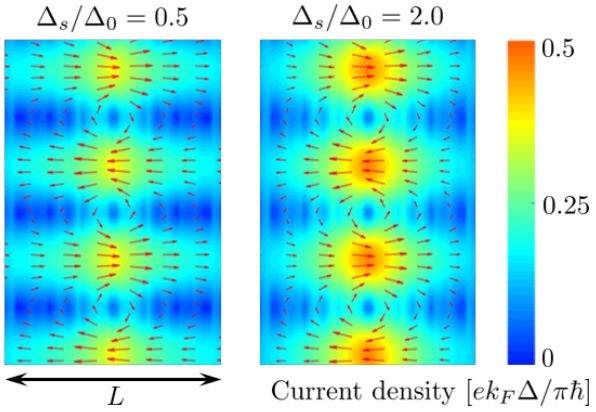

Figure 4.3: Scale plots of the current density through the normal region of a d-wave junction exposed to a uniform magnetic field when left and right superconductor have equal orientation and subdominant s-wave gap. The current is calculated numerically from equation (4.24), (4.3) and (4.7) and with $\Delta\varphi = \pi/2$, $k_B T = \Delta$, $l_m/L = 0.6$.

We can easily find the total current in the case with $\alpha_L = \alpha_R$. Using the same method as in the pure d-wave pairing we find the current

$$I_x = \frac{\frac{7+\sin^2(2\alpha)}{15} + \frac{\Delta_s^2}{\Delta_0^2}}{1+\frac{\Delta_s^2}{\Delta_0^2}} I_{c,0} \frac{\sin\left(\frac{e}{\hbar}\Phi\right)}{\frac{e}{\hbar}\Phi} \sin\Delta\varphi. \tag{4.25}$$

The total current is on the same form as in equation (4.23), but with a modified factor of suppression. With a subdominant s-wave gap we find the current to be larger than in the pure d-wave case and in the limit $\Delta_s \gg \Delta_0$ the total current is not suppressed by the d-wave gap and the pure s-wave case is re-obtained.

$\underline{\alpha_L = \alpha, \alpha_R = \alpha - \pi/2}$

The current density and total current found above, with a subdominant s-wave gap and equal orientation of the d-wave part in left and right superconductor, were not very surprising, as its pattern look like a combination of the pure d-wave case and the pure s-wave case. However, if we let the d-wave part of the left and right superconductor be oriented with a difference of $\pi/2$ the situation is dramatically changed. Now the phase shift $\Delta\beta$ is non-zero and θ-dependent. In order to understand the current pattern we need to consider the structure of the Aharonov-Bohm phase shift, γ. From (4.7) we notice that $\gamma(x_0, y_0, \theta) = \gamma(-x_0, y_0, -\theta)$ and thus, if $\Delta\beta = 0$, then

$\delta I_k(x_0, y_0, \theta) = \delta I_k(-x_0, y_0, -\theta)$. When finding the current density we integrate over both negative and positive angles and thus find a current density to be symmetric around the $x_0 = 0$ axis. Now that we have an extra phase shift $\Delta\beta$ dependent on θ this symmetry is broken. To understand the pattern we consider the expression for δI_k in equation (4.24) in the high temperature regime and consider the special case with $\alpha = \pm\pi/4$:

$$\delta I_k \approx \frac{e(\Delta_0^2 + \Delta_s^2)}{\hbar k_B T} \frac{\sin^2(2\theta) + \Delta_s^2/\Delta_0^2}{1 + \Delta_s^2/\Delta_0^2} \sin\left(\Delta\varphi - \gamma_k \pm \Delta\beta\right), \tag{4.26}$$

with

$$\Delta\beta = 2\arctan\left(\frac{\Delta_s/\Delta_0}{\sin(2\theta)}\right) - \mathrm{sgn}(\theta)\pi \tag{4.27}$$

which is an odd function of θ. In order to find the current density we integrate $\cos\theta\delta I_k(\theta)$ from $-\pi/2$ and $\pi/2$, which is equivalent to integrate $\cos\theta\,[\delta I_k(\theta) + \delta I_k(-\theta)]$ over only positive angles from 0 to $\pi/2$. With $\alpha = \pm\pi/4$ we have

$$\delta I_k(\theta, x_0) + \delta I_k(-\theta, x_0) \approx 2\frac{e\Delta_0^2}{\hbar k_B T} \sin\left(\Delta\varphi - \frac{2L}{l_m^2} y_0\right) \left(\sin^2(2\theta) + \Delta_s^2/\Delta_0^2\right) \cos\left(\frac{2L}{l_m^2} x_0 \tan\theta \pm \Delta\beta(\theta)\right). \tag{4.28}$$

When $\Delta_s = 0$, i.e. in the pure d-wave case, the last factor in (4.28) is

$$-\cos\left(\frac{2L}{l_m^2} x_0 \tan\theta\right) \tag{4.29}$$

which has largest absolute value at $x_0 = 0$ in correspondence with the pattern in the rightmost scale plot in figure 4.2. We will now consider the case with $\Delta_s/\Delta_0 \gtrsim \sqrt{2}$ in which the effect from the subdominant gap is most prominent and we can write

$$\arctan\left(\frac{1}{\frac{\Delta_0}{\Delta_s}\sin(2\theta)}\right) \approx -\frac{\Delta_0}{\Delta_s}\sin(2\theta) + \mathrm{sgn}(\theta)\frac{\pi}{2}. \tag{4.30}$$

For small angles, θ, the last factor in (4.28) can be written as

$$\cos\left(2\theta\left(\frac{L}{l_m^2} x_0 \mp \frac{\Delta_0}{\Delta_s}\right)\right) \tag{4.31}$$

with its maximum when

$$\frac{x_0}{L} \approx \pm\frac{\Delta_0}{\Delta_s}\frac{l_m^2}{L^2} \tag{4.32}$$

where the upper (lower) sign corresponds to $\alpha = \pm\pi/4$. The maximum current is no longer in the middle of the junction, but shifted towards one of the superconductors. When the orientation in the left and right superconductor is $\alpha_L = \pi/4$ and $\alpha_R = -\pi/4$, respectively, the maximum current is shifted to the right and when the orientation is $\alpha_L = -\pi/4$ and $\alpha_R = \pi/4$ the maximum current is

shifted towards the left superconductor. The rightmost scale plot in figure 4.4 illustrates this effect.

We keep the subdominant gap and let the orientation in the left and right superconductor differ by $\pi/2$, like we did above. However, we will let $\alpha = 0$ so that $\alpha_L = 0$ and $\alpha_R = -\pi/2$. Now we have

$$\delta I_k(\theta, x_0) \approx \frac{e(\Delta_0^2 + \Delta_s^2)}{\hbar k_B T} \frac{\cos^2(2\theta) + \Delta_s^2/\Delta_0^2}{1 + \Delta_s^2/\Delta_0^2} \sin\left(\Delta\varphi - \gamma_k + \Delta\beta\right) \tag{4.33}$$

with

$$\Delta\beta = 2\arctan\left(\frac{\Delta_s/\Delta_0}{\cos(2\theta)}\right) - \pi, \tag{4.34}$$

which is now an even function of θ. We expect the current to be symmetric around $x_0 = 0$, as $\delta I_k(x_0, y_0, \theta) = \delta I_k(-x_0, y_0, -\theta)$, like we had in the pure d-wave case. However, despite this symmetry the phase $\Delta\beta$ has an important effect on the pattern. To get more insight we again consider the contribution from both positive and negative angles:

$$\delta I_k(\theta, x_0) + \delta I_k(-\theta, x_0) \approx 2\frac{e\Delta_0^2}{\hbar k_B T}\left(\cos^2(2\theta) + \Delta_s^2/\Delta_0^2\right) \sin\left(\Delta\varphi - \frac{2L}{l_m^2} y_0 + \Delta\beta\right) \cos\left(\frac{2L}{l_m^2} x_0 \tan\theta\right). \tag{4.35}$$

The phase $\Delta\beta$ now appears together with y_0 instead of x_0 like we had in the $\alpha = \pi/4$ case. The expression gives largest current at $x_0 = 0$ like for the pure d-wave case. If we increase $|x_0|$ we find the maximum current at smaller angles $|\theta|$ as $|x_0 \tan\theta|$ is conserved if we increase $|x_0|$ and decrease $|\theta|$. But decreasing $|\theta|$ means decreasing $\Delta\beta$, and would require a decrease in y_0 to keep the current at its maximum. Thus an increase in x_0 correspond to a decrease in y_0. This is different from the pure d-wave case, with $\Delta\beta = 0$, in which an increase in x_0 did not affect the y_0-dependence, only the overall magnitude. In the pure d-wave case we observed flat current channels with the maximums and minimums at conserved y_0 as $|x_0|$ is increased, see left scale plot in figure 4.2. In the scale plot to the left in figure 4.4 we can see how the channels are bent at x_0 as a consequence of the θ-dependent phase $\Delta\beta$ resulting from the subdominant s-wave gap.

For other orientations, $0 < \alpha < \pi/4$, $\Delta\beta$ is neither an odd nor an even function of θ and it is not as easy to consider the case analytically. The middle scale plot in figure 4.4 shows the current density for $\alpha = \pi/8$ and we understand how the pattern change from the case with $\alpha = 0$ to $\alpha = \pi/2$.

In the high temperature, low field regime with $\Delta_s \gg \Delta_0$ the total current is again found to be proportional to the Fraunhofer factor, with a suppression factor which in general is quite complicated, but which will qualitatively be the same as for the case with $\alpha_L = \alpha_R$.

The d-wave superconductors have shown to give rise to a current pattern which is very different from ordinary s-wave pattern. In the pure case without subdominant s-wave gap we found that

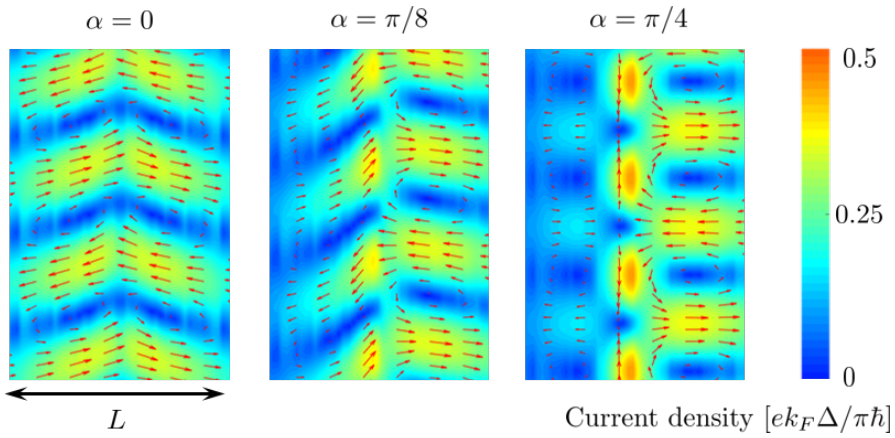

Figure 4.4: Scale plots of the current density through the normal region of a d-wave junction exposed to a uniform field when left and right superconductor have orientations $\alpha_L = \alpha$ and $\alpha_R = \alpha - \pi/2$ and a subdominant s-wave gap. The current is calculated numerically from equation (4.24), (4.3) and (4.7) and with $\Delta\varphi = \pi/2$, $kBT = \Delta$, $l_m/L = 0.6$.

the current vortices are modified to current channels oriented long the orientation of the gap parameters. In the case with subdominant s-wave gap parameter we found that the symmetry of the pattern is lost as a consequence of an extra θ-dependent phase shift, $\Delta\beta(\theta)$. With this property the current density could be much larger in one side of the junction than the other and this anomaly pattern can open for new ways of controlling the current in Josephson junctions.

4.3 Low-T_c SFS junction in weak magntic field

In section 2.9 we considered the Zeeman effect in an SFS junction with normal s-wave pairing in the superconductors in which the energy levels were split into two extra states. We insert the energy levels (3.42) into equation (4.2) and find in the high temperature regime $k_B T \gtrsim \Delta$

$$\begin{aligned}\delta I_k &= \frac{2e\Delta}{\hbar}\sum_{\sigma=\pm}\sin\left(\frac{\Delta\varphi}{2}-\frac{\gamma}{2}+\sigma\frac{k_F L h}{2\mu}\cos\theta\right)\tanh\left(\frac{\Delta}{2k_B T}\cos\left(\frac{\Delta\varphi}{2}-\frac{\gamma}{2}+\sigma\frac{k_F L h}{2\mu}\cos\theta\right)\right)\\ &\approx \frac{e\Delta^2}{\hbar k_B T}\cos\left(\frac{k_F L h}{\mu}\cos\theta\right)\sin\left(\Delta\varphi-\gamma\right).\end{aligned} \tag{4.36}$$

This expression is similar to what we found in the normal SNS case (4.6), but with a factor depending on the Zeeman field, h, and the angle, θ. The current pattern is thus expected to look similar to the SNS case, however we have here assumed small angles which, according to the expression for γ, yields a smaller variation along the junction and the vortices will be dragged compared to the SNS case with all angles taken into account. Note that this is not due to the Zeeman splitting, but to the angle restriction of the momenta. The contribution from a positive angle θ and its corresponding

negative angle $-\theta$ yields

$$\delta I_k(\theta) + \delta I_k(-\theta) \approx \frac{2e\Delta^2}{\hbar k_B T} \cos\left(\frac{k_F L h}{\mu}\cos\theta\right)\cos\left(\frac{2L}{l_m^2}x_0\tan\theta\right)\sin\left(\Delta\varphi - \frac{2L}{l_m^2}y_0\right). \tag{4.37}$$

An increase in the Zeeman field strength h require an increase in θ in order to maintain the magnitude of the current and this would again require $|x_0|$ to decrease. Thus we expect the vortices to shrink as h is increased. We are considering only small angles θ and due to the factor $\cos\theta$ in the integral for I_x (4.1) the small angle states dominate even more. For low fields $l_m/L \gtrsim 0.5$ this yields a small variation along the junction as the argument in the middle factor is small for any x_0. The effect of the shrinking vortices will thus be less prominent. The Zeeman field will instead have an important effect on the strength and direction of the current. The above expression will be maximized at $(k_F L h/\mu)\cos\theta = 2n\pi$, and have a period of $\Delta h = \pi\mu/k_F L$. At $h = (n+1/2)\pi\mu/k_F L$ the current will be at its minimum and at $h = (2n+1)\pi\mu/k_F L$ the current will be at its maximum, but the direction will be reversed compared with the current at $h = 0$. In figure 4.3 the current density is found numerically for three different values of h and we observe a pattern in correspondence with the analysis done here. Note that the rightmost scale plot differ from the leftmost scale plot in the way that the current has opposite direction.

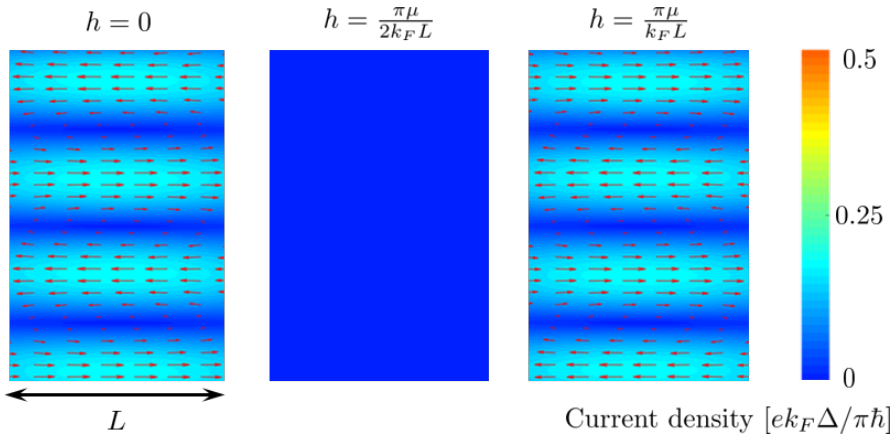

Figure 4.5: Scale plots of the current density through the normal region of an SFS junction exposed to a uniform field, with three different values for the Zeeman field, h. The current is calculated numerically from equation (4.36), (4.3) and (4.7) and with $\Delta\varphi = \pi/2$, $kBT = \Delta$, $l_m/L = 0.6$, $k_F L = 100$, $|\theta| < \theta_{\max} = \pi/8$.

We find the total current by using the same method as in the previous sections and in appendix B:

$$I_x = I_{c,0}A(h)\frac{\sin\left(\frac{e}{\hbar}\Phi\right)}{\frac{e}{\hbar}\Phi}\sin\Delta\varphi \tag{4.38}$$

where we have defined

$$A(h) \equiv \int_0^{\theta_{\max}} d\theta \cos\theta \cos\left(\frac{k_F L h}{\mu}\cos\theta\right). \tag{4.39}$$

The integral $A(h)$ will depend on what angles we allow, restricted by $\pm\theta_{\max}$, and can not in general be solved analytically. In figure 4.3, the factor is found numerically for three different $\theta_{\max}$. With all three choices the factor $A(h)$ is zero for certain values of h/μ. Thus for certain choices of h the critical current is zero and the total current is completely cancelled. For certain ranges of h, $A(h) < 0$ and the current is reversed. The periodic behavior in h accompanied by the reversal current may be caused by 0-π oscillations in the current. Cooper pairs in a ferromagnet oscillate due to the center-of-mass momentum they acquire due to the spin-split bands. Therefore, the order parameter also oscillates, and vanishes at certain values of h (or the length L). When it reappears, it has changed sign, which is equivalent to a π-shift and thus the current is reversed.

The weak spin-orbit coupling alone will, as stated in section 3.4, have no effect on the current density. The Zeeman effect however, has shown that the current direction as well as the current strength in the junction can be controlled by scaling the Zeeman value. Unlike the s-wave pattern, the SFS pattern will not change significantly by the Zeeman splitting in a uniform field.

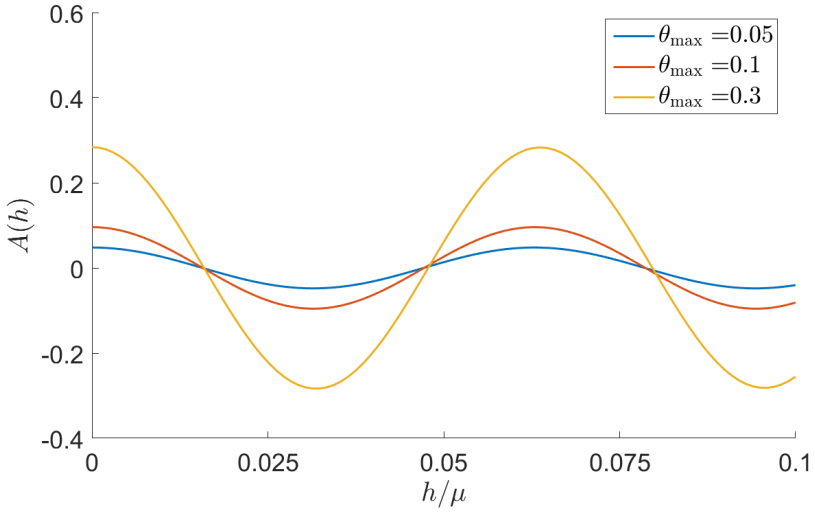

Figure 4.6: A plot of the factor $A(h)$ which limits the critical current in an SFS juction when exposed to a uniform magnetic field. The angle $\theta_{\max}$ determines the maximum angle of incidence in the junction.

Chapter 5

Energy spectrum in a strong magnetic field

So far we have considered magnetic fields where only the influence of the vector potential on the phase was taken into account. However, we have neglected the curvature, due to the Lorentz force, of the trajectories. We will in this chapter consider an SNS-junction in a strong magnetic field, in which the trajectories will be curved. Hoppe *et. al* [43] and Rakyta *et. al* [44] have considered a single NS surface in the strong magnetic field, but the SNS-junction in such strong fields has not been explored. We will differ between two types of semi-classical orbits, A and B, shown in figure 5.1. In the first scenario, A, the radius of the cyclotron of the state is so small that the state will traverse along the junction via skipping orbits and never make it from one superconductor to the other. In this scenario we thus expect the current across the junction to be zero. In the second scenario, either the hole or the electron will make it over to the other superconductor and be Andreev reflected at the superconducting interface. Due to the retro reflection the Andreev reflected particle will not necessarily make it back to the original superconductor, which is illustrated in the middle figure. The last illustration in figure 5.1 is a scenario in which both the electron as well as the hole make it across the junction. There are infinitely many other scenarios, which can be a combination of the three scenarios in figure 5.1 and in our classification we only differ between the case in which no particles make it across the junction, A, and the case in which some particles make it across, B.

Also in the strong field the Josephson current will be carried by the Andreev bound states and we will start by identifying the ABS energy levels of the junction, like we did in chapter 3. Since we can not ignore the curvature of the trajectories in the strong field we can not consider the semiclassical trajectory from section 3.1. The Bohr-sommerfeld quantization condition is no longer applicable and we will instead set up the wave functions in each region of the junction and use boundary conditions to solve the system.

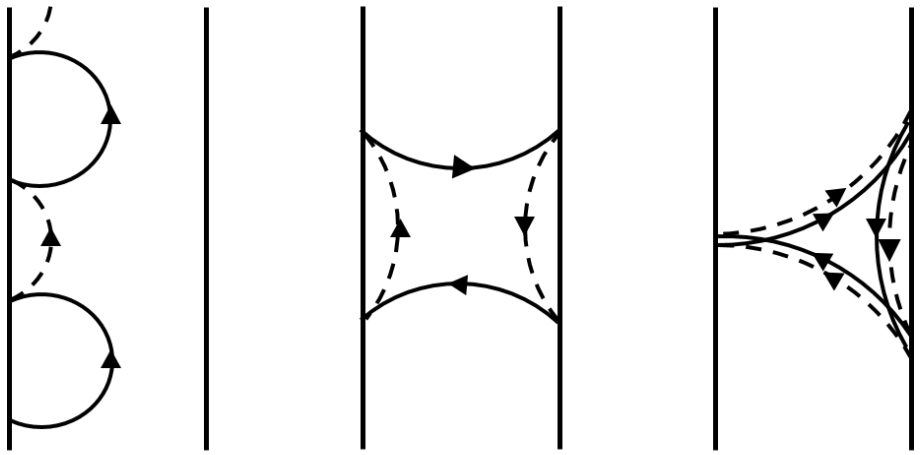

Figure 5.1: Classification of possible semiclassical orbits in Josephson junction exposed to a strong magnetic field. The solid (dashed) lines correspond to electron (hole) trajectory segments. The arrows indicate the direction of the group velocity.

We let the field be uniform and parallel to the interfaces and assume the field to be screened completely in the superconductors. Using the coordinate system from section 3.1 the magnetic field is given as

$$\boldsymbol{B} = B\left[\Theta\left(x+\frac{L}{2}\right)-\Theta\left(x-\frac{L}{2}\right)\right]\hat{z} \tag{5.1}$$

where $\Theta(x)$ is the Heaviside step function. The vector potential

$$\boldsymbol{A} = -By\left[\Theta\left(x+\frac{L}{2}\right)-\Theta\left(x-\frac{L}{2}\right)\right]\hat{x} \tag{5.2}$$

is thus a good choice of gauge as it satisfies $\nabla\times\boldsymbol{A}=\boldsymbol{B}$ and is zero in both superconductors. We allow for barriers at the interfaces and the overall Hamiltonian is

$$h(x,y) = \frac{1}{2m}\left(\boldsymbol{p}-q\boldsymbol{A}\right)^2 - \mu + V_L\delta(x+L/2) + V_R\delta(x-L/2). \tag{5.3}$$

5.1 Wave functions in the superconducting region

We will identify the wave functions in each region, starting with the superconductors. We can ignore the spin degeneracy and use the wave functions from equation (2.29) and (2.30):

$$\Psi_e^{\pm}(x,y) = \begin{pmatrix} 1 \\ e^{-i(\eta+\varphi)} \end{pmatrix} e^{i(\pm k_x^+ x + k_y^+ y)}, \qquad \Psi_h^{\pm}(x,y) = \begin{pmatrix} e^{-i(\eta-\varphi)} \\ 1 \end{pmatrix} e^{i(\pm k_x^+ x + k_y^+ y)} \tag{5.4}$$

where Ψ_e^+ are right-going electrons, Ψ_e^- are left-going electrons, Ψ_h^+ are left-going holes and Ψ_h^- are right-going holes. The direction of the wave functions is determined by the group velocity as discussed in section 2.2. In the short junction regime we will only consider energies within the gap, $E_{\boldsymbol{k}} < \Delta$, as stated in section 3.2.2. For such energies the wave vectors (2.14) will get imaginary parts and must decay in the superconductors. Consequently, there will be no incoming subgap wave-functions from the superconductor into the normal metal and we need only to consider the outgoing wave-functions in the superconducting regions. We let $k_y^+ \approx k_y^- \equiv k_y$ in the Andreev approximation and the total wave functions in the left (L) and right (R) region will thus be

$$\begin{aligned}\Psi_L(x-L/2,y) &= \left[a_1\begin{pmatrix}1\\ e^{-i(\eta+\varphi_L)}\end{pmatrix}e^{-ik_x^+x} + a_2\begin{pmatrix}e^{-i(\eta-\varphi_L)}\\ 1\end{pmatrix}e^{ik_x^-x}\right]e^{ik_yy}\\ \Psi_R(x+L/2,y) &= \left[b_1\begin{pmatrix}1\\ e^{-i(\eta+\varphi_R)}\end{pmatrix}e^{ik_x^+x} + b_2\begin{pmatrix}e^{-i(\eta-\varphi_R)}\\ 1\end{pmatrix}e^{-ik_x^-x}\right]e^{ik_yy}.\end{aligned} \tag{5.5}$$

We have allowed for different phases φ_L and φ_R in each region and absorbed a phase factor $\exp(\pm ik_xL/2)$ in the coefficients in order to simplify the boundary equations.

5.2 Wave functions in the normal region

In the normal region we have a strong magnetic field and we must include the vector potential in the Hamiltonian:

$$h_N = \frac{1}{2m}\left(\boldsymbol{p}-q\boldsymbol{A}\right)^2 - \mu_N. \tag{5.6}$$

As our system is invariant in the y-direction, but not in the x-direction, we let the wave functions have plane waves in the y-direction, and let the x-dependent parts be on a general form, $\Phi_{e/h}^{(N)}(x)$:

$$\tilde{\Psi}_e^{(N)} = \begin{pmatrix}\Phi_e^{(N)}(x)\\ 0\end{pmatrix}e^{ik_yy} \qquad \tilde{\Psi}_h^{(N)} = \begin{pmatrix}0\\ \Phi_h^{(N)}(x)\end{pmatrix}e^{ik_yy}. \tag{5.7}$$

The functions $\Phi_{e/h}^{(N)}$ will be determined by inserting the wave functions, along with the Hailitonian, h_N, in the BdG-equations (2.21a). With the vector potential given in equation (5.2) we can not separate the wave functions into a general x-dependent part and a y-dependent plane wave part as we have done in equation (5.7). We will instead use the vector potential

$$\tilde{\boldsymbol{A}} = B\left[\left(x+\frac{L}{2}\right)\Theta\left(x+\frac{L}{2}\right) - \left(x-\frac{L}{2}\right)\Theta\left(x-\frac{L}{2}\right)\right]\hat{y} \tag{5.8}$$

which also satisfies $\nabla\times\tilde{\boldsymbol{A}} = \boldsymbol{B}$ with $\boldsymbol{B}$ given in equation (5.1). But, unlike the vector potential given in equation (5.2), $\tilde{\boldsymbol{A}}$ will be finite also in the right superconductor. Our strategy is thus to use the vector potential $\tilde{\boldsymbol{A}}$ to find the wave functions, $\tilde{\Psi}^{(N)}$, in the normal region and then do a gauge trans-

formation, $\tilde{\Psi}^{(N)} \rightarrow \Psi^{(N)}$, according to appendix A, back to the vector potential $\boldsymbol{A}$ given in equation (5.2).

In the normal region we have $\tilde{\boldsymbol{A}} = B\left(x+\frac{L}{2}\right)\hat{y}$ and inserting this in the Hamiltonian (5.6) along with the two-dimensional momentum operator yields

$$h_N = -\frac{\hbar^2}{2m}\frac{\partial^2}{\partial x^2} + \frac{e^2B^2}{2m}\left[x+\frac{L}{2} \pm i\frac{\hbar}{eB}\frac{\partial}{\partial y}\right]^2 - \mu_N. \tag{5.9}$$

We insert the wave functions (5.7) together with the Hamiltonian, h_N, in the BdG-equations (2.21a) and must solve

$$h_{e/h}^{(N)}\Phi^{e/h}(x)e^{ik_y y} = \pm E\Phi^{e/h}(x)e^{ik_y y}. \tag{5.10}$$

Since the y-separable of the wave function is a plane wave, we can replace $\partial/\partial y$ with ik_y in the Hamiltonian:

$$h_N = -\frac{\hbar^2}{2m}\frac{\partial^2}{\partial x^2} + \frac{e^2B^2}{2m}\left[x+\frac{L}{2} \mp \frac{\hbar k_y}{eB}\right]^2 - \mu_N, \tag{5.11}$$

where the term $\hbar k_y/eB$ in the bracket will play the role as a guiding center, traversing parallel to the interfaces. After doing this replacement, equation (5.10) yields

$$-\frac{\hbar^2}{2m}\frac{\partial^2\Phi^{e/h}}{\partial x^2} + \frac{e^2B^2}{2m}\left[x+\frac{L}{2} \mp \frac{\hbar k_y}{eB}\right]^2\Phi^{e/h} = \left[\pm E+\mu_N\right]\Phi^{e/h}. \tag{5.12}$$

In order to simplify the equation we introduce the new variables

$$\begin{aligned}\xi_{e/h} &= \frac{\sqrt{2}}{l_m}\left(x+\frac{L}{2} \pm l_m^2 k_y\right)\\ a_{e/h} &= -\frac{ml_m^2}{\hbar^2}\left[\pm E+\mu_N\right],\end{aligned} \tag{5.13}$$

with $l_m = \sqrt{\hbar/eB}$ as the magnetic length. Equation (5.12) can now be written as

$$\frac{\partial^2\Phi^{e/h}}{\partial\xi_{e/h}^2} - \left[\frac{\xi_{e/h}^2}{4} + a_{e/h}\right]\Phi^{e/h} = 0. \tag{5.14}$$

This equation is a parabolic cylinder differential equation [74] and has solutions of the form

$$\begin{aligned}\Phi_1^{e/h}(a_{e/h},\xi_{e/h}) &= e^{-\frac{1}{4}\xi_{e/h}^2}M\left(\frac{1}{2}a_{e/h}+\frac{1}{4},\frac{1}{2},\frac{1}{2}\xi_{e/h}^2\right)\\ \Phi_2^{e/h}(a_{e/h},\xi_{e/h}) &= e^{-\frac{1}{4}\xi_{e/h}^2}M\left(\frac{1}{2}a_{e/h}+\frac{3}{4},\frac{3}{2},\frac{1}{2}\xi_{e/h}^2\right)\end{aligned} \tag{5.15}$$

where $M(a,b,z)$ is the Kummer's function [74]:

$$\begin{aligned} M(a,b,z) &= 1 + \frac{az}{b} + \frac{(a)_2 z^2}{(b)_2 2!} + \ldots + \frac{(a)_n z^n}{(b)_n n!} + \ldots, \\ (a)_n &= a(a+1)(a+2)\ldots(a+n-1), \quad (a)_0 = 1. \end{aligned} \tag{5.16}$$

The general solution for $\Phi^{e/h}(x)$ will be a linear combination of $\Phi_1^{e/h}$ and $\Phi_2^{e/h}$ and the total wave function in the normal region and with the gauge from equation (5.8) will be given as

$$\tilde{\Psi}_N(x,y) = \left[c_1 \begin{pmatrix} \Phi_1^e(x) \\ 0 \end{pmatrix} + c_2 \begin{pmatrix} \Phi_2^e(x) \\ 0 \end{pmatrix} + c_3 \begin{pmatrix} 0 \\ \Phi_1^h(x) \end{pmatrix} + c_4 \begin{pmatrix} 0 \\ \Phi_2^h(x) \end{pmatrix} \right] e^{ik_y y}. \tag{5.17}$$

We must now do a transformation $\tilde{\boldsymbol{A}} \to \boldsymbol{A}$, $\tilde{\Psi}_N \to \Psi_N$. From appendix A we have that such a transformation yields

$$\boldsymbol{A} = \tilde{\boldsymbol{A}} + \nabla\chi, \qquad \Psi_N = e^{i\frac{q}{\hbar}\chi}\tilde{\Psi}_N, \tag{5.18}$$

where χ is given as

$$\chi = -By\left[\left(x + \frac{L}{2}\right)\Theta\left(x + \frac{L}{2}\right) - \left(x - \frac{L}{2}\right)\Theta\left(x - \frac{L}{2}\right) \right]. \tag{5.19}$$

After doing this transformation we find the wave functions in the normal region and in the gauge from equation (5.8) to be

$$\begin{aligned} \Psi_N(x,y) &= \exp\left(-i\frac{qB}{\hbar}y\left(x + \frac{L}{2}\right)\right)\tilde{\Psi}_N(x,y) \\ &= \exp\left(\pm i\frac{\xi_{e/h}y}{\sqrt{2}l_m} - ik_y y\right)\tilde{\Psi}_N(x,y) \\ &= c_1 \begin{pmatrix} \Phi_1^e \\ 0 \end{pmatrix} e^{i\xi_e y/l_m\sqrt{2}} + c_2 \begin{pmatrix} \Phi_2^e \\ 0 \end{pmatrix} e^{i\xi_e y/l_m\sqrt{2}} + c_3 \begin{pmatrix} 0 \\ \Phi_1^h \end{pmatrix} e^{-i\xi_h y/l_m\sqrt{2}} + c_4 \begin{pmatrix} 0 \\ \Phi_2^h \end{pmatrix} e^{-i\xi_h y/l_m\sqrt{2}}. \end{aligned} \tag{5.20}$$

5.3 Boundary conditions

We have now found the wave functions in each region with unknown coefficients a_1, a_2, b_1, b_2, c_1, …, c_4 that must satisfy the boundary conditions at the superconducting interfaces. Charge conservation yields continuous wave-functions at the interfaces:

$$\begin{aligned} \Psi_L(-L/2,y) &= \Psi_N(-L/2,y) \equiv \Psi(-L/2,y), \\ \Psi_R(L/2,y) &= \Psi_N(L/2,y) \equiv \Psi(L/2,y). \end{aligned} \tag{5.21}$$

The boundary conditions for the derivatives will not be continuous due to the delta potentials and the choice of gauge (5.2). We find the boundary conditions for the derivatives at the left interface

by integrating the BdG-equations (2.21) over a small distance ϵ around $x = -L/2$ and then let $\epsilon \to 0$:

$$0 = \lim_{\epsilon\to 0}\int_{-L/2-\epsilon}^{-L/2+\epsilon} E_{\boldsymbol{k}}\Psi(x,y)dx = \lim_{\epsilon\to 0}\int_{-L/2-\epsilon}^{-L/2+\epsilon}\begin{pmatrix} h(x,y) & \Delta(x) \\ \Delta^*(x) & -h(x,y)\end{pmatrix}\Psi(x,y)dx \tag{5.22}$$

which gives

$$\begin{aligned}
0 &= \lim_{\epsilon\to 0}\int_{-L/2-\epsilon}^{-L/2+\epsilon} h(x,y)\Psi(x,y)dx \\
&= \lim_{\epsilon\to 0}\int_{-L/2-\epsilon}^{-L/2+\epsilon}\frac{\hbar^2}{2m}\Bigg[-\left(\frac{\partial^2}{\partial x^2}+\frac{\partial^2}{\partial y^2}\right) - i\frac{qBy}{\hbar}\left(\frac{\partial}{\partial x}\Theta\left(x+\frac{L}{2}\right)+\Theta\left(x+\frac{L}{2}\right)\frac{\partial}{\partial x}\right) \\
&\qquad + \frac{q^2B^2y^2}{\hbar^2}\Theta\left(x+\frac{L}{2}\right) - \frac{2m}{\hbar^2}\mu + \frac{2m}{\hbar^2}V_L\delta\left(x+\frac{L}{2}\right)\Bigg]\Psi(x,y)dx \\
&= -\frac{\hbar^2}{2m}\frac{\partial^2\Psi_N}{\partial x^2}\bigg|_{x=-L/2} + \frac{\hbar^2}{2m}\frac{\partial^2\Psi_L}{\partial x^2}\bigg|_{x=-L/2} + \left(-i\frac{\hbar qBy}{2m}+V_L\right)\Psi\bigg|_{x=-L/2}.
\end{aligned}$$

Hence, the boundary condition at the left interface for the derivatives is

$$\frac{\partial\Psi_L}{\partial x}\bigg|_{x=-L/2} - \frac{\partial\Psi_N}{\partial x}\bigg|_{x=-L/2} = \left(i\frac{qBy}{\hbar} - \frac{2m}{\hbar^2}V_L\right)\Psi(-L/2,y). \tag{5.24}$$

and by similar calculations we find

$$\frac{\partial\Psi_R}{\partial x}\bigg|_{x=L/2} - \frac{\partial\Psi_N}{\partial x}\bigg|_{x=L/2} = \left(i\frac{qBy}{\hbar} + \frac{2m}{\hbar^2}V_R\right)\Psi(L/2,y). \tag{5.25}$$

as boundary condition at the right interface. The y-dependency in the boundary condition is a result of the choice of gauge. If we instead had chosen the $\tilde{\boldsymbol{A}}$ gauge the y-dependency would instead enter in the wave functions. The consequence from the y-dependency is that we get y-dependent ABS energies in correspondence with the energies found in the weak field.

5.4 ABS energy

The ABS energy levels can now be found by inserting the wave functions in the superconducting (5.5) and normal region (5.20) into the boundary conditions (5.21), (5.24), (5.25). We insert the resulting system of equations in a homogeneous matrix equation of the form

$$M\begin{pmatrix} a_1 & a_2 & b_1 & b_2 & c_1 & c_2 & c_3 & c_4\end{pmatrix}^T = 0 \tag{5.26}$$

where M is an 8×8-matrix. The ABS energies, E, are included in the above equation via the variable η in the superconducting wave functions (5.5) and via the variables $a_{e/h}$ (5.13) in the normal region wave functions (5.20). These energies are found by letting the determinant $\det(M)$ be zero, which is required for the system of equations to have non-trivial solutions. It turns out to be difficult to

find an analytical expression for the ABS energies, even when asymptotical limits [74] are used for the parabolic cylinder functions (5.15), and we will instead solve the system numerically.

Rakyta *et. al.* [44] found the energy levels for a superconductor-normal metal-vacuum junction (SNV) and from a semiclassical analysis they identified the orbit classifications from figure 5.1 in a corresponding SNV-case. Figure 5.2(a) and 5.2(b) show a reproduction of the results from ref. [44] with the semiclassical orbits from figure 5.1 indicated. It turns out that, for certain values, the numerical calculations are rather difficult and for the corresponding SNS-case we are only able to find the energy levels for small k_y/k_F, see figure 5.3(a) and 5.3(b). For small k_y/k_F the SNV and SNS energies correspond and we assume the states of figure 5.3(a) to be classified as scenario A, and the states of figure 5.3(b) to be classified as scenario B (B:1 or B:2), in correspondence with the SNV case. This is also confirmed by the consideration of the energies in terms of the phase difference, $\Delta\varphi$, shown in figure 5.4(a) and 5.4(b). From this we find that the energy levels of scenario A are independent of $\Delta\varphi$ unlike the energy levels of scenario B. This indicate that the orbits are classified as scenario A, and the phase difference will thus have no impact on the energy levels or the Josephson current, as these orbits will have small radii and thus be prevented from traveling between the superconductors. In scenario B, however, the states will make it across the junction and the phase difference will affect the energy levels. From this analysis we have used a quantum mechanical approach to find the energy levels, but we are still able to interpret the result semiclassically and thus get more insight of the effect of the strong field.

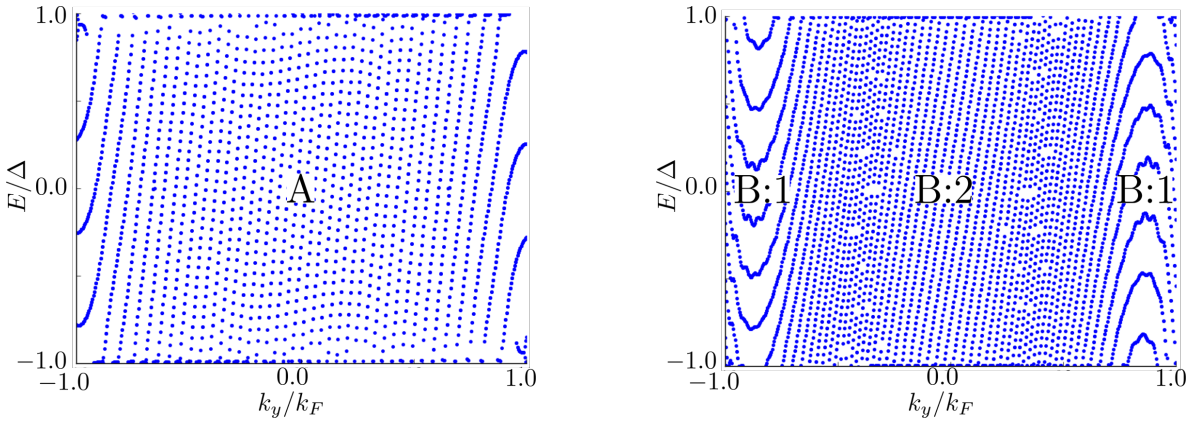

Figure 5.2: The energy spectrum in a superconductor-normal metal-vacuum junction, reproduced from ref. [44]. The parameters are $E_F = 10\Delta$, $k_F W = 106.7$ and (a) $l_m k_F = 20\sqrt{2}$, (b) $l_m k_F = 40$.

In the above results we have let $E_F = 10\Delta$, in which the numerical computations can be done in the high field, $W/k_F l_m^2 \gtrsim 0.1$. We want to compare the results in this chapter with the energies

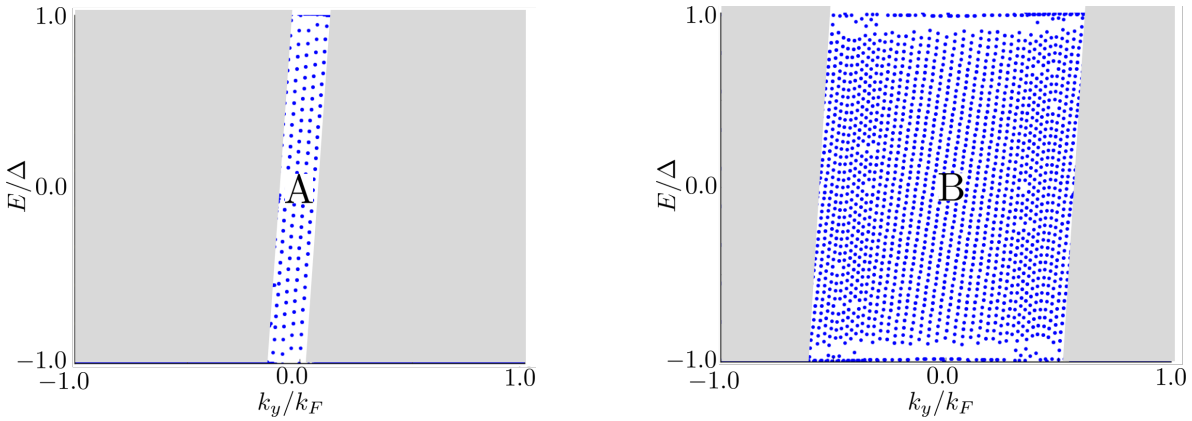

Figure 5.3: The energy spectrum in a superconductor-normal metal-superconductor junction. The parameters are $E_F = 10\Delta$, $k_F W = 106.7$, $Z = 0$, $k_F y = 0$, $\varphi = 0$ and (a) $l_m k_F = 20\sqrt{2}$, (b) $l_m k_F = 40$. In the grey areas, the numerical calculations are difficult.

and currents found for the weak field in chapter 3 and 4. In chapter 3 the Andreev approximation ($\Delta \ll E_F$) was used and we will now use $E_F = 500\Delta$ in which the numerical calculations can be done for weak magnetic fields, $W/k_F l_m^2 \lesssim 0.1$. Figure 5.4 shows the energy levels for a weak field, $W/k_F l_m^2 = 0.05$, at two different positions, y, along the surface normal. The energy levels are found to have a periodicity, $\Delta y = 2\pi l_m^2/L$, which correspond to the y-dependency of the energy levels found in the weak field approach (3.11). Thus we have found that the general approch used in this chapter without any assumption on the semiclassical trajectory correspond to the semiclassical approach used in chapter 3.

The current can be found numerically in a similar fashion as in chapter 4, with the current along the junction given by

$$I_x(\Delta\varphi) = \int dy \int \frac{dk_y}{2\pi} \delta I(\boldsymbol{r}, \boldsymbol{k}), \tag{5.27}$$

with

$$\delta I(\boldsymbol{r}, \boldsymbol{k}) = -2k_B T \sum_i \left[2\cosh\left(\frac{E_i}{2k_B T} \right) \right] \tag{5.28}$$

found from equation (2.42) and (2.37). However, the actual numerical calculations turns out to be rather difficult for certain parameter ranges, and a complete presentation of the current vs field strength could not be made.

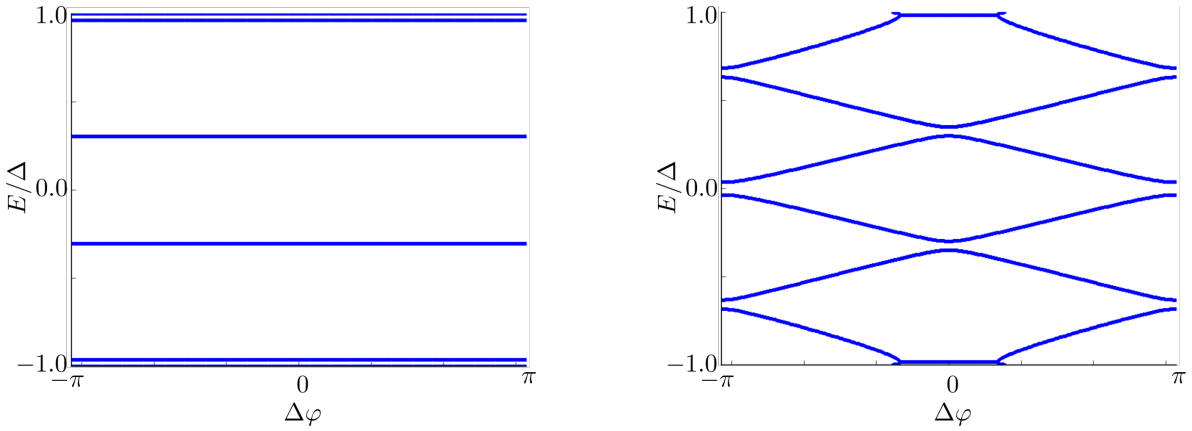

(a) (b)

Figure 5.4: The energy spectrum in terms of the superconducting phase difference, $\Delta\varphi$, in an SNS junction. The parameters are $E_F = 10\Delta$, $k_F W = 106.7$, $Z = 0$, $k_y = 0$, $k_F y = 0$, and (a) $l_m k_F = 20\sqrt{2}$, (b) $l_m k_F = 40$.

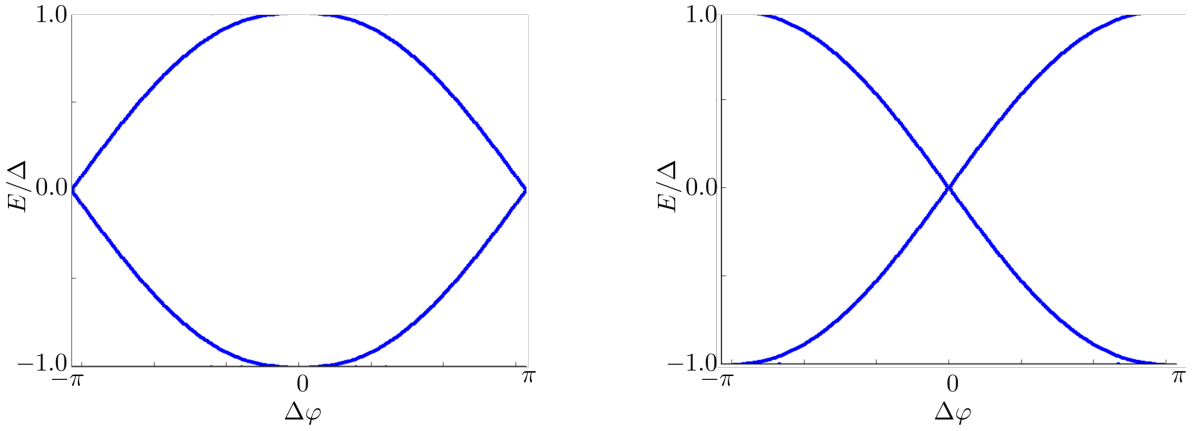

(a) (b)

Figure 5.5: The energy spectrum in terms of the superconducting phase difference, $\Delta\varphi$, in an SNS junction. The parameters are $E_F = 500\Delta$, $k_F W = 106.7$, $Z = 0$, $k_y = 0$, $l_m k_F = 20\sqrt{2}$ and (a) $k_F y = 0$, (b) $k_F y = \frac{\pi l_m^2}{2L}$.

Chapter 6

Conclusion and outlook

In this thesis we have studied how the supercurrent density and the critical current in an SNS-junction is affected by a weak external magnetic field. The result found in an ordinary s-wave SNS-junction is already known, but we have here also considered high-T_c junctions of d-wave superconductors and SFS-junctions with the normal metal substituted by a ferromagnet. Moreover, we have studied how the Andreev bound states in an SNS-junction is affected by a strong magnetic field, when the curvature of the semiclassical trajectories can not be neglected.

In chapter 3 we found the energy levels of the Andreev bound states, using Bohr-Sommerfeld quantization, and the Andreev levels were then used in chapter 4 to find the current density and total current in the junction. In the ordinary low-T_c junction, a chain of Josephson vortices appeared in the center of the junction along the interface and the critical current was found to be the familiar Fraunhofer oscillations, in accordance with earlier research.

In the high-T_c junction the current vortices were modified to current channels oriented along the orientation of the gap parameter. In the case with subdominant s-wave gap, we found that the symmetry of the pattern is lost as a consequence of an extra θ-dependent phase shift, $\Delta\beta(\theta)$. For certain orientations in the presence of the subdominant s-wave gap, this would give much larger current density in one side of the junction than in the other.

In the SFS junction we treated the Zeeman effect and the spin-orbit effect separately. We found that the weak spin-orbit coupling alone has no effect on the Andreev bound state energies. The Zeeman splitting was shown to have an effect on the strength and direction of the Josephson current, but the pattern did not change significantly, compared with the low-T_c SNS-junction. The critical current, both in the high-T_c SNS junction and the low-T_c SFS junction did both have the Fraunhofer factor, however the critical current was now suppressed even more, and for certain values of the Zeeman field the total current would be completely cancelled and also reversed.

In chapter 5 we used analytical methods to find the wave functions and matching conditions in an SNS-junction exposed to a strong magnetic field. The system was then solved numerically, and the Andreev bound state energies were found. We were able to classify two kinds of semiclassical orbits in the junction, one of which the states traverse along the interfaces and do not contribute to the current, and one kind where the cyclotron radius is larger and the Andreev bound state travels between the superconductors.

In the consideration of the current density in the weak magnetic field we assumed the magnetic field to be uniform. In ordinary SNS-junctions, modulated magnetic fields give rise to different current pattern and the critical currents will in some cases not decay as Fraunhofer oscillations [39]. It could be of interest to consider how the supercurrents in high-T_c junctions or in SFS-junctions are affected when the magnetic field is modulated. Moreover, in the strong magnetic field the parabolic cylinder functions made the numerical calculations rather difficult and slow. In future work it could be relevant to investigate numerical methods which can handle these functions in an efficient way such that one may understand how the current of the junction is affected by the strong field, not only the ABS energies. To get an even better understanding of the situation one should do a more thorough semiclassical analysis, similar to what was done by Rakyta $et.\ al.$ [44], and classify the orbits in a more subtle way.

Appendix A

Gauge invariant vector potential and phase

The presence of a magnetic field, $\boldsymbol{B}$, and an electric field, $\boldsymbol{E}$, would give rise to a vector potential, $\boldsymbol{A}$, defined by $\boldsymbol{B} = \nabla \times \boldsymbol{A}$, and a scalar potential, v, defined by $\boldsymbol{E} = -\nabla v - \frac{\partial \boldsymbol{A}}{\partial t}$. The potentials $\boldsymbol{A}$ and v are not physical sizes and must be gauge invariant, that is we may do the transformation

$$\begin{aligned} \boldsymbol{A}' &= \boldsymbol{A} + \nabla\chi \\ v' &= v - \frac{\partial \chi}{\partial t} \end{aligned} \tag{A.1}$$

where χ is any function of position and time, without changing the physical system. We will in this section show that such a transformation implies a transformation in the wavefunction Ψ as well. Considering the time-dependent Schrödinger equation yields

$$\begin{aligned} i\hbar\frac{\partial \Psi}{\partial t} &= \left[\frac{1}{2m}\left(\frac{\hbar}{i}\nabla - q\boldsymbol{A}\right)^2 + qv - \mu_N\right]\Psi \\ &= \left[\frac{1}{2m}\left(\frac{\hbar}{i}\nabla - q\boldsymbol{A}' + q\nabla\chi\right)^2 + qv' + q\frac{\partial\chi}{\partial t} - \mu_N\right]\Psi, \end{aligned} \tag{A.2}$$

which by rearranging and using that

$$e^{iq\chi/\hbar}\left(\frac{\hbar}{i}\nabla + q\nabla\chi\right)\Psi = \frac{\hbar}{i}\nabla\left(e^{iq\chi/\hbar}\Psi\right), \tag{A.3}$$

gives

$$\begin{aligned} i\hbar\frac{\partial}{\partial t}\left(\Psi e^{iq\chi/\hbar}\right) &= e^{iq\chi/\hbar}\left[\frac{1}{2m}\left(\frac{\hbar}{i}\nabla - q\boldsymbol{A}' + q\nabla\chi\right)^2 + qv'\right]\Psi \\ &= \left[\frac{1}{2m}\left(\frac{\hbar}{i}\nabla - q\boldsymbol{A}'\right)^2 + qv'\right]\left(\Psi e^{iq\chi/\hbar}\right). \end{aligned} \tag{A.4}$$

The Schrödinger equation in the transformed system is now on the same form as the original system,

$$i\hbar\frac{\partial\Psi'}{\partial t} = \left[\frac{1}{2m}\left(\frac{\hbar}{i}\nabla - q\boldsymbol{A}'\right)^2 + qv'\right]\Psi', \tag{A.5}$$

with the transformed wave function $\Psi' = e^{iqf/\hbar}\Psi$. Thus a gauge transformation $\boldsymbol{A} \to \boldsymbol{A} + \nabla\chi$ imply a transformation $\phi \to \phi + q\chi/\hbar$ in the phase. The gauge invariant phase will thus be on the form

$$\phi_{\mathrm{GI}} = \phi - \frac{q}{\hbar}\int \boldsymbol{A}\cdot d\boldsymbol{r}, \tag{A.6}$$

as a transformation $\phi \to \phi + q\chi/\hbar$ and $\boldsymbol{A} \to \boldsymbol{A} + \nabla\chi$ will keep ϕ_{GI} unchanged:

$$\begin{aligned}\phi_{\mathrm{GI}} &\to \phi + \frac{q}{\hbar}\chi - \frac{q}{\hbar}\int\left(\boldsymbol{A} + \nabla\chi\right)\cdot d\boldsymbol{r} = \phi - \frac{q}{\hbar}\int \boldsymbol{A}\cdot d\boldsymbol{r} + \frac{q}{\hbar}\chi - \frac{q}{\hbar}\chi \\ &= \phi - \frac{q}{\hbar}\int \boldsymbol{A}\cdot d\boldsymbol{r}.\end{aligned} \tag{A.7}$$

Appendix B

Current in a low-T_c SNS junction exposed to a weak uniform magnetic field

We will calculate the current in a low-T_c junction exposed to a uniform magnetic field [1]. As stated in equation (4.1) and (4.6) the total current in the junction will be given as

$$I_x(\Delta\varphi) = \int dy \int \frac{dk_y}{2\pi} \delta I(\boldsymbol{r}, \boldsymbol{k}), \tag{B.1}$$

with

$$\delta I_k(\Delta\varphi) \approx \frac{e\Delta^2}{\hbar k_B T} \sin\left(\Delta\varphi - \gamma_k\right). \tag{B.2}$$

We consider the system of section 3.1. In the presence of a vector potential, $\boldsymbol{A}$, a state traversing along a trajectory from the left superconductor, S_L, to the right superconductor, S_R, will accumulate a phase

$$\gamma = -\frac{2e}{\hbar} \int_{S_L}^{S_R} \boldsymbol{A} \cdot d\boldsymbol{l} \tag{B.3}$$

due to gauge invariance explained in appendix A. This is the Aharonov-Bohm phase shift which we here will calculate for a uniform magnetic field, $\boldsymbol{B}$. As the field is assumed to be completely screened from the superconductors, it is given as

$$\boldsymbol{B} = B\left[\Theta(x + L/2) - \Theta(x - L/2)\right]\hat{z}, \tag{B.4}$$

and we choose the gauge of the $\boldsymbol{A}$-field as

$$\boldsymbol{A} = -By\left[\Theta(x + L/2) - \Theta(x - L/2)\right]\hat{x}. \tag{B.5}$$

[1] This derivation was done by A. Brøyn in a specialization project [39] and is inspired by the approach used by Ostroukh et. al (2016) [37].

The Aharonov-Bohm phase shift, $\gamma(x_0, y_0, \theta_k)$, is calculated from equation (B.3) by integration along a path through the point (x_0, y_0) at an angle θ_k with the x-axis, as shown in figure 3.1. The trajectory will be given by the line

$$y(x) = y_0 - x_0 \tan\theta_k + x \tan\theta_k, \tag{B.6}$$

and using this in equation (3.10) we find the phase shift:

$$\begin{aligned} \gamma &= -\frac{2e}{\hbar}\int_L^R \boldsymbol{A}\cdot d\boldsymbol{l} = B\frac{2e}{\hbar}\int_{-L/2}^{L/2} y(x)dx \\ &= \frac{2L}{l_m^2}\left(y_0 - x_0\tan\theta_k\right). \end{aligned} \tag{B.7}$$

We combine equation (B.1) and (B.2):

$$I_x = \frac{I_{c,0}}{2W}\int_{-W/2}^{W/2} dy_0 \int_{\pi/2}^{\pi/2} d\theta_k \cos\theta_k \sin(\Delta\varphi - \gamma), \tag{B.8}$$

with

$$I_{c,0} = \frac{k_F W e \Delta^2}{4\pi\hbar k_B T}. \tag{B.9}$$

From equation (B.3) we notice that $\gamma(x_0, y_0, \theta_k) = -\gamma(x_0, -y_0, -\theta_k)$ which allows us to write

$$I_x = \frac{I_{c,0}}{W}\sin(\Delta\varphi)\int_{-W/2}^{W/2} dy_0 \int_0^{\pi/2} d\theta_k \cos\theta_k \cos\gamma. \tag{B.10}$$

The integral over y_0 gives

$$\int_{-W/2}^{W/2} dy_0 \cos\gamma = \frac{l_m^2}{L}\sin\left(\frac{LW}{l_m^2}\right)\cos\left(\frac{2L}{l_m^2}x_0\tan\theta_k\right) \approx \frac{l_m^2}{L}\sin\left(\frac{LW}{l_m^2}\right), \tag{B.11}$$

where the last equality is taken in the low field regime ($l_m \gg L$) in order to simplify the analytical expression. The total current is thus

$$I_x = I_{c,0}\frac{\sin\left(\frac{e}{\hbar}\Phi\right)}{\frac{e}{\hbar}\Phi}\sin\Delta\varphi \tag{B.12}$$

with $\Phi = BLW$ as the magnetic flux and we find the critical current at $\Delta\varphi = \pi/2$:

$$I_{c,\text{const}} = I_{c,0}\left|\frac{\sin\left(\frac{e}{\hbar}\Phi\right)}{\frac{e}{\hbar}\Phi}\right| \tag{B.13}$$

which is the well known Fraunhofer oscillations.

Bibliography

[1] Dirk van Delft and Peter Kes. The discovery of superconductivity. 63(9):38–43, September 2010. ISSN 0031-9228, 1945-0699. URL http://physicstoday.scitation.org/doi/full/10.1063/1.3490499.

[2] W. Meissner and R. Ochsenfeld. Ein neuer effekt bei eintritt der supraleitfähigkeit. *Naturwissenschaften*, 21(44):787–788, 1933. ISSN 1432-1904. URL http://dx.doi.org/10.1007/BF01504252.

[3] A M Forrest. Meissner and ochsenfeld revisited. *European Journal of Physics*, 4(2):117, 1983. URL http://stacks.iop.org/0143-0807/4/i=2/a=011.

[4] J. Bardeen, L. N. Cooper, and J. R. Schrieffer. Theory of superconductivity. *Phys. Rev.*, 108:1175–1204, December 1957. URL http://link.aps.org/doi/10.1103/PhysRev.108.1175.

[5] J. G. Bednorz and K. A. Müller. Possible hightc superconductivity in the balacuo system. *Zeitschrift für Physik B Condensed Matter*, 64(2):189–193, 1986. ISSN 1431-584X. doi: 10.1007/BF01303701. URL http://dx.doi.org/10.1007/BF01303701.

[6] N.E. Bickers, D.J. Scalapino, and R.T. Scalettar. Cdw and sdw mediated pairing interactions. *International Journal of Modern Physics B*, 01(03n04):687–695, 1987. doi: 10.1142/S0217979287001079. URL http://www.worldscientific.com/doi/abs/10.1142/S0217979287001079.

[7] Masahiko Inui, Sebastian Doniach, Peter J. Hirschfeld, and Andrei E. Ruckenstein. Coexistence of antiferromagnetism and superconductivity in a mean-field theory of high-T_c superconductors. *Phys. Rev. B*, 37:2320–2323, Feb 1988. doi: 10.1103/PhysRevB.37.2320. URL https://link.aps.org/doi/10.1103/PhysRevB.37.2320.

[8] C. Gros, D. Poilblanc, T.M. Rice, and F.C. Zhang. Superconductivity in correlated wavefunctions. *Physica C: Superconductivity*, 153:543 – 548, 1988. ISSN 0921-4534. doi: http://dx.doi.org/10.1016/0921-4534(88)90715-0. URL http://www.sciencedirect.com/science/article/pii/0921453488907150.

[9] Gabriel Kotliar and Jialin Liu. Superexchange mechanism and d-wave superconductivity. *Phys. Rev. B*, 38:5142–5145, Sep 1988. doi: 10.1103/PhysRevB.38.5142. URL https://link.aps.org/doi/10.1103/PhysRevB.38.5142.

[10] T. Lofwander, V. S. Shumeiko, and G. Wendin. TOPICAL REVIEW: Andreev bound states in high-T_c superconducting junctions. *Superconductor Science Technology*, 14:R53–R77, May 2001. doi: 10.1088/0953-2048/14/5/201.

[11] Elbio Dagotto. Correlated electrons in high-temperature superconductors. *Rev. Mod. Phys.*, 66:763–840, Jul 1994. doi: 10.1103/RevModPhys.66.763. URL https://link.aps.org/doi/10.1103/RevModPhys.66.763.

[12] R. D. Parks. *Superconductivity*. CRC Press, 1969. ISBN 978-0-8247-1521-2.

[13] B. Pannetier and H. Courtois. Andreev reflection and proximity effect. *Journal of Low Temperature Physics*, 118(5):599–615, 2000. ISSN 1573-7357. URL http://dx.doi.org/10.1023/A:1004635226825.

[14] Linder Jacob and Robinson Jason W. A. Superconducting spintronics. *Nat Phys*, 11(4):307–315, apr 2015. ISSN 1745-2473. doi: http://dx.doi.org/10.1038/nphys324210.1038/nphys3242.

[15] P. M. Tedrow and R. Meservey. Spin-dependent tunneling into ferromagnetic nickel. *Phys. Rev. Lett.*, 26:192–195, Jan 1971. doi: 10.1103/PhysRevLett.26.192. URL https://link.aps.org/doi/10.1103/PhysRevLett.26.192.

[16] P. M. Tedrow and R. Meservey. Spin polarization of electrons tunneling from films of fe, co, ni, and gd. *Phys. Rev. B*, 7:318–326, Jan 1973. doi: 10.1103/PhysRevB.7.318. URL https://link.aps.org/doi/10.1103/PhysRevB.7.318.

[17] JM Rowell. Magnetic field dependence of the josephson tunnel current. *Physical Review Letters*, 11(5):200, 1963. URL http://journals.aps.org/prl/abstract/10.1103/PhysRevLett.11.200.

[18] Michael Tinkham. *Introduction to Superconductivity*. Courier Corporation, 1996. ISBN 978-0-486-13472-7.

[19] Antonio Barone and Gianfranco Paternò. *Physics and applications of the Josephson effect*. Wiley, 1982. ISBN 978-0-471-01469-0.

[20] Jarillo-Herrero P. Oostinga J. B. Vandersypen L. M. K. Heersche, H. B. and A. F. Morpurgo. Bipolar supercurrent in graphene. *Nature*, 446:56–59, 2007. ISSN 0028-0836. URL http://dx.doi.org/10.1038/nature05555.

[21] CaladoV. E., GoswamiS., NandaG., DiezM., AkhmerovA. R., WatanabeK., TaniguchiT., KlapwijkT. M., and VandersypenL. M. K. Ballistic Josephson junctions in edge-contacted graphene. *Nat Nano*, 10(9):761–764, September 2015. ISSN 1748-3387. URL http://dx.doi.org/10.1038/nnano.2015.156.

[22] M. T. Allen, O. Shtanko, I. C. Fulga, J. I. J. Wang, D. Nurgaliev, K. Watanabe, T. Taniguchi, A. R. Akhmerov, P. Jarillo-Herrero, L. S. Levitov, and A. Yacoby. Visualization of phase-coherent electron interference in a ballistic graphene josephson junction, 2015. URL https://arxiv.org/abs/1506.06734.

[23] Zhu-M. J. Fal'ko V. I. Mishchenko A. Kretinin A. V. Novoselov K. S. Woods C. R. Watanabe K. Taniguchi T. Geim A. K. Ben Shalom, M. and J. R. Prance. Quantum oscillations of the critical current and high-field superconducting proximity in ballistic graphene. *Nat Phys*, 12(4):318–322, April 2016. ISSN 1745-2473. URL http://dx.doi.org/10.1038/nphys3592.

[24] M. Veldhorst, M. Snelder, M. Hoek, T. Gang, V. K. Guduru, X. L. Wang, U. Zeitler, W. G. van der Wiel, A. A. Golubov, H. Hilgenkamp, and A. Brinkman. Josephson supercurrent through a topological insulator surface state. *Nat Mater*, 11(5):417–421, May 2012. ISSN 1476-1122. URL http://dx.doi.org/10.1038/nmat3255.

[25] J. R. Williams, A. J. Bestwick, P. Gallagher, Seung Sae Hong, Y. Cui, Andrew S. Bleich, J. G. Analytis, I. R. Fisher, and D. Goldhaber-Gordon. Unconventional josephson effect in hybrid superconductor-topological insulator devices. *Phys. Rev. Lett.*, 109:056803, Jul 2012. URL http://link.aps.org/doi/10.1103/PhysRevLett.109.056803.

[26] Sean Hart, Hechen Ren, Timo Wagner, Philipp Leubner, Mathias Muhlbauer, Christoph Brune, Hartmut Buhmann, Laurens W. Molenkamp, and Amir Yacoby. Induced superconductivity in the quantum spin Hall edge. *Nat Phys*, 10(9):638–643, September 2014. ISSN 1745-2473. URL http://dx.doi.org/10.1038/nphys3036.

[27] Vlad S. Pribiag, BeukmanArjan J. A., Fanming Qu, Maja C. Cassidy, Christophe Charpentier, Werner Wegscheider, and Leo P. Kouwenhoven. Edge-mode superconductivity in a two-dimensional topological insulator. *Nat Nano*, 10(7):593–597, July 2015. ISSN 1748-3387. URL http://dx.doi.org/10.1038/nnano.2015.86.

[28] A.A. Abrikosov. The magnetic properties of superconducting alloys. *Journal of Physics and Chemistry of Solids*, 2(3):199–208, 1957. ISSN 0022-3697. URL http://www.sciencedirect.com/science/article/pii/0022369757900835.

[29] J. C. Cuevas and F. S. Bergeret. Magnetic interference patterns and vortices in diffusive sns junctions. 2007. URL http://journals.aps.org/prl/abstract/10.1103/PhysRevLett.99.217002.

[30] F. S. Bergeret and J. C. Cuevas. The Vortex State and Josephson Critical Current of a Diffusive SNS Junction. *Journal of Low Temperature Physics*, 153(5):304–324, 2008. ISSN 1573-7357. doi: 10.1007/s10909-008-9826-2. URL http://dx.doi.org/10.1007/s10909-008-9826-2.

[31] Mohammad Alidoust, Granville Sewell, and Jacob Linder. Non-fraunhofer interference pattern in inhomogeneous ferromagnetic josephson junctions. *Phys. Rev. Lett.*, 108:037001, Jan 2012. URL http://link.aps.org/doi/10.1103/PhysRevLett.108.037001.

[32] Mohammad Alidoust and Klaus Halterman. Proximity induced vortices and long-range triplet supercurrents in ferromagnetic josephson junctions and spin valves. 2015. URL http://aip.scitation.org/doi/full/10.1063/1.4908287.

[33] Morten Amundsen and Jacob Linder. General solution of 2d and 3d superconducting quasiclassical systems: coalescing vortices and nanoisland geometries. Mar 2015. URL https://www.ncbi.nlm.nih.gov/pmc/articles/PMC4785343/.

[34] J. P. Heida, B. J. van Wees, T. M. Klapwijk, and G. Borghs. Nonlocal supercurrent in mesoscopic josephson junctions. *Phys. Rev. B*, 57:R5618–R5621, Mar 1998. URL http://link.aps.org/doi/10.1103/PhysRevB.57.R5618.

[35] Victor Barzykin and Alexandre M. Zagoskin. Coherent transport and nonlocality in mesoscopic SNS junctions: anomalous magnetic interference patterns. *Superlattices and Microstructures*, 25(5):797 – 807, 1999. ISSN 0749-6036. doi: http://dx.doi.org/10.1006/spmi.1999.0731. URL http://www.sciencedirect.com/science/article/pii/S0749603699907310.

[36] Minsoo Kim, Dongchan Jeong, Gil-Ho Lee, Yun-Sok Shin, Hyun-Woo Lee, and Hu-Jong Lee. Tuning Locality of Pair Coherence in Graphene-based Andreev Interferometers. *Scientific Reports*, 5:8715, March 2015. URL http://dx.doi.org/10.1038/srep08715.

[37] V. P. Ostroukh, B. Baxevanis, A. R. Akhmerov, and C. W. J. Beenakker. Two-dimensional josephson vortex lattice and anomalously slow decay of the fraunhofer oscillations in a ballistic sns junction with a warped fermi surface. *Phys. Rev. B*, 94:094514, Sep 2016. URL http://link.aps.org/doi/10.1103/PhysRevB.94.094514.

[38] Hendrik Meier, Vladimir I. Fal'ko, and Leonid I. Glazman. Edge effects in the magnetic interference pattern of a ballistic sns junction. *Phys. Rev. B*, 93:184506, May 2016. URL http://link.aps.org/doi/10.1103/PhysRevB.93.184506.

[39] Anna Brø yn. Supercurrent transport by andreev bound states in an external magnetic field. *Specialization project*.

[40] L. Landau. Diamagnetismus der metalle. *Zeitschrift für Physik*, 64(9):629–637, 1930. ISSN 0044-3328. doi: 10.1007/BF01397213. URL http://dx.doi.org/10.1007/BF01397213.

[41] Hideaki Takayanagi and Tatsushi Akazaki. Semiconductor-coupled superconducting junctions using nbn electrodes with high hc2 and tc. *Physica B: Condensed Matter*, 249:462 – 466, 1998. ISSN 0921-4526. doi: http://dx.doi.org/10.1016/S0921-4526(98)00164-1. URL http://www.sciencedirect.com/science/article/pii/S0921452698001641.

[42] T. D. Moore and D. A. Williams. Andreev reflection at high magnetic fields. *Phys. Rev. B*, 59: 7308–7311, Mar 1999. doi: 10.1103/PhysRevB.59.7308. URL https://link.aps.org/doi/10.1103/PhysRevB.59.7308.

[43] H Hoppe, U Zülicke, and Gerd Schön. Andreev reflection in strong magnetic fields. *Physical review letters*, 84(8):1804, 2000.

[44] Péter Rakyta, Andor Kormányos, Zoltán Kaufmann, and József Cserti. Andreev edge channels and magnetic focusing in normal-superconductor systems: A semiclassical analysis. *Physical Review B*, 76(6):064516, 2007.

[45] Yakov I. Granovskii. Sommerfeld formula and Dirac's theory. *Physics-Uspekhi*, 47(5):523, 2004. URL http://stacks.iop.org/1063-7869/47/i=5/a=L06.

[46] K. Fossheim and A. Sudbø. *Superconductivity: Physics and Applications*. Wiley, Chichester, West Sussex, 2004. ISBN 9780470844526.

[47] P. G. de Gennes. Boundary effects in superconductors. *Rev. Mod. Phys.*, 36:225–237, Jan 1964. URL http://link.aps.org/doi/10.1103/RevModPhys.36.225.

[48] G. E. Blonder, M. Tinkham, and T. M. Klapwijk. Transition from metallic to tunneling regimes in superconducting microconstrictions: Excess current, charge imbalance, and supercurrent conversion. *Phys. Rev. B*, 25:4515–4532, Apr 1982. URL http://link.aps.org/doi/10.1103/PhysRevB.25.4515.

[49] A. F. Andreev. The thermal conductivity of the intermediate state in superconductors. *Sov. Phys. JETP*, 19:1228 – 1231, Nov 1964. URL http://www.jetp.ac.ru/cgi-bin/e/index/e/19/5/p1228?a=list.

[50] H. A. Blom, A. Kadigrobov, A. M. Zagoskin, R. I. Shekhter, and M. Jonson. Dissipative electron transport through andreev interferometers. *Phys. Rev. B*, 57:9995–10016, Apr 1998. URL http://link.aps.org/doi/10.1103/PhysRevB.57.9995.

[51] P. A. M. Benistant, H. van Kempen, and P. Wyder. Direct observation of andreev reflection. *Phys. Rev. Lett.*, 51:817–820, Aug 1983. URL http://link.aps.org/doi/10.1103/PhysRevLett.51.817.

[52] B. D. Josephson. Possible new effects in superconductive tunnelling. *Physics Letters*, 1(7):251 – 253, 1962. ISSN 0031-9163. URL http://www.sciencedirect.com/science/article/pii/0031916362913690.

[53] Meng Xiang-Guo, Wang Ji-Suo, and Liang Bao-Long. Cooper-Pair Number-Phase Quantization for Inductance Coupling Circuit Including Josephson Junctions. *Chinese Physics Letters*, 25(4):1419, 2008. URL http://stacks.iop.org/0256-307X/25/i=4/a=069.

[54] A. A. Golubov, M. Yu. Kupriyanov, and E. Il'ichev. The current-phase relation in josephson junctions. *Rev. Mod. Phys.*, 76:411–469, Apr 2004. URL http://link.aps.org/doi/10.1103/RevModPhys.76.411.

[55] SHINYA Hasuo and Takeshi Imamura. Digital logic circuits. *Proceedings of the IEEE*, 77(8): 1177–1193, 1989. URL http://ieeexplore.ieee.org/document/34118/.

[56] R. Kleiner and P. Müller. Intrinsic josephson effects in high-t_c superconductors. *Phys. Rev. B*, 49:1327–1341, Jan 1994. URL http://link.aps.org/doi/10.1103/PhysRevB.49.1327.

[57] D. A. Wollman, D. J. Van Harlingen, W. C. Lee, D. M. Ginsberg, and A. J. Leggett. Experimental determination of the superconducting pairing state in ybco from the phase coherence of ybco-pb dc squids. *Phys. Rev. Lett.*, 71:2134–2137, Sep 1993. doi: 10.1103/PhysRevLett.71.2134. URL https://link.aps.org/doi/10.1103/PhysRevLett.71.2134.

[58] C. C. Tsuei, J. R. Kirtley, C. C. Chi, Lock See Yu-Jahnes, A. Gupta, T. Shaw, J. Z. Sun, and M. B. Ketchen. Pairing symmetry and flux quantization in a tricrystal superconducting ring of $Yba_2cu_3o_{7-\delta}$. *Phys. Rev. Lett.*, 73:593–596, Jul 1994. doi: 10.1103/PhysRevLett.73.593. URL https://link.aps.org/doi/10.1103/PhysRevLett.73.593.

[59] D. A. Wollman, D. J. Van Harlingen, W. C. Lee, D. M. Ginsberg, and A. J. Leggett. Experimental determination of the superconducting pairing state in ybco from the phase coherence of ybco-pb dc squids. *Phys. Rev. Lett.*, 71:2134–2137, Sep 1993. doi: 10.1103/PhysRevLett.71.2134. URL https://link.aps.org/doi/10.1103/PhysRevLett.71.2134.

[60] Yukio Tanaka and Satoshi Kashiwaya. Theory of tunneling spectroscopy of d-wave superconductors. *Physical review letters*, 74(17):3451, 1995.

[61] Yu A Bychkov and E I Rashba. Oscillatory effects and the magnetic susceptibility of carriers in inversion layers. *Journal of Physics C: Solid State Physics*, 17(33):6039, 1984. URL http://stacks.iop.org/0022-3719/17/i=33/a=015.

[62] C. W. J. Beenakker. Universal limit of critical-current fluctuations in mesoscopic josephson junctions. *Phys. Rev. Lett.*, 67:3836–3839, Dec 1991. URL http://link.aps.org/doi/10.1103/PhysRevLett.67.3836.

[63] Xin-Zhong Yan and Chia-Ren Hu. Magnetic field effect in josephson tunneling between *d*-wave superconductors. *Phys. Rev. Lett.*, 83:1656–1659, Aug 1999. doi: 10.1103/PhysRevLett.83.1656. URL https://link.aps.org/doi/10.1103/PhysRevLett.83.1656.

[64] E. V. Bezuglyi, A. S. Rozhavsky, I. D. Vagner, and P. Wyder. Combined effect of zeeman splitting and spin-orbit interaction on the josephson current in a superconductor–two-dimensional electron gas–superconductor structure. *Phys. Rev. B*, 66:052508, Aug 2002. doi: 10.1103/PhysRevB.66.052508. URL https://link.aps.org/doi/10.1103/PhysRevB.66.052508.

[65] Y. Aharonov and D. Bohm. Significance of electromagnetic potentials in the quantum theory. *Phys. Rev.*, 115:485–491, Aug 1959. URL http://link.aps.org/doi/10.1103/PhysRev.115.485.

[66] IO Kulik. Macroscopic quantization and the proximity effect in sns junctions. *Soviet Journal of Experimental and Theoretical Physics*, 30:944, 1969. URL http://www.jetp.ac.ru/cgi-bin/e/index/e/30/5/p944?a=list.

[67] Masashige Matsumoto and Hiroyuki Shiba. Coexistence of different symmetry order parameters near a surface in d-wave superconductors i. *Journal of the Physical Society of Japan*, 64 (9):3384–3396, 1995. doi: 10.1143/JPSJ.64.3384. URL http://dx.doi.org/10.1143/JPSJ.64.3384.

[68] Masashige Matsumoto and Hiroyuki Shiba. Coexistence of different symmetry order parameters near a surface in d-wave superconductors ii. *Journal of the Physical Society of Japan*, 64 (12):4867–4881, 1995. doi: 10.1143/jpsj.64.4867.

[69] S. Kashiwaya, Y. Tanaka, M. Koyanagi, H. Takashima, and K. Kajimura. Tunneling spectroscopy of d-wave superconductors. *Journal of Physics and Chemistry of Solids*, 56(12):1721 – 1723, 1995. ISSN 0022-3697. doi: http://dx.doi.org/10.1016/0022-3697(95)00135-2. URL http://www.sciencedirect.com/science/article/pii/0022369795001352. Proceedings of the Conference on Spectroscopies in Novel Superconductors.

[70] Masashige Matsumoto and Hiroyuki Shiba. Coexistence of different symmetry order parameters near a surface in d-wave superconductors iii. *Journal of the Physical Society of Japan*, 65 (7):2194–2203, 1996. doi: 10.1143/JPSJ.65.2194. URL http://dx.doi.org/10.1143/JPSJ.65.2194.

[71] M. Fogelström, D. Rainer, and J. A. Sauls. Tunneling into current-carrying surface states of high-tc superconductors. *Physical Review Letters*, 79(2):281–284, 1997. ISSN 0031-9007.

[72] Y. Tanuma, Y. Tanaka, M. Ogata, and S. Kashiwaya. Quasiparticle states near surfaces of high-t_c superconductors based on the extended $t-j$ model. *Phys. Rev. B*, 60:9817–9826,

Oct 1999. doi: 10.1103/PhysRevB.60.9817. URL https://link.aps.org/doi/10.1103/PhysRevB.60.9817.

[73] Jian-Xin Zhu and C. S. Ting. Spontaneous flux in a d-wave superconductor with time-reversal-symmetry-broken pairing state at 110-oriented boundaries. *Phys. Rev. B*, 60:R3739–R3742, Aug 1999. doi: 10.1103/PhysRevB.60.R3739. URL https://link.aps.org/doi/10.1103/PhysRevB.60.R3739.

[74] Milton Abramowitz and Irene A Stegun. *Handbook of mathematical functions: with formulas, graphs, and mathematical tables*, volume 55. Courier Corporation, 1964.